AD NUMBER
ADB016788
LIMITATION CHANGES
TO: **Approved for public release; distribution is unlimited.**
FROM: **Distribution authorized to U.S. Gov't. agencies only; Test and Evaluation; AUG 1976. Other requests shall be referred to Air Force Armament Lab., Eglin AFB, FL.**
AUTHORITY
USADTC ltr 10 Dec 1979

THIS REPORT HAS BEEN DELIMITED
AND CLEARED FOR PUBLIC RELEASE
UNDER DOD DIRECTIVE 5200.20 AND
NO RESTRICTIONS ARE IMPOSED UPON
ITS USE AND DISCLOSURE.

DISTRIBUTION STATEMENT A

APPROVED FOR PUBLIC RELEASE;
DISTRIBUTION UNLIMITED.

AFATL-TR-76-90

DESIGN CONSIDERATIONS FOR AN IMPULSE CORRECTED, BODY FIXED, LASER GUIDED, FIN STABILIZED ROCKET

BALLISTICS BRANCH
GUNS, ROCKETS AND EXPLOSIVES DIVISION

AUGUST 1976

FINAL REPORT: JANUARY 1974 - JULY 1976

AIR FORCE ARMAMENT LABORATORY
AIR FORCE SYSTEMS COMMAND • UNITED STATES AIR FORCE
EGLIN AIR FORCE BASE, FLORIDA

UNCLASSIFIED

SECURITY CLASSIFICATION OF THIS PAGE (When Data Entered)

REPORT DOCUMENTATION PAGE

READ INSTRUCTIONS BEFORE COMPLETING FORM

14

1. REPORT NUMBER
AFATL-TR-76-9Ø

2. GOVT ACCESSION NO.

3. RECIPIENT'S CATALOG NUMBER

9

6

4. TITLE (and Subtitle)
DESIGN CONSIDERATIONS FOR AN IMPULSE CORRECTED, BODY FIXED, LASER GUIDED, FIN STABILIZED ROCKET.

5. TYPE OF REPORT & PERIOD COVERED
FINAL rept.
Jan[redacted] [redacted]974-Jul[redacted] [redacted]976,

6. PERFORMING ORG. REPORT NUMBER

10

7. AUTHOR(s)
Kenneth K./Cobb

8. CONTRACT OR GRANT NUMBER(s)

9. PERFORMING ORGANIZATION NAME AND ADDRESS
Guns, Rockets and Explosives Division (DLDL)

10. PROGRAM ELEMENT, PROJECT, TASK AREA & WORK UNIT NUMBERS
62602F
16 2547 0308
17 Ø3

11. CONTROLLING OFFICE NAME AND ADDRESS
Air Force Armament Laboratory
Armament Development and Test Center
Eglin Air Force Base, FL 32542

11

12. REPORT DATE
Aug[redacted] [redacted]976

13. NUMBER OF PAGES
101

14. MONITORING AGENCY NAME & ADDRESS (if different from Controlling Office)

12 101p.

15. SECURITY CLASS. (of this report)
UNCLASSIFIED

15a. DECLASSIFICATION/DOWNGRADING SCHEDULE

16. DISTRIBUTION STATEMENT (of this Report)

Distribution limited to U.S. Government agencies only; this report documents test and evaluation; distribution limitation applied August 1976. Other requests for this document must be referred to the Air Force Armament Laboratory (DLDL), Eglin Air Force Base, Florida 32542.

17. DISTRIBUTION STATEMENT (of the abstract entered in Block 20, if different from Report)

18. SUPPLEMENTARY NOTES

Available in DDC

19. KEY WORDS (Continue on reverse side if necessary and identify by block number)

Body Fixed Guidance System
Impulse Correction

20. ABSTRACT (Continue on reverse side if necessary and identify by block number)

This report is an analysis of the dynamics and accuracy of a laser guided fin stabilized rocket. The guidance uses a quadrant detector, pursuit guidance, and is a body fixed system (no gyroscopic or relative wind reference). Corrections are made using short action time explosive strips located forward of the center of mass.

Several guidance consideration which affect the accuracy or effectiveness of

Next pg

DD FORM 1 JAN 73 1473 EDITION OF 1 NOV 65 IS OBSOLETE

UNCLASSIFIED 400 936

SECURITY CLASSIFICATION OF THIS PAGE (When Data Entered)

LB

(Item 20 concluded) this system are analyzed in this report. Some of these considerations are: phasing of the laser pulse frequency and the pitch frequency; the relation between the trim misalignment, the pitch frequency, and the roll rate; the maximum expected correction as a function of the physical and aerodynamic characteristics of the rocket; target motion and wind; and the dead zone size.

PREFACE

This work was done under Project 25470308 in the Ballistics Branch of the Guns, Rockets and Explosives Division. The effort commenced on this program in July 1973. The knowledge gained from this work has been used and will continue to be used to support the Advanced Tactical Rocket System. The effort has been carried on periodically since 1973. The author is indebted to Billy Walker and Gus Osterlow for computer programming on the six-degree-of-freedom simulation. Particular appreciation is extended to Gus Osterlow for setting up numerical integration techniques, and other assistance in computer numerical analysis as well as computer programming.

This technical report has been reviewed and is approved for publication.

FOR THE COMMANDER

Gerald P. D'Arcy

GERALD P. D'ARCY, Colonel, USAF
Chief, Guns, Rockets and Explosives Division

(The reverse of this page is blank)

TABLE OF CONTENTS

LIST OF FIGURES

LIST OF TABLES

(The reverse of this page is blank)

SECTION I

INTRODUCTION

During the past 2-1/2 years a study has been made to determine the feasibility of using an explosive charge to give terminal correction to a fin stabilized rocket using a fixed-body seeker. Figure 1 is a sketch of the type guidance head being considered. Figure 2 is a sketch of the rocket and associated four quadrant detecting correction method to be employed. A pulsed laser image reflected from the target is received in one of the four quadrants indicating that the longitudinal axis of the missile is not in line with the target. The seeker logic then fires an explosive strip (action time approximately 10^{-4} seconds) in the image quadrant. The explosive strips are expended in a predetermined sequence. In this manner the velocity vector (to the extent that the angle of attack is small when the correction is made) is turned in line with the target. Part of the correction comes from motion of the cg due to the linear momentum explosive impulse, and the remainder comes from the lift force generated by the angle of attack. The angle of attack is induced primarily by the moment of the impulse which is forward of the center of gravity.

In studying the guidance system it is necessary to simulate the motion of the rocket, the logic and correction of the guidance system, and all associated errors. Two simulation computer programs are used in this study. The first is a simple closed form solution to the pitching motion which is used in analyzing the pitching frequency, angle of attack, and magnitude of the impulse correction for the high force, short time duration impulses employed. The second computer program is a complete six-degree-of-freedom program which models the entire guidance system. This includes physical and aerodynamic properties of the rocket, the guidance logic, the force and moment of the impulse corrections, atmospheric conditions and target motion.

The advantages of the type of guidance being considered are that it is simple and inexpensive. The guidance package contains no gyros or other moving parts.

The following phenomena can adversely affect the accuracy of this body-fixed system, and an understanding of them is essential in developing the system:

(1) Limited correction from explosive impulse strips; the total correction to be obtained from this type of guidance is determined by the total impulse per strip, the number of strips, the physical and aerodynamic properties of the rocket, and the type of trajectory being considered.

(2) Angle of attack when guidance correction made; the angle of attack of the rocket, induced by impulse correction or trim misalignment, is erroneously interpreted by the seeker as an error in the direction of the velocity vector.

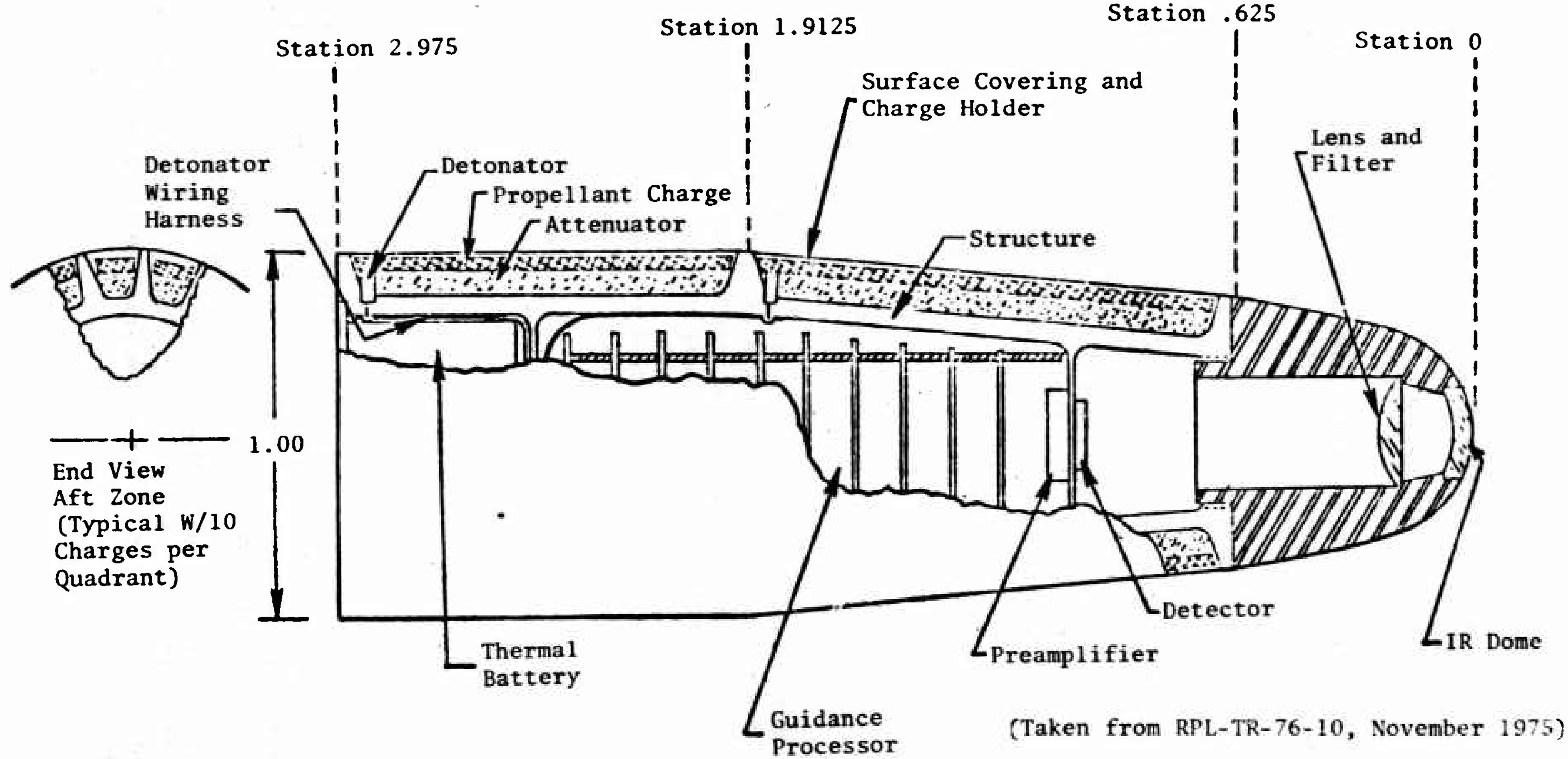

(Taken from RPL-TR-76-10, November 1975)

(All Dimensions in Calibers)

Figure 1. Impulse Control Guidance Head

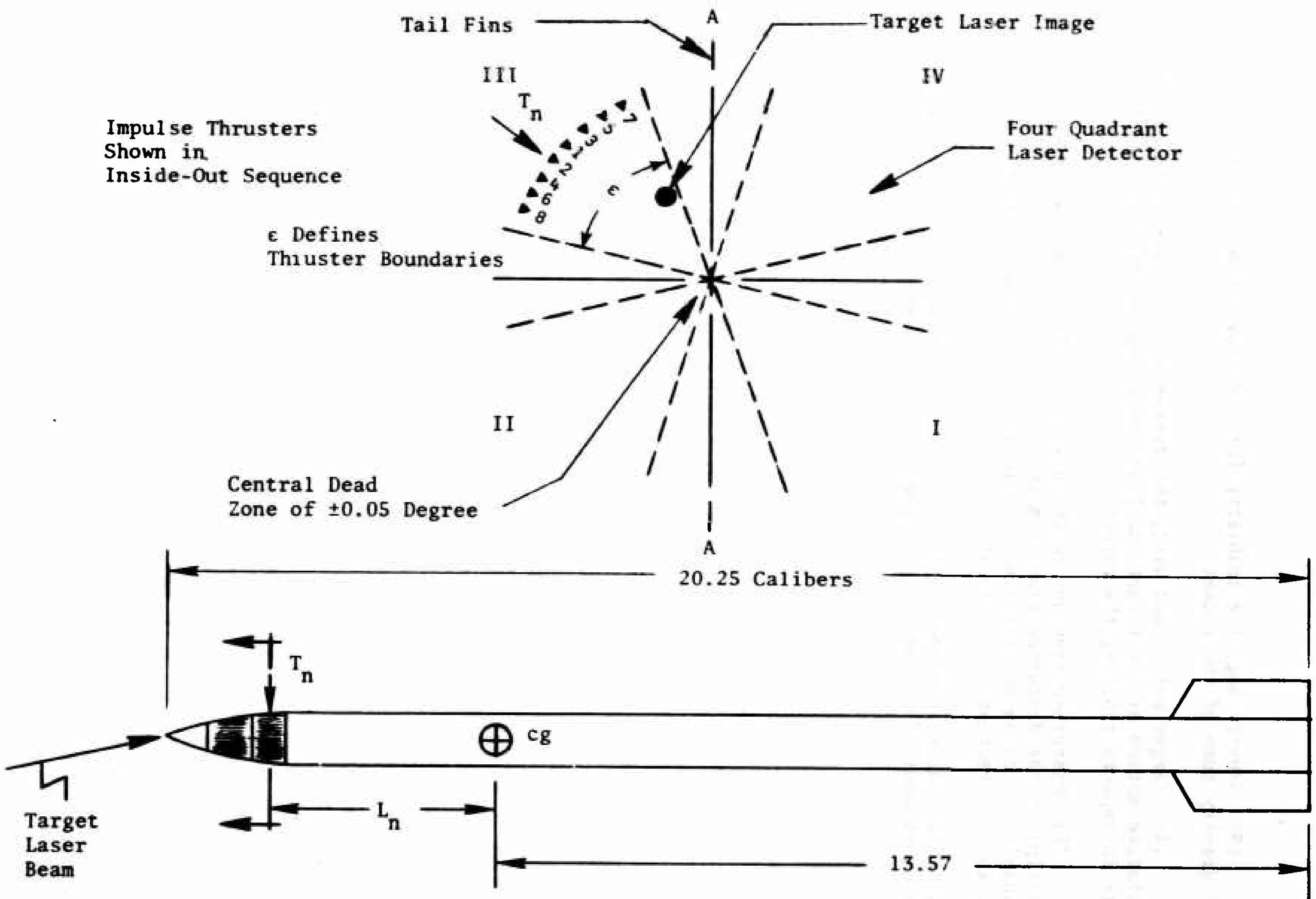

Figure 2. Impulse Control Geometry

(3) Gravity sag; the inability for the logic to account for the normal gravity turn of the rocket.

(4) Target motion and wind; the system does not take into account the relative motion of the target (no lead computing capability), and this results in impacts trailing the target.

(5) Disturbed flow due to the blast wave from the impulse explosive strip; if the disturbed flow from the explosive strip changes the aerodynamic forces on the missile for a long enough period of time, an unpredictable correction would result.

All of the above phenomena will be considered in detail in this report and an assessment of the accuracy of the system will be given.

SECTION II

GENERAL GUIDANCE CONSIDERATIONS AND SIMULATION MODELS

1. BASIC GUIDANCE SYSTEM

The guidance corrections are initiated by the seeker determining the off axis quadrant of a reflected laser beam from the designated target. The line of sight laser reflection is focused by the lens (Figure 1) onto the detector. The seeker logic determines the quadrant of the focused beam (Figure 2) to the limits of the dead zone. The dead zone may be a small area at the center of the field of view, or a region on the perpendicular lines separating the quadrants. For the system being considered the size of the dead zone is on the order of 0.1 degree.

The seeker receives a signal each time the laser pulses. The primary laser pulse frequency considered in this report is 20 per second. Upon receiving a signal in one of the four quadrants, the seeker logic will designate an explosive strip (thruster) in the same quadrant to fire (Figure 2). In determining the target quadrant the seeker has determined the line of sight to the target with respect to the longitudinal axis to within 90 degrees. There is essentially no time delay between reception of laser image and completion of thrust action (less than 10^{-4} seconds), and this is one of the advantages of the system. The logic of the sequencing of the thrusters may be varied. Also the number, the total impulse and the location of the thrusters may be varied. These variations will have an effect on the accuracy and will be discussed in detail in later sections of this report. The amount of correction which can be obtained from a configuration of thrusters is basic to the guidance, and is discussed in Section IV.

The guidance being considered here is fixed body. This means there are no gyroscopes or any other moving parts to identify an inertial reference or rocket relative motion. The guidance system can only determine the angle between the target and the longitudinal axis (no floating head as in the laser guided bomb). It is desired to correct the direction of the velocity vector to the target, but by the nature of the system this is done only to the extent that the angle of attack is small when correction is initiated. Figure 3 illustrates this point where at 3.3 seconds of flight a target offset 50 feet amounts to a 0.9 degree correction. If the angle of attack of the missile is any sizeable fraction of this, then unacceptable errors result (the effect on accuracy of this error will be considered later in this report).

Angle of attack errors can be induced by the impulse correction itself. In general the explosive strip will be located forward of the rocket center of gravity as shown in Figure 2. As a result of the explosive impulse the

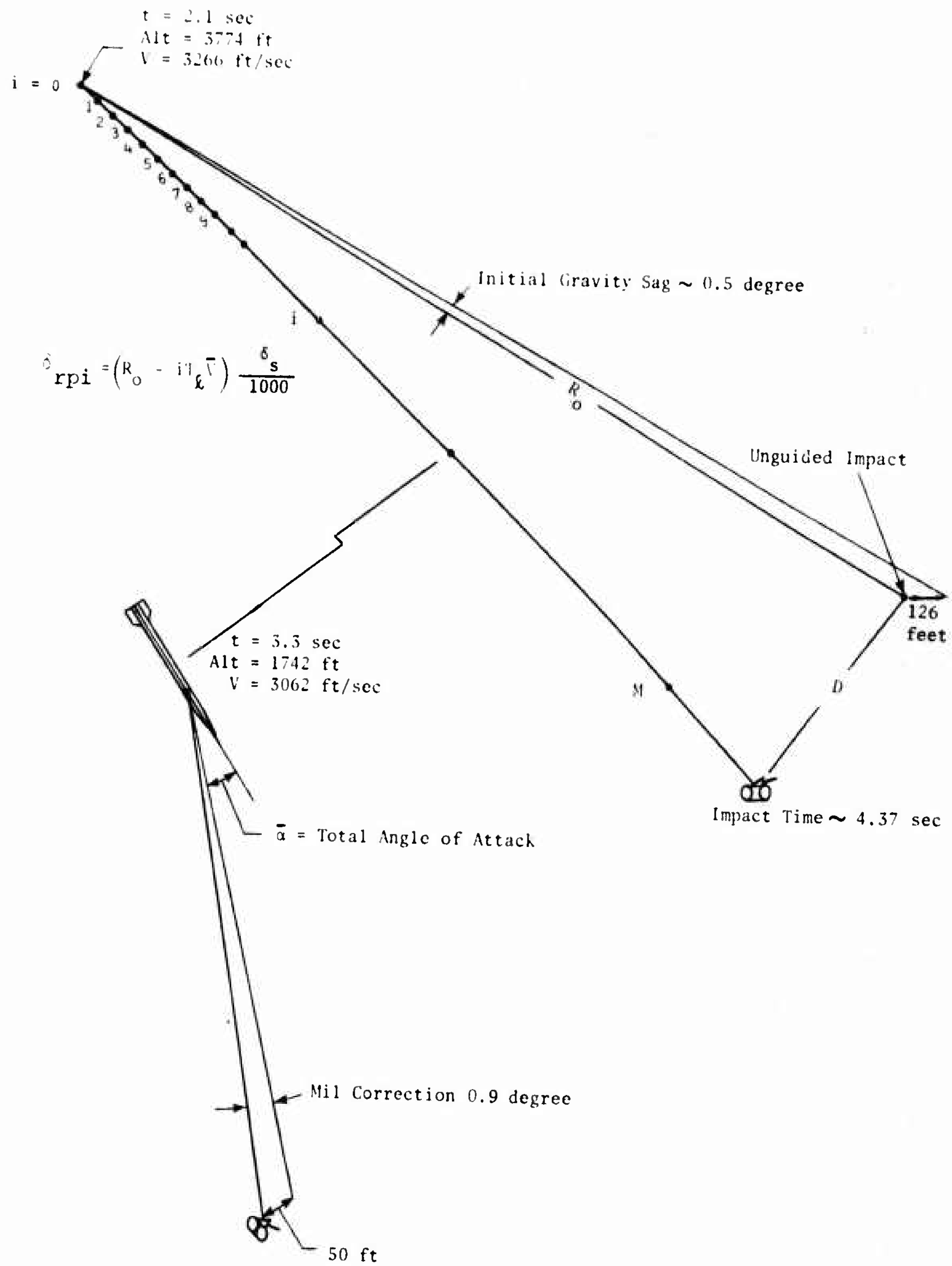

Figure 3. Laser Trajectory Corrections

missile will incur an angle of attack which will oscillate and damp according to the physical and aerodynamic properties of the missile. On the following laser pulse a residual angle of attack will be interpreted as a target direction error to correct. Since we are attempting to correct the velocity vector to the target, accuracy will be reduced. The relationship between the laser pulse frequency, missile pitch frequency, angle of attack, and accuracy will be discussed in Section III.

The explosive strip when detonated will also cause a blast wave and associated disturbed flow over the missile. If this disturbance affected the missile long enough, it could result in an undesired angle of attack which could reduce accuracy. A test to determine if this was a problem was run and is discussed in Section VII.

Another source of angle of attack error is trim misalignment. This results in an angle of attack in the trim plane rotating with the spin frequency of the missile. The relationship between the static trim misalignment, the spin, pitch frequency, and the resulting trim angle will be given in Section V. A method for controlling the magnitude of the trim arm with the spin and thereby reducing the guidance error is also given.

Gravity sag is a source of error in this system. It results from the guidance system correcting to the line of sight direction to the target without regard to the normal gravity turn of the missile. This is depicted in Figure 3, where at guidance initiation (2.1 seconds) the velocity vector is pointed 126 feet downrange of the unguided impact point. The zero angle-of-attack missile will incorrectly detect a target at the unguided impact point as being about 0.5 degree down. Corrections will be initiated and will result in the missile having to correct back to the target in the latter part of the trajectory. The missile won't be able to correct all the way back to the target and will impact short. Figure 4 shows the angle between the longitudinal axis and the target as a function of space slant range to the target for a nominal rocket configuration. The three trajectories are unguided with the target being located on, 50 feet short of, and 50 feet beyond the unguided impact. Generally the gravity sag error is decreased by increasing the total impulse per correction. This will be shown in the six-degree-of-freedom accuracy study.

The guidance system being considered uses pursuit guidance (i.e., correction directly toward the target). This results in the missile trailing the target if there is relative motion between the missile and the target. The relative motion can result from the target moving, or a wind causing the rocket to move with respect to the target, or both. This error can be reduced by increasing the total impulse per thrust. This will be demonstrated in Section III.

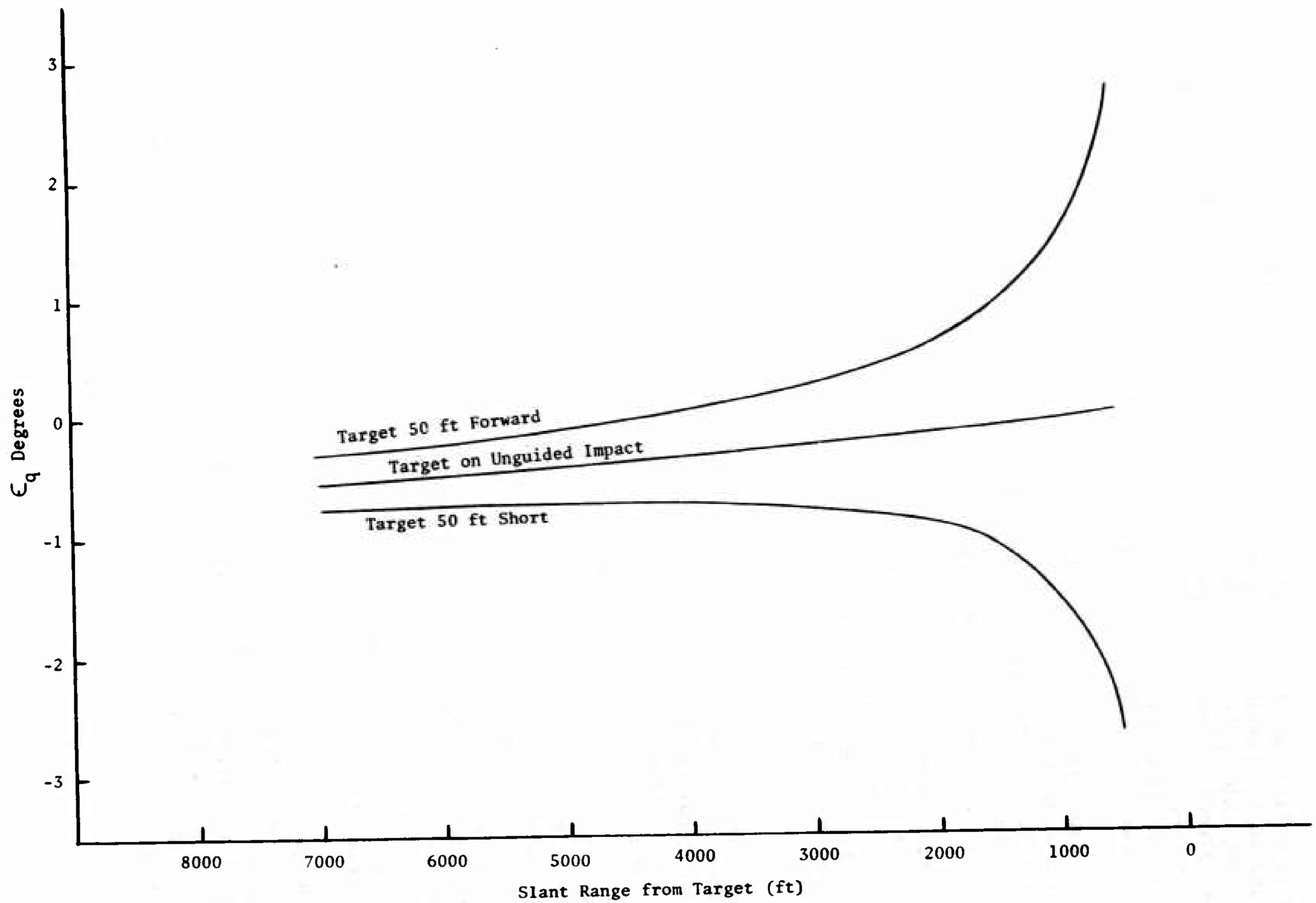

Figure 4. Angle Between Longitudinal Axis and Target

2. NOMINAL TRAJECTORY, BASELINE ROCKET

The final configurations of the unguided and guided version of the Advanced Tactical Rocket (ATR) have not been determined at this time. The approximate dimensions, mass, moments of inertia and aerodynamic coefficients will be given below. These data are based on preliminary design work and aerodynamic test at AEDC (References 1 and 2). Most of the analysis in this and later sections will deal with the baseline rocket and modifications of this configuration.

The rocket being considered is a 4-inch diameter rocket which burns for about 2 seconds giving an axial impulse of approximately 5560 lb-sec. The physical characteristics of the baseline rocket are given in Table 1, the primary aerodynamic properties in Table 2, and the performance for two dive angles in Table 3. All symbols are defined following the tables. For the 30-degree dive, 450 knot, 6000-foot aircraft launch conditions, the baseline rocket at burnout has a velocity of 3295 ft/sec. The burnout mass is 1.759 slugs, the cg is 4.697 feet from the base and the transverse moment of inertia is 4.997 slug-ft^2. At guidance initiation (2.1 seconds), the velocity is 3278 ft/sec, the altitude 3769 feet, the velocity vector has turned over from the initial 30 degrees to 31.9 degrees and the slant range to unguided impact has shortened from approximately 11,300 feet initially to 7030 feet.

TABLE 1. BASELINE CONFIGURATION PHYSICAL CHARACTERISTICS

t (sec)	M (slugs)	I_x (slug-ft^2)	I_y (slug-ft^2)	X_{cg} (ft base)	-L (ft cg)	T (lbs)
0	2.477	0.0643	8.01	3.909		2780
2.0	1.759	0.05425	4.997	4.6967		2780 terminate
2.1	GUIDANCE COMMENCE				1.6	

TABLE 2. PRIMARY AERODYNAMIC CHARACTERISTICS

Mach	C_x	$C_{n\alpha}$	C_p (ft) Base	C_{m_α}	C_{mq}	$C_{\ell\delta}$	$C_{\ell p}$
2.0	0.49	11.00	1.792	-95.84	-4108	0.075	-6.4
2.5	0.41	9.396	2.008	-75.79	-3540	0.052	-6.25
2.75	0.377	8.995	2.154	-68.61	-3427		
3.0	0.344	8.594	2.30	-61.79	-3315	0.035	-6.0
3.5	0.31	7.964	2.617	-49.69	-3156	0.015	-3.9
$f_c = 1$	See Appendix C for force and moment equations						

TABLE 3. PERFORMANCE

t (sec)	Alt (ft)	X (ft)	Slant Range (ft)	V (ft/sec)	$\dot{X}$ (ft/sec)	$\dot{Z}$ (ft/sec)	Dive Angle (degrees)	Spin Rate (rev/sec)	Remarks
30 degree Dive									
0	6000	0	11306	760	658	380	30	0	
2.0	3946	3372	7358	3282	2788	1733	31.86	13.36	Burnout
2.1	3774	3651	7031	3266	2772	1726	31.91	13.28	Guidance
4.37	0	9583	0	2855	2393	1558	33.06	14.89	Impact
37.5 degree Dive									
0	6000	0	9490	760	603.0	462.7	37.5	0	
2.0	3526	3086	5536	3288	2548	2078	39.19	13.39	Burnout
2.1	3319	3340	5208	3271	2533	2069	39.23	13.30	Guidance
3.76	0	7353	0	2969	2275	1908	40.00	14.40	Impact

LIST OF SYMBOLS

t	=	time from launch
M	=	mass of rocket
I_x	=	axial moment of inertia
I_y	=	transverse moment of inertia
X_{cg}	=	distance to cg from base
$-L$	=	forward distance to the thruster from the cg
T	=	axial thrust
C_x	=	axial drag (thrust off)
$C_{N\alpha}$	=	normal force coefficient derivative due to α
$C_{m\alpha}$	=	restoring moment coefficient derivative due to α
C_{mq}	=	damping moment coefficient derivative due to q
Alt	=	altitude
X	=	down range distance
SL	=	slant range
V	=	velocity of the rocket
$\dot{X}$	=	X component of velocity of cg
$\dot{Z}$	=	Z component of velocity of cg
$C_{\ell\delta}$	=	spin driving moment coefficient
$C_{\ell p}$	=	spin damping moment coefficient
f_c	=	fin cant parameter (1.0 for this configuration)

3. LINEAR PITCHING AND SWERVE MOTION

The linear equations of motion for a rolling missile are described in many publications including Reference 3. Appendix B gives a simplified version of the equations for angular motion for a rolling fin stabilized missile.[a] For the slow roll rates considered (10 to 20 hertz), the nutation is only about 1 percent greater than the precession frequency. The frequency for pure pitching motion will be between these two frequencies. Then for the more complicated case of motion induced by side impulse, the planar motion solution will give most of the information required to understand the motion.

For the impulse guidance being considered it is important to understand the relationship between the motion of the rocket after side impulse, and all of the parameters affecting the motion. The equations determining the angular and swerving motion for the planar motion case are derived in Appendix A (see Figure A-1). In the derivation of these equations the usual small angle and magnitude simplifications are made. Steady state conditions (velocity, spin, etc) are also assumed.

The quantities of importance are the angle of attack $\alpha_{(t2)}$, the pitch frequency (ω_1) and the side deflection or swerve (δ_s).[b] These quantities are listed in the following equations:

$$\alpha_{(t_2)} = e^{\lambda t_2} \left[\alpha_\tau \cos \omega_1 t_2 + \left(\frac{\dot{\alpha}_\tau}{\omega_1} - \frac{K_{\dot{\alpha}} \alpha_\tau}{2\omega_1} \right) \sin \omega_1 t_2 \right] \tag{A-23}$$

$$\alpha_\tau = \alpha_p \left[e^{\lambda \tau} \left(-\cos \omega_1 \tau + \frac{K_{\dot{\alpha}}}{2\omega_1} \sin \omega_1 \tau \right) + 1 \right] \tag{A-19}$$

$$\lambda = K_{\dot{\alpha}} / 2$$

---

[a]The equation in Appendix B omits magnus terms and terms which are considered small for the high static margin missile considered in Section 2.

[b]In computing the swerve for a rolling missile an average thrust is computed. Equation (A-32) Appendix A. The linear spin equation is also given in Appendix A.

$$\dot{\alpha}_\tau = \alpha_p \omega_1 \; e^{\lambda \tau} \quad \sin \omega_1 \tau \left[1 + \left(\frac{K_{\dot{\alpha}}}{2\omega_1} \right)^2 \right] \qquad \text{(A-20)}$$

$$\omega_1 = \sqrt{-K_\alpha - \left(K_{\dot{\alpha}}^2 / 4 \right)} \qquad \text{(A-15)}$$

$$\alpha_p = \frac{-\bar{F}_s L}{K_\alpha I_y} + \frac{\bar{F}_s C_{mq} d}{2MV^2 C_{m\alpha}} \qquad \text{(A-16)}^a$$

$$K_\alpha = \rho V^2 \pi d^3 C_{m\alpha} / 8I_y \qquad \text{(A-10)}$$

$$K_{\dot{\alpha}} = \rho \pi d^4 V \left(C_{mq} + C_{m\dot{\alpha}} \right) / 16I_y \qquad \text{(A-12)}$$

$$\delta_s = \frac{-fV}{d} C_{N\alpha} \alpha_p \left[e^{\lambda \tau} \quad \frac{K_{\dot{\alpha}}^2}{4K_\alpha \omega_1} \quad \sin \omega_1 \tau + 2\tau \right] + \frac{\bar{F}_s \tau}{MV} \qquad \text{(A-29)}$$

δ_s = Change in velocity vector direction in radians

$\alpha_{(t_2)}$ = Missile angle of attack at time t_2

τ = Thrust termination time

---

[a] It is of particular interest that the second term in α_p involves C_{mq} alone without $C_{m\dot{\alpha}}$. This suggests that it may be possible to extract C_{mq} separately from free flight range test to the extent that $C_{m\alpha}$ and $\bar{F}_s$ are known.

t_2 = Time after side thrust termination, $t_2 = 0$ when $t = \tau$

α_τ = The missile angle of attack at side thrust termination

$\dot{\alpha}_\tau$ = Missile angle of attack rate at side thrust termination time

M = Missile mass

V = Missile velocity (constant in above equations)

ρ = Air density (average)

s = Missile reference area

d = Missile reference diameter

Q = Dynamic pressure = $\rho V^2/2$

I_x = Missile axial moment of inertia

I_y = Missile transverse moment of inertia

$\bar{F}_s$ = Average constant side force (See Equation (A-32)

f = $\rho sd/2M$

q = Pitch rate ($\dot{\theta}$ for this geometry)

$\dot{\alpha}$ = Angle of attack rate

α_p = The particular constant in the differential equation solution for α_τ

$C_{N\alpha}$ = Normal force coefficient derivative due to α

C_{mq} = Damping moment coefficient derivative due to q ($q = \dot{\theta}$)

$C_{m\dot{\alpha}}$ = Damping moment coefficient derivative due to $\dot{\alpha}$

L = Distance from cg to application of side force (negative if forward of cg)

In order to have the angle of attack small when a correction is made, the pitch frequency must be about 1/2 the laser pulse frequency (see

Section III). For the baseline configuration Equation (A-15) gives an average pitch frequency during guidance of 10.3 hertz. The angle of attack at lase time will be some fraction of the maximum angle of attack.

Figure 5 is a plot of data from the above equations for the baseline configuration. The maximum angle of attack (α_m) is obtained from Equation (A-23) and is plotted as it varies with total impulse. It is desired to keep the angle as small as feasible. The mil change in the velocity vector, (δ_s Equation A-29), as it varies with the strip impulse is also plotted. This value should be large to obtain large side corrections (see Section IV).

The distance the rocket must move before the maximum angle of attack damps to 0.25 degree is also plotted in Figure 5. The 0.25 degree was selected since it is necessary to have the angle of attack this small to obtain sufficient accuracy (see Section III). The plot was made from Equation (A-23). For reasonable impulses (4 lb-sec and above) the distance to damp to 0.25 degree would be greater than 700 feet. This means that we cannot rely on damping to have a small angle of attack when corrections are made.

Figure 6 gives the mil correction and maximum angle of attack for the baseline configuration plotted versus the distance of the thrust center forward of the cg location. The plot shows that the maximum angle of attack is extremely small ~ (.005 degree) if the side thrust is located at the center of gravity (L = 0). The mil correction for this thrust location is 0.888 mil. This is about 59 percent of the nominal value (1.493 mils), corresponding to the center of thrust located 1.453 feet (4.479 calibers) forward of the cg. Because of the smaller angle of attack the guidance system is more accurate for the thrust center close to the cg (this is demonstrated in Section III). The angle of attack, the mil correction and simplicity of design (modular concept) must be considered in the design.

Figure 7 is a plot of the angle of attack versus time taken from Equation (A-23). Also plotted on the same curve is the angle of attack output from the six-degree-of-freedom program. The plot shows the agreement is very good for the first 1/2 cycle after guidance initiation. The small difference in peak value is due to a slightly smaller constant value of C_{mq} being used in the planar equations than the Mach dependent C_{mq} used in the 6-D program. The angles will be quite different after 2.15 seconds since the rocket will be getting thrust of various phase in the 6-D program while the rocket in the linear model is performing pure damped pitching motion from one impulse. The six-degree-of-freedom motion is driven by the thrust application at the laser pulse frequency.

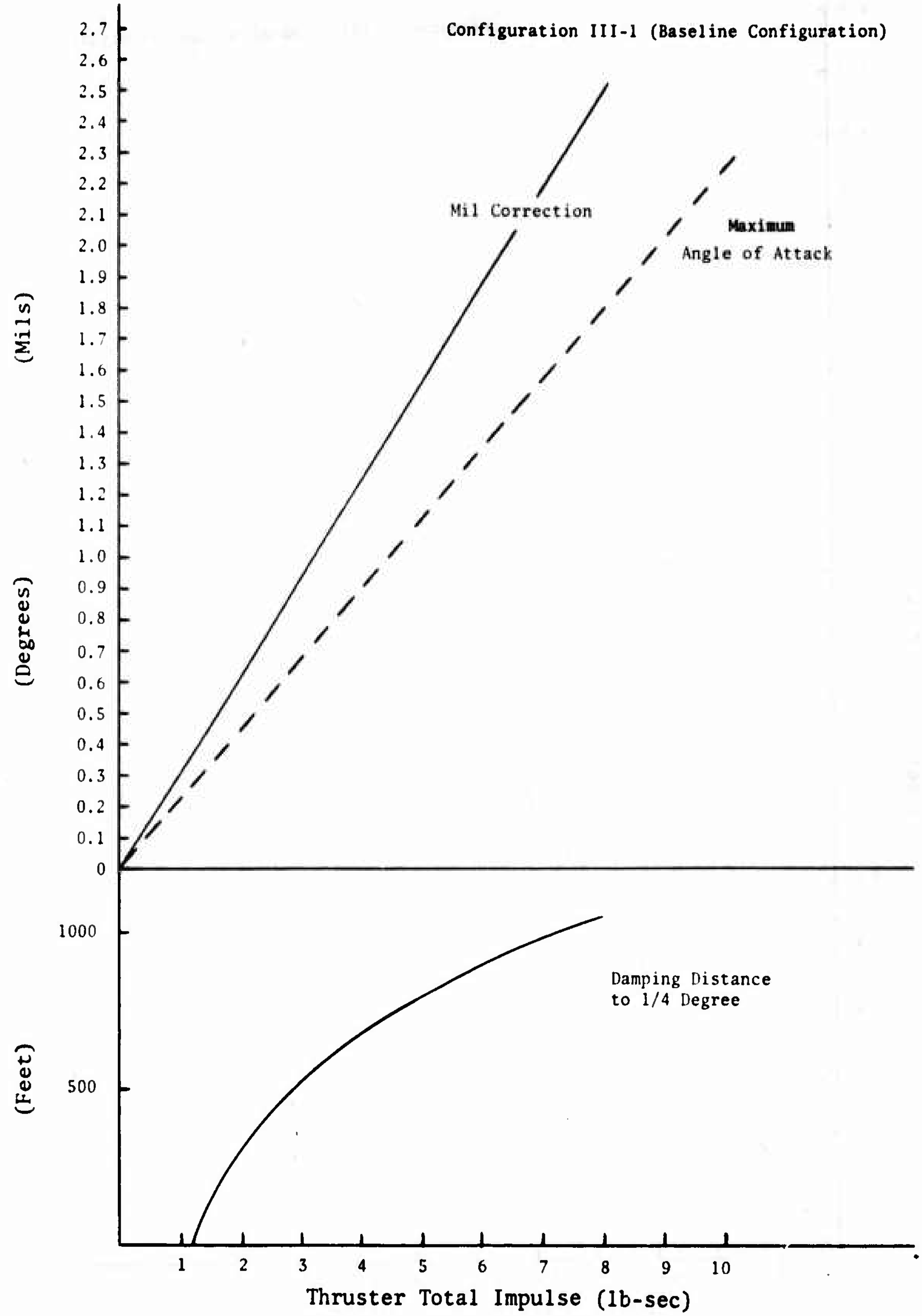

Figure 5. Mil Correction, Angle of Attack, Distance to Damp versus Total Impulse

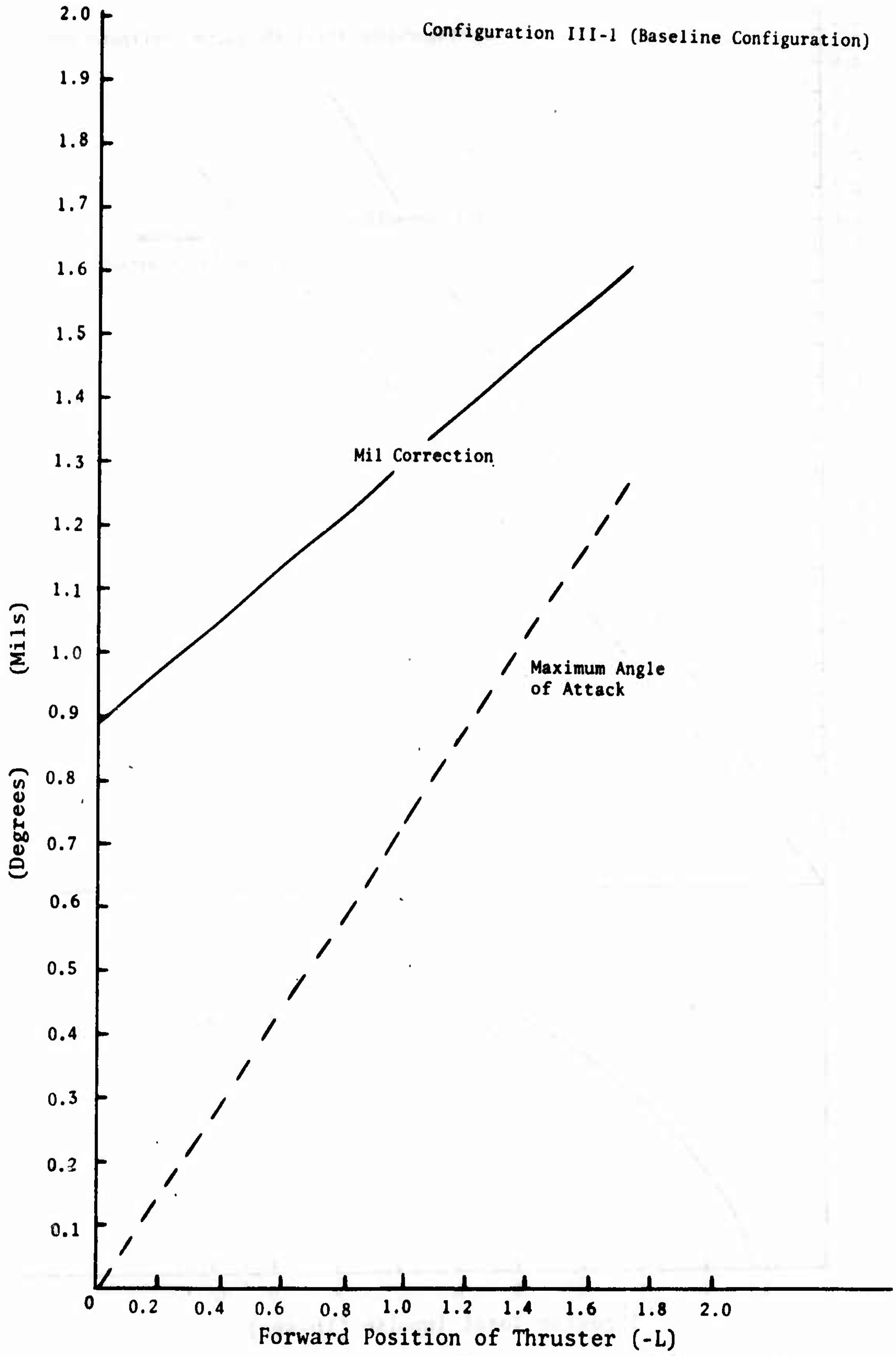

Figure 6. Correction versus Thrust Position "L"

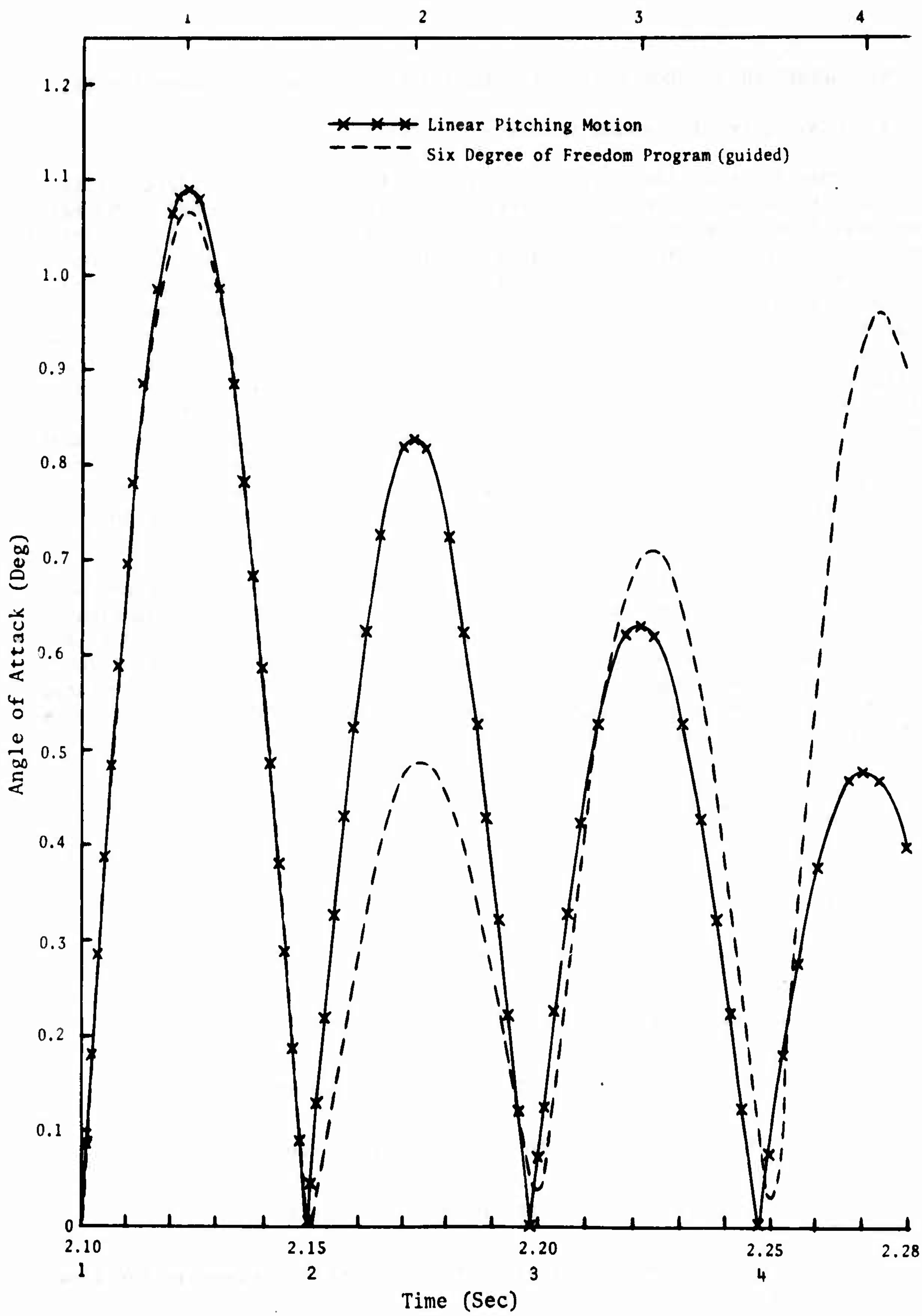

Figure 7. Angle of Attack versus Time

4. SIX-DEGREE-OF-FREEDOM GUIDANCE SIMULATION AND ACCURACY ANALYSIS MODEL

a. Six-Degree-of-Freedom Guidance Simulation

In order to study the complex guidance problem being considered it is necessary to use a six-degree-of-freedom computer guidance model. The basic model was taken from Reference 4. This computer model is set up in terms of modules which can be used independently. The modules used directly from Reference 4 were the engine module (rocket axial thrust), the steady wind and air data modules, translational and rotational rigid body dynamics modules, the transformation module (body fixed $\rightleftarrows$ inertial coordinates), and the program termination and miss distance calculation module. Integration of the state variables is performed using an Adams-Moulton (fourth-order) integration algorithm with Runga-Kutta start and fixed integration step. The equations for the explosive side thrusting forces and associated moments (which are unique to the system being considered in this report) and the aerodynamic forces and moments were written as separate modules in this study. The accuracy analysis methods and equations were also done in this study.

A general model of the forces and moments generated by the forward position explosive thrusters has been set up and programmed. The equations and logic of this fixed body model are given in Appendix C. The model is not complicated by the necessity of actuating control valves, control surfaces, or other complicating mechanisms. Upon the reception of a simulated lazer target image, error signals are generated in the fixed body reference system according to Equation (1):

$$\begin{aligned} \varepsilon_q &= \mathrm{Tan}^{-1} R_z/R_x \\ \varepsilon_r &= \mathrm{Tan}^{-1} R_y/R_x \end{aligned} \tag{1}$$

ε_q = Pitch error signal of target

ε_r = Yaw error signal of target

R_x = X position of target in body axis system

R_y = Y position of target in body axis system

R_z = Z position of target in body axis system

·ces and moments are then applied to the rocket as given in the flow ·gic and equations of Appendix C.

The program allows for a variable number of thrusters, thrust magnitude and position of each individual thruster, field of view, dead zone size, and sequencing of thrusters. The computer program has been expanded to include various thruster sequencing and other options not included in Appendix C.

In order to obtain adequate accuracy during the short burn time of the explosive (order of 10^{-4} seconds), it is necessary to go to integration times of about 1/10 the explosive action time. To reduce the computer running time and still retain accuracy it is necessary to change integration step size at the beginning and end of each explosive thruster burn.

The body axis aerodynamic forces and moments are also listed in Appendix C. The forces include the axial drag, and the normal forces (due to angle of attack). The moments include the spin driving and damping moments, the pitching and yawing moments due to angle of attack, the damping moments due to body rates and angle of attack rates, and the magnus moments. The axial drag and spin moment coefficients are input to the program as functions of the Mach number and total angle of attack ($\overline{\alpha}$). All other coefficients are input to the program as functions of Mach number and either α or β (angle of attack components, see Figure C-6)

$$\alpha = \mathrm{Tan}^{-1}\left[w/u\right]$$

$$\beta = \mathrm{Tan}^{-1}\left[v/u\right]$$

$$\overline{\alpha} = \mathrm{Tan}^{-1}\sqrt{\left[v^2 + w^2\right] / \left[u^2 + v^2 + w^2\right]}$$

u, v, w = components of missile velocity in x, y, z body axis system.

b. Accuracy Analysis Model

In evaluating the accuracy of a configuration of the system, a target position is simulated in the ground plane. This position is within a few hundred feet of the non-perturbed unguided impact point of the rocket. In order to get a statistical evaluation of the accuracy, it is necessary to simulate a number of targets. Figure 8 shows a normal distribution of impact points for the unguided version of the rocket (x_e and y_e are the inertial coordinates in ground plane). The cross marks give the impact points for a 37.5 degree dive at a 10,000-foot slant range for a normal distribution. The standard deviation in x_e and y_e are equal to 7 mils perpendicular to the trajectory (impacts in x_e and y_e are assumed independent). The pattern is stretched out in the x direction since the 7 mil error goes as the cosecant of the dive angle in the ground plane.

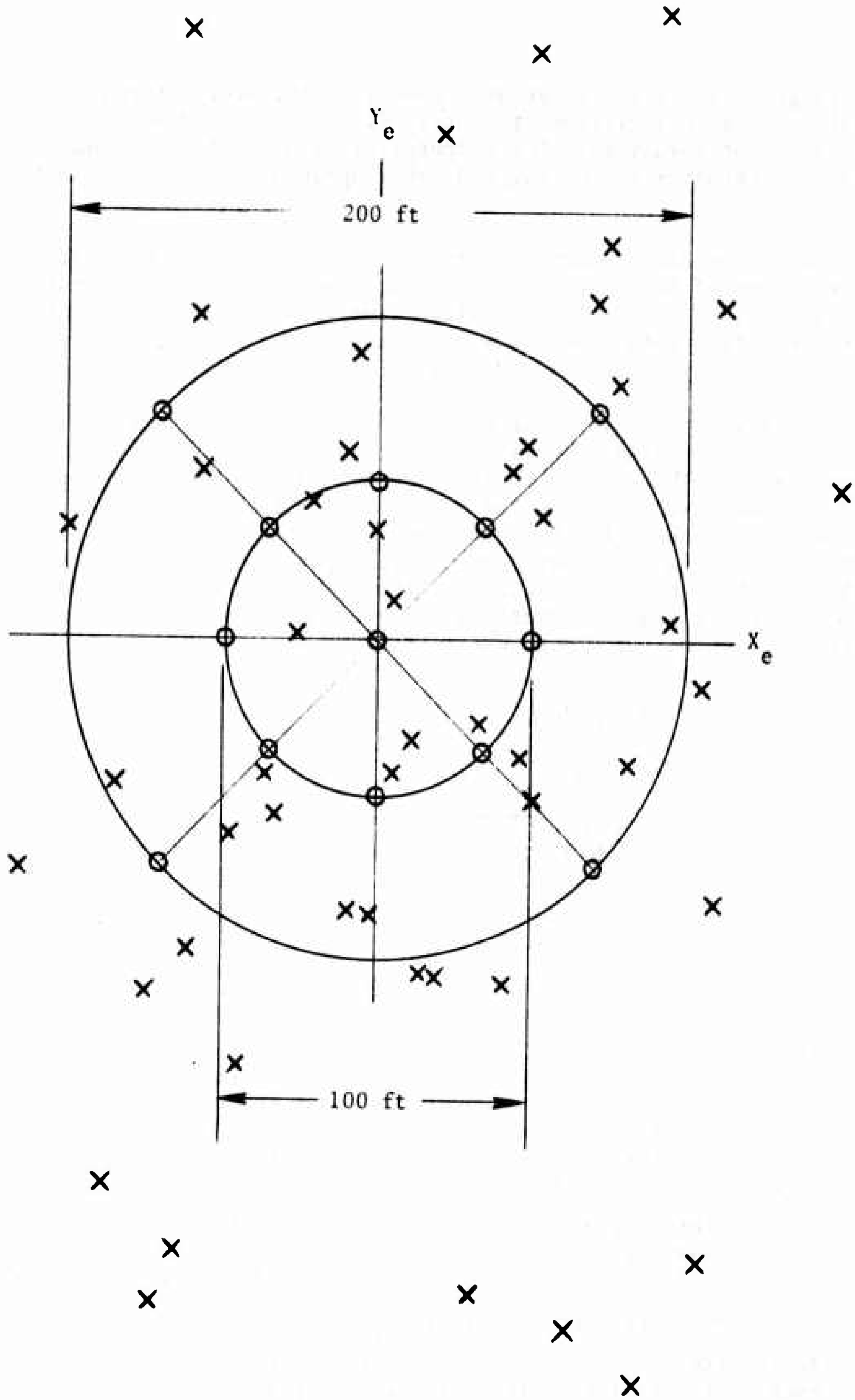

Figure 8. Target Array

The procedure employed in evaluating the accuracy is to use the unguided impact points as targets for the guided version. The guided version would impact at the center of the array if guidance were not activated. In order to reduce computer time and better analyze accuracy with regard to target position, the 13 circles (Figure 8) were used as the target array for most of the accuracy analysis done. One of the target circles is located at the center of the pattern. Eight targets are 50 feet from the center separated by 45 degrees starting with a downrange position. The last four targets are located 100 feet from the center, 90 degrees apart starting 45 degrees between x_e and y_e. It is shown in Section VII that for most cases the difference in accuracy between the symmetrical target array (circles) and the random normal array (marks) is small.

The accuracy of a configuration is stated in terms of a mean point of impact, and a circular error probable (CEP) radius. Figure 9 shows the mean point of impact (with respect to the targets) for the array of 13 targets (circles Figure 8).[a] The data is for baseline configuration, a 30-degree dive from 6000 feet. Δx_e and Δy_e are the x_e and y_e miss distances for the 13 trajectories. The standard deviations of the impact point are calculated by the following formula.[b]

$$\sigma_{\Delta x_{ep}} = \sqrt{\frac{\sum_{i}^{N}\left(\Delta X_{epi} - \overline{\Delta X}_{ep}\right)^2}{N - 1}}$$

$$\sigma_{\Delta y_e} = \sqrt{\frac{\sum_{i}^{N}\left(\Delta Y_{ei} - \overline{\Delta Y}_{e}\right)^2}{N - 1}}$$

where

ΔX_{epi} , ΔY_{ei} = the difference between component impact and target position for target i

$\overline{\Delta X}_{ep}$, $\overline{\Delta Y}_e$ = the mean value of ΔX_{epi} and ΔY_{ei}

$\sigma_{\Delta x_{ep}}$ and $\sigma_{\Delta y_e}$ are converted to a CEP according to Reference 5. (See Figure C-5). The computer program prints out the mean point of impact, the standard deviation of the impacts, the CEP, and other data of interest for the total number of targets in the target array. The same data can be obtained for any combination of the targets in the array.

---

[a]The ΔX_{epi} listed means the miss distance perpendicular to the trajectory.

[b]For small N, N-1 is replaced by N.

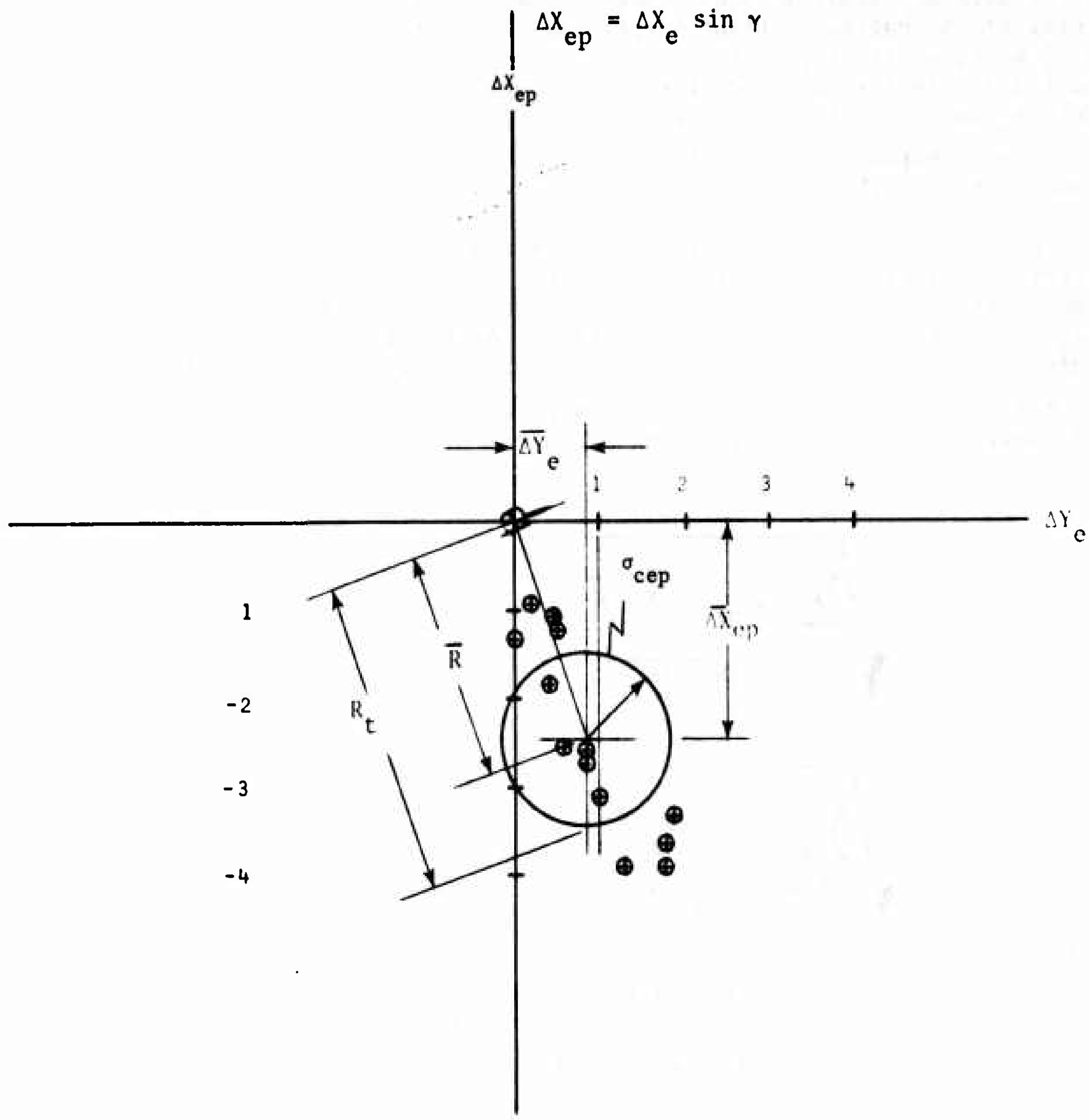

(All Dimensions in Feet)

Figure 9. Target Miss Statistics

Table 4 is the computer printout for the target array given in Figure 8. For this particular case the target array was broken down into five groups (information on miss distance for long as compared to short targets can be obtained in this manner). The fourth column is for all 13 targets. The first row is the missile average angle of attack when a target image is received (at lase time).[a] The standard deviation of the various means are listed in the row following the statistic.

The perpendicular miss, $\Delta\bar{X}_{ep}$ mean, is the miss distance perpendicular to the trajectory and is obtained by multiplying the average miss in the horizontal plane by the sin of the dive angle. The y mean is $\Delta\bar{Y}e$. The radial miss distance is the distance to the mean point of impact as listed in Figure 9. The data in Table 4 is for a launch of 30 degrees from 6000 feet altitude.

The statistics of this section are not meant to portray rigorous statistical definitions. The methodology is set up to evaluate error sources and get an approximate value for the system miss distances.

[a]All angles are in degrees and distances in feet.

TABLE 4. GUIDANCE SUMMARY STATISTICS

	Target Sub Arrays				
	1-5	1-9	6-9	10-13	All 1-13
Mean Lase Time Angle of Attack $\bar{\alpha}_\ell$ (deg) Standard Deviation (deg)	0.077 0.013	0.079 0.018	0.081 0.008	0.079 0.004	0.079 0.010
Mean Perpendicular Miss Distance (Down Range) $\Delta \bar{X}_{ep}$ (ft) Standard Deviation (ft)	-2.78 0.61	-2.89 0.95	-3.03 1.24	-1.55 0.56	-2.48 1.05
Mean Miss Distance (Cross Range) $\bar{Y}$ (ft) Standard Deviation (ft)	0.93 0.45	1.08 0.58	1.28 0.66	0.36 0.19	0.86 0.59
Mean Radial Miss Distance $\bar{R}$ (ft)	2.93	3.09	3.29	1.59	2.63
Circular Error Probability σ_{cep} (ft)	0.62	0.89	1.10	0.44	0.96
Total Miss $R_t = \bar{R} + \sigma_{cep}$ (ft)	3.55	3.98	4.39	2.03	3.59
Mean Dead Zone Occurrences	21.4	20.3	19.0	17.0	19.3
Mean Overexpenditures of Thrusters	0	0.11	0.25	0	0.08

SECTION III

RELATION BETWEEN THE LASER PULSE FREQUENCY AND PITCH FREQUENCY

As mentioned previously in this report, the angle of attack of the missile must be relatively small when a correction is made since the angle of attack is interpreted as an error in the velocity vector direction. It was also shown in Section II that there was not sufficient damping between laser pulses to reduce the angle of attack to acceptable values. The method used to overcome this problem is to have the missile pitch frequency, (essentially the same as nutation and precession frequencies for slow roll see Section II), slightly larger than 1/2 the laser pulse frequency (LPF). Under these conditions the angle of attack tends to be small when a correction is made, and the angle of attack error (due to pitch frequency being above 1/2 the LPF) is opposite the correction side of the previous correction. The latter tends to cause out of phase corrections and prevents resonant angle of attack buildup.

The above can be qualitatively understood from Figure 10.[a] A correction is made toward the target where the initial velocity vector is V_1. The angle of attack moves to α_{1m} and swings back through the zero angle of attack position, (since the pitch frequency is a little over 1/2 the LPF). The second correction is made when the angle of attack is $\alpha_{2\ell}$ and the correction $\overline{F}_2$ is generally in the opposite direction of the angular velocity. This tends to cause the random error corrections to be out of phase with the angular velocity and prevents a resonant buildup of angle of attack. If the pitch frequency were less than 1/2 LPF a resonant buildup of the angle of attack would occur, and the accuracy would be greatly reduced. This is clearly demonstrated from the 6-D output given below.

Figure 13 is a plot of the average angle of attack at lase (correction) time for 15 variations of the natural pitch frequency of baseline configuration. The different pitch frequencies were obtained by varying the cg location of this configuration (see Table 5). Each of the 12 points in Figure 13 represents the results of running trajectories for the target array given in

[a]Figure 10 shows planar motion; however, for the high impulse system being considered the six-degree-of-freedom motion is nearly planar. 6-D plots of the angular motion (α vs β) are shown in Figures 11 and 12 (same trajectory). Figure 11 is in the body fixed coordinate system and Figure 12 is in the fixed plane. Figure 12 shows that for the slow roll, and out of phase fast impulse being considered, the motion is nearly planar in the plane of the impulse.

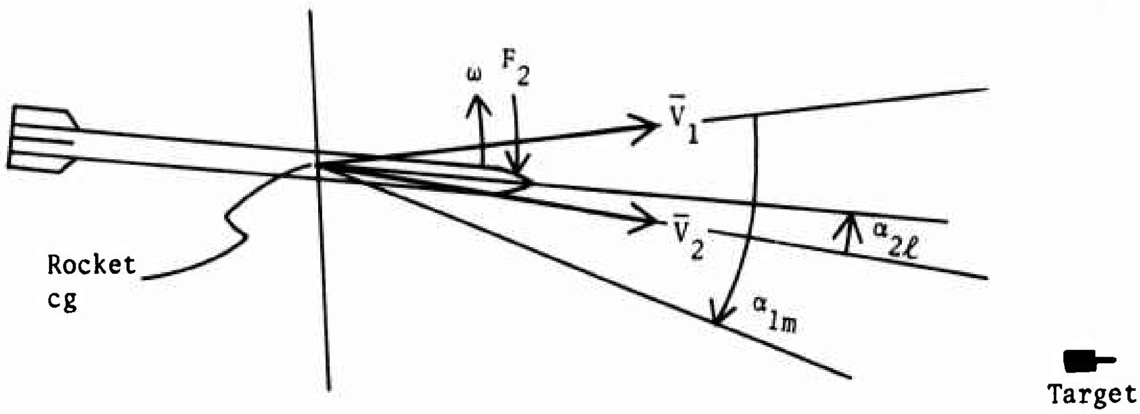

Figure 10. Idealized Thruster Correction

ω	=	angular velocity
α_{1m}	=	maximum angle of attack on first swing
$\bar{V}_1$	=	velocity prior to first correction
$\bar{V}_2$	=	velocity after first correction
$\alpha_{2\ell}$	=	Angle of attack when second correction is made at second laser pulse
$\bar{F}_2$	=	second thrust force

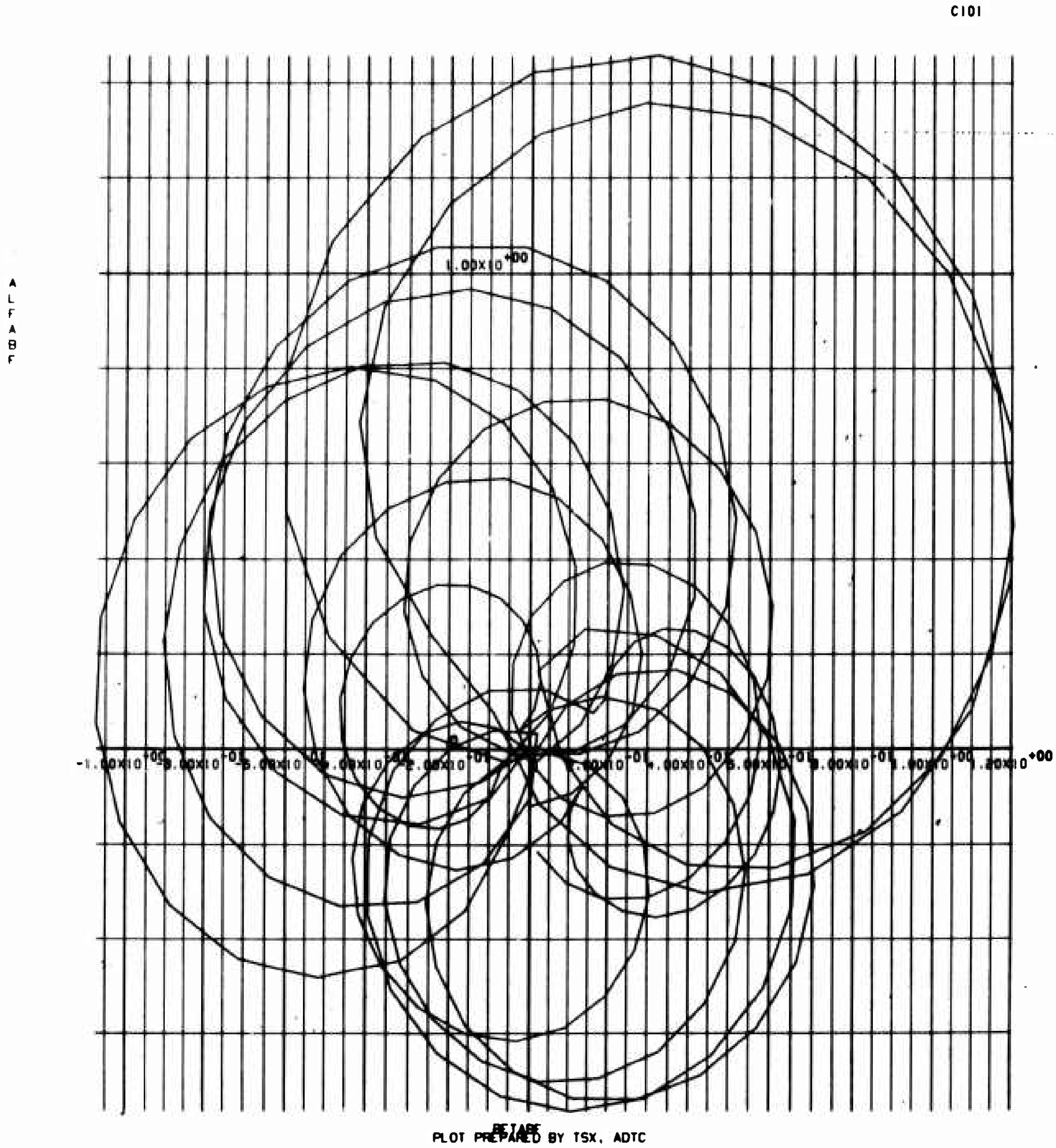

Figure 11. Alpha Versus Beta Body Fixed Coordinates

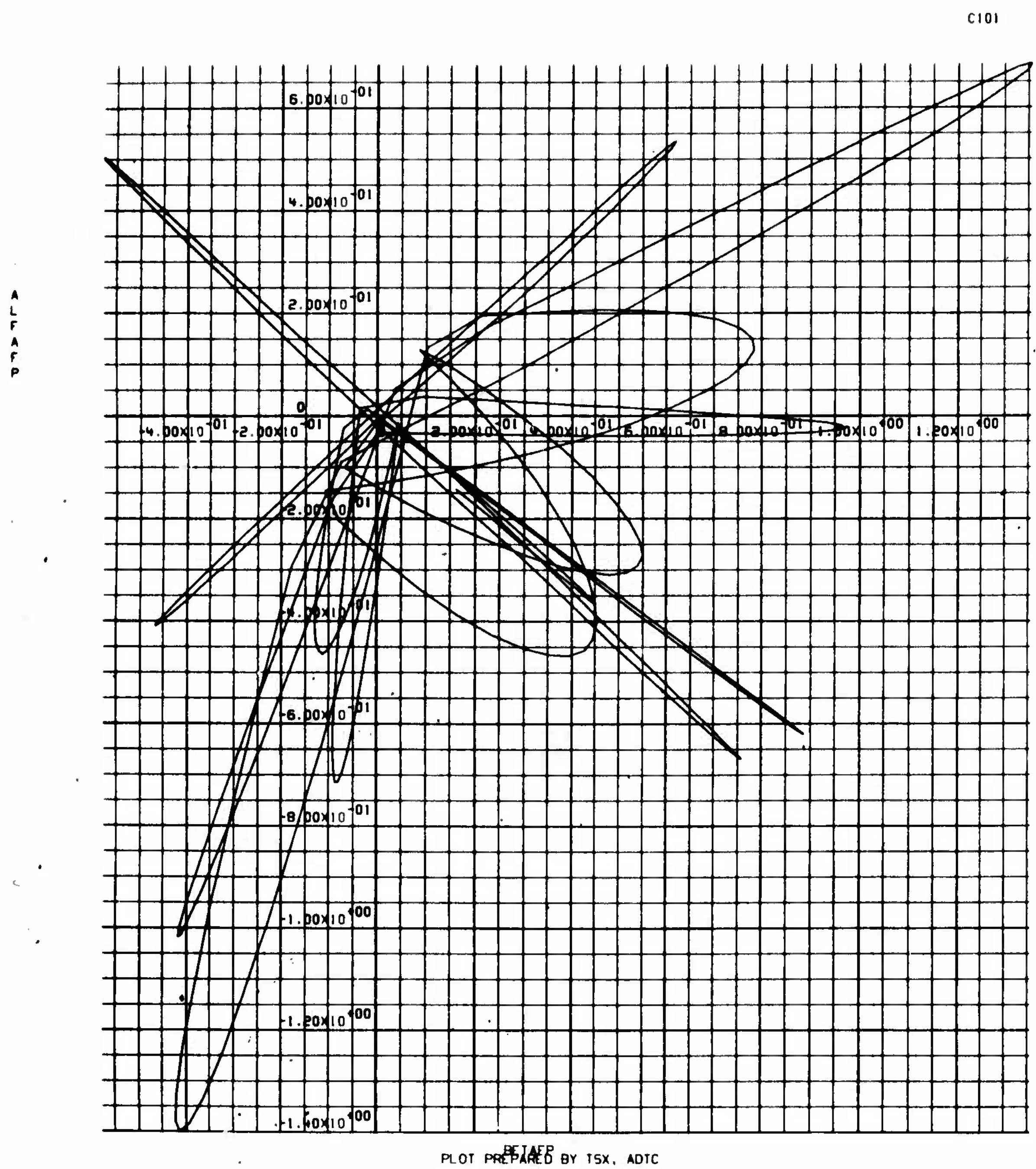

Figure 12. Alpha Versus Beta Fixed Plane Coordinates

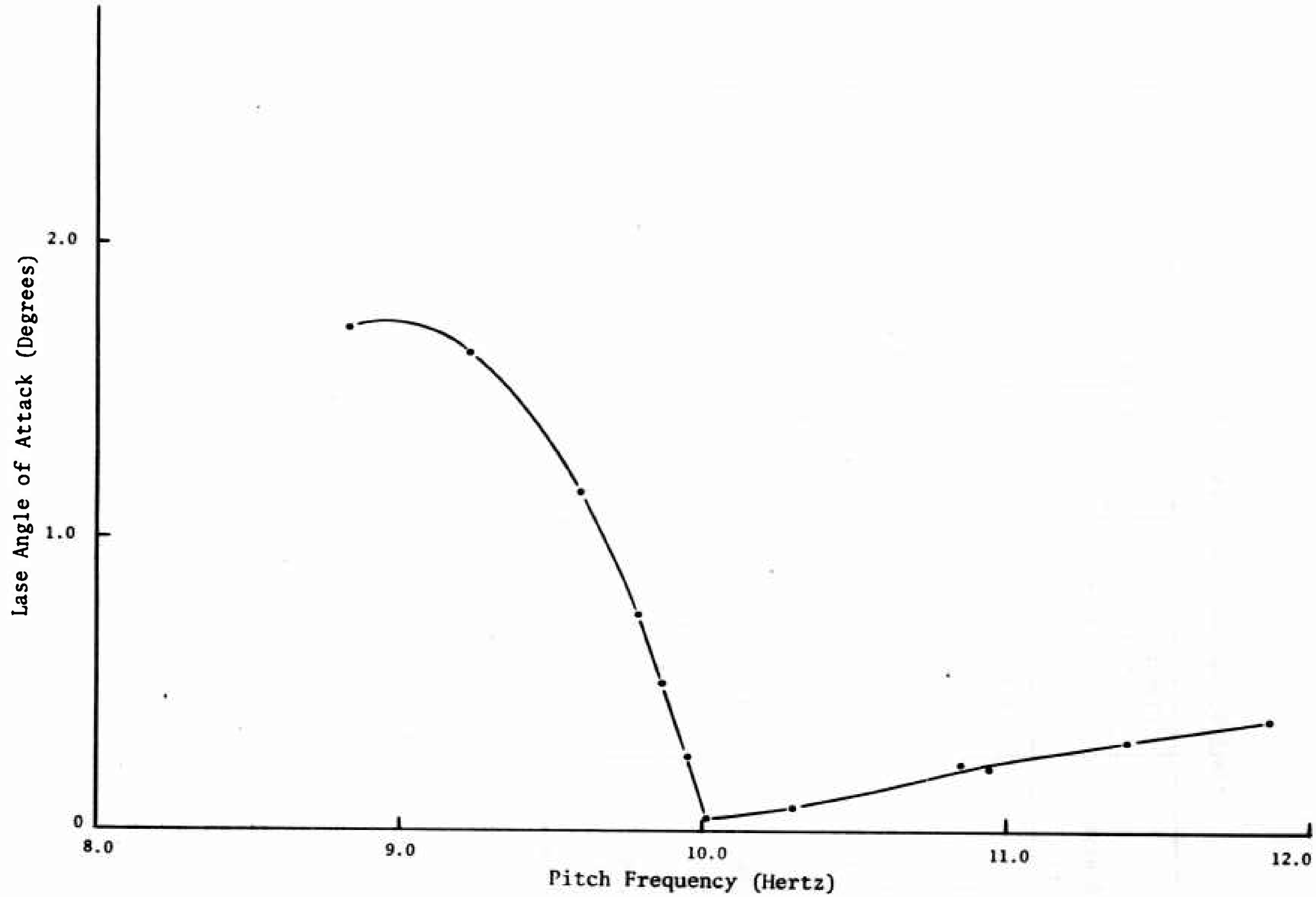

Figure 13. Average Angle of Attack at Lase Time versus Pitch Frequency

TABLE 5. ACCURACY DATA VERSUS PITCH FREQUENCY

CG Base (ft)	Planar Linear Theory Data		Six-Degrees-of-Freedom Output		
	ω_1 (hertz)	α_m (deg)	$\bar{\alpha}_\ell$ (deg)	$\bar{R}$ (ft)	σ CEP (ft)
4.0305	8.83	1.24	1.71	12.0	19.8
4.196	9.23		1.63	19.9	16.5
4.362	9.60	1.16	1.16	20.8	17.1
4.445	9.78		0.74	18.7	10.0
4.487	9.86		0.50	15.5	8.0
4.5287	9.95	1.12	0.24	7.3	3.0
4.57	10.04		0.042	2.3	0.5
4.6967	10.3		0.079	2.63	0.96
4.976	10.85	1.04	0.22	6.8	2.5
5.0287	10.95		0.21	5.7	1.8
5.2787	11.42		0.30	8.1	2.7
5.5287	11.87		0.37	10.4	4.4

Figure 8 (13 targets). The plot shows that above the natural pitch frequency the average angle of attack at lase is related to the angle attained from a natural swing from the last impulse.

$$\alpha_{\ell 2} \simeq \alpha_m \sin \omega\tau_\ell = \alpha_m \sin \frac{2\pi f_1}{f_\ell} \tag{2}$$

This equation gives a fairly close approximation of the curve (Figure 13) above a frequency of 10 hertz. Below a frequency of 10 hertz the angle of attack builds up drastically. This is due to the bias angle of attack error being in the direction to generally cause subsequent impulses to be in phase with the angular velocity. This creates a large buildup in angle of attack. This is also shown in Figure 14 where the upper curve is for the frequency of 10.3 hertz (above resonance) and the lower curve is for a frequency of 9.78 hertz in the resonant region. It is obvious that for the 9.78 pitch frequency the angle of attack is building up and is up to about 2.0 degrees at 2.86 seconds (the plot covers only about 1/3 the guided flight). The plot shows the average angle of attack at lase time is also building up. From Table 5 it is seen that the average angle of attack at lase for the 9.78 pitch frequency is 0.74 degree compared to 0.079 for the 10.3 pitch frequency.

The effect of the angle of attack and resonant condition on guided accuracy are shown in Table 5 and Figure 15. Table 5 lists the frequencies (ω_1) and maximum angle of attack (α_m) from the planar equations (Section II), and some of the statistics from the 6-D output summary statistics (mean angle of attack at lase ($\bar{\alpha}_\ell$), mean point of impact ($\bar{R}$), and σ_{cep}). The distance from target to mean point of impact and CEP values are plotted versus the pitch frequency in Figure 15. The angle of attack is again plotted to illustrate the relationship between resonance angle of attack and guided accuracy of this system.

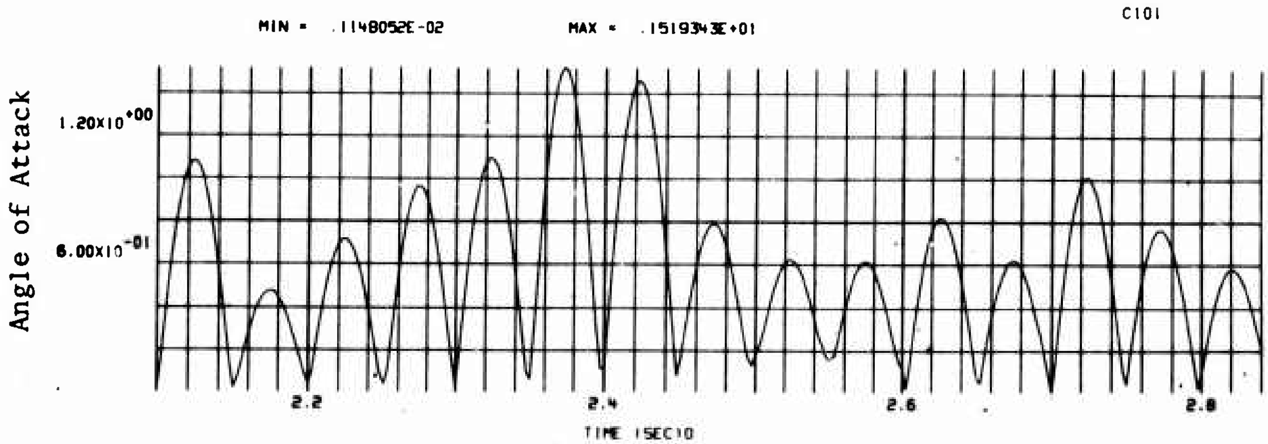

Pitch Frequency ~ 10.3. Slightly Above 1/2 LPF

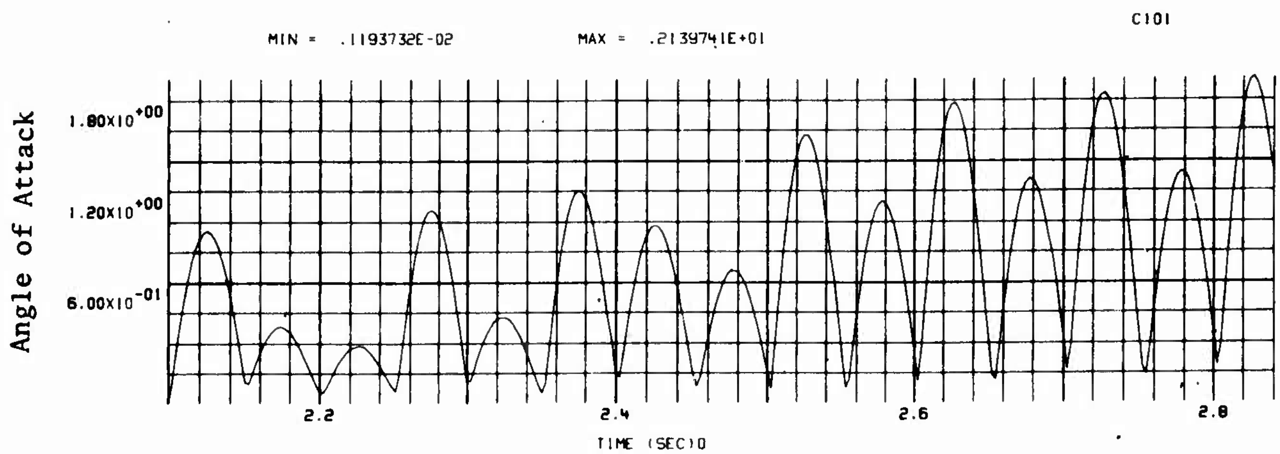

Pitch Frequency ~ 9.78. Slightly Below 1/2 LPF

Figure 14. Angle of Attack Versus Time, Two Pitch Frequencies

PLOT PREPARED BY TSX, ADTC

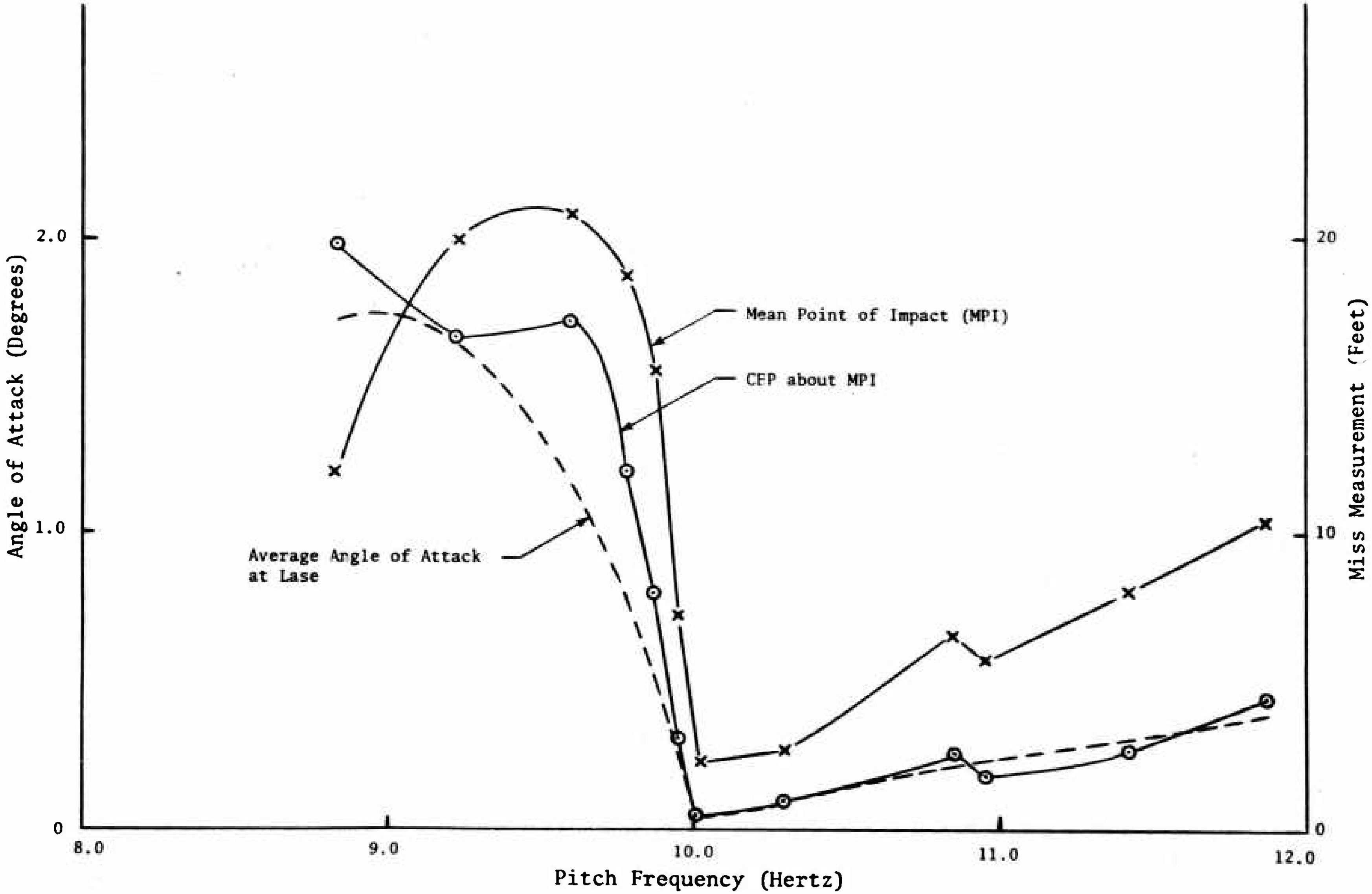

Figure 15. Average Lase Angle of Attack, Mean Point of Impact, and CEP versus Pitch Frequency

SECTION IV

APPROXIMATE MAXIMUM EXPECTED CORRECTION

1. CORRECTION ASSUMING IMPULSE EXACTLY TOWARD TARGET

In the system being considered, the correction toward the target is a result of the thrust impulses from the explosive strips in the guidance head. The explosive strips are limited in number and total impulse and the maximum expected correction toward the target will be limited.

The angular change in the direction of the velocity vector on each thrust will result from the rigid body impulse and the lift on the missile due to the impulse induced angle of attack. The correction will be a function of the magnitude of the impulse, the distance from the rocket cg to the center of the impulse, and the physical and aerodynamic properites of the rocket. The equation for the velocity vector angular correction is derived in Section II and Appendix A (Equation A-29). All the parameters involved in obtaining the angular correction (δ_S) are given in the equation. This equation was derived using a planar linear theory model, however, the results obtained from using the equation compare favorably with the data from the six-degree-of-freedom program.

Equation A-29 gives the angular correction to the velocity vector, but it is desired to get the distance correction on the ground. In order to get the distance correction on the ground it is necessary to consider the distance from the impact when the correction is made. Figure 16 is a pictorial view of the missile being corrected at each laser impulse as it approaches the target. The approximate distance to impact at the i'th lase is

$$R_i \sim \left(R_o - iT_\ell \overline{V}\right) \tag{3}$$

where

R_i = Approximate distance to impact at the i'th lase

i = i'th lase. $i = 0, 1, 2, \ldots N$

R_o = Distance to impact at guidance initiation

$\overline{V}$ = Average rocket velocity to impact determined from time of flight and R_o

T_ℓ = Period between laser pulses

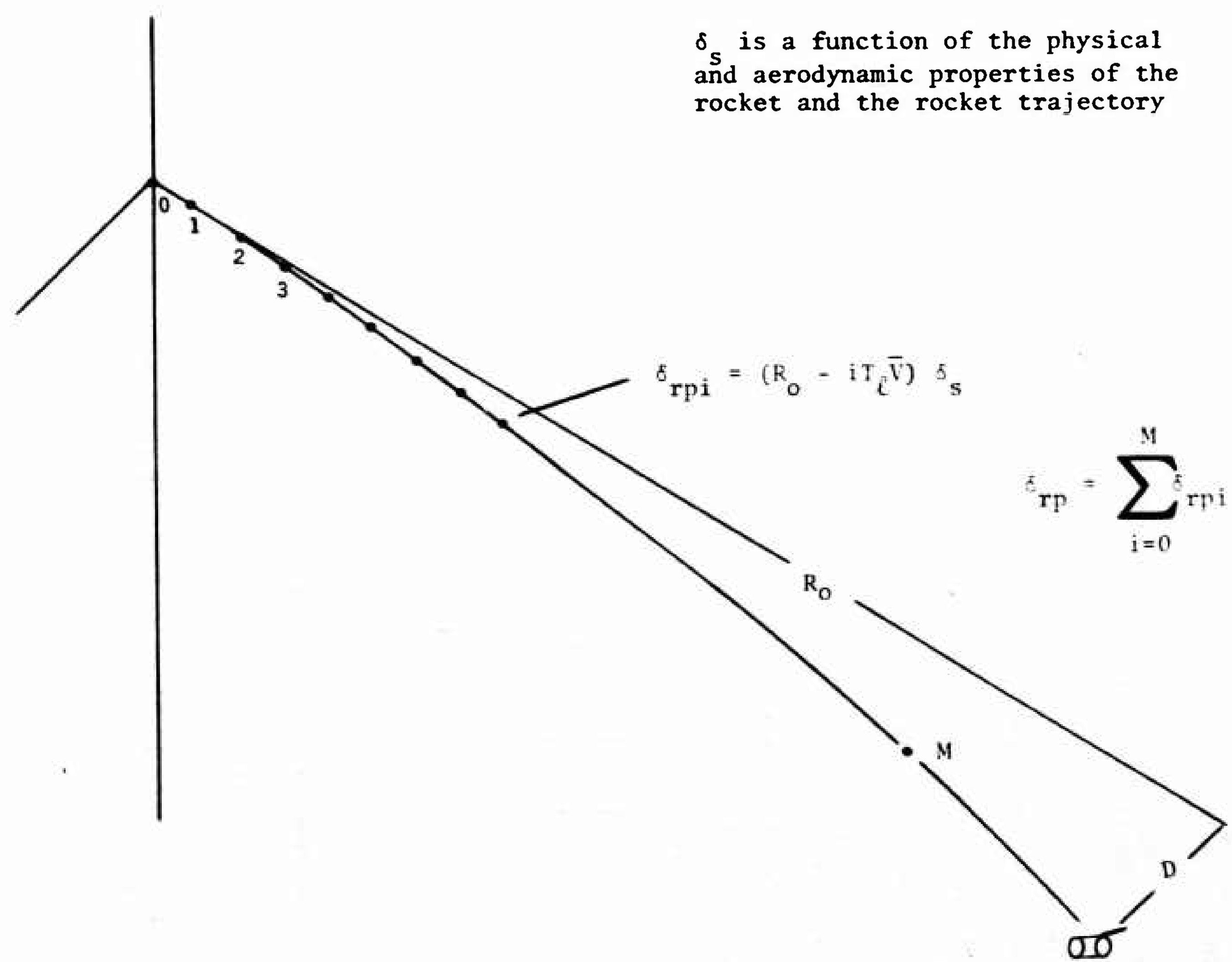

Figure 16. Magnitude of Correction

The ground perpendicular correction due to the i'th lase is

$$\delta_{rpi} = \delta_s R_i \tag{4}$$

δ_s = Angular correction to velocity vector in radians (See Equation A-29).

The total correction is the sum of these individual corrections through the last correction before impact.

In computing the total maximum correction it will be assumed that the guidance head has a central dead zone, and that the target is removed enough from the unguided impact point so that the target image does not fall in the dead zone. Under these conditions the total number of impulses will be the number of thrusters (N) when the target is at sufficient range so that the guided flight time (T_f) is greater than $(N-1)T_\ell$. The maximum value of i (See Figure 3) for this case is (N-1). For shorter ranges, $T_f < (N-1)T_\ell$, the maximum value of i is the integer part of (T_f/T_ℓ). The maximum value of i is given in the following equations:

$$M = \text{Integer Part of} \left(\frac{T_f}{T_\ell} \right), \quad \text{for } \frac{T_f}{T_\ell} \leq (N-1) \tag{5}$$

$$M = (N-1), \quad \text{for } \frac{T_f}{T_\ell} > (N-1)$$

where:

M = Maximum value of i (See Figure 3)

T_f = Guided flight time.

The average velocity is given in terms of the time of flight by the following equation:

$$\bar{V} = R_o/T_f \tag{6}$$

The total correction is now obtained by summing Equation (4) from zero to M where M is given by Equation (5) and V by Equation (6).[a]

$$\delta_{rp} = \sum_{i=0}^{M} \delta_s R_i = (M + 1) R_o \left\{ 1 - \frac{T_\ell}{T_f} \frac{M}{2} \right\} \delta_s \tag{7}$$

2. EFFECT OF FOUR QUADRANT DETECTOR

Since the target is detected to within 90 degrees, the correction toward the target will in general be in error. This is demonstrated in Figure 17 where a hypothetical case for one quadrant is shown. The correction for the target image shown is applied at the angle ε_f rather than the correct angle ε_{tg}. Where ε_f is the quadrant angle defining the direction of the applied thrust and ε_{tg} is the angle defining the direction to the target.

For better values for correction to target, the error angle $(\varepsilon_{tg} - \varepsilon_f)$, of the applied thrust direction should be taken into account. The thrust will then have the following component in the direction toward the target.

$$\bar{F}_{tg} = \bar{F} \cos (\varepsilon_{tg} - \varepsilon_f) \tag{8}$$

$\bar{F}_{tg}$ = Component of thrust toward the target

$\varepsilon_{tg} - \varepsilon_f$ = The error angle of the applied thrust

The thrust will also have a component perpendicular to the target direction.

$$\bar{F}_p = \bar{F} \sin (\varepsilon_{tg} - \varepsilon_f) \tag{9}$$

$\bar{F}_p$ = Component of the thrust perpendicular to the target direction

It will be assumed that the perpendicular component of the thrust will average to zero since the thrust is just as likely to be on one side of the target as the other. It is necessary to find the expected value of the error angle in order to compute the expected component of the thrust toward the target.

---

[a]In the derivation of this equation the fact that $\sum_{i=0}^{M} i = M(M + 1)/2$ was used.

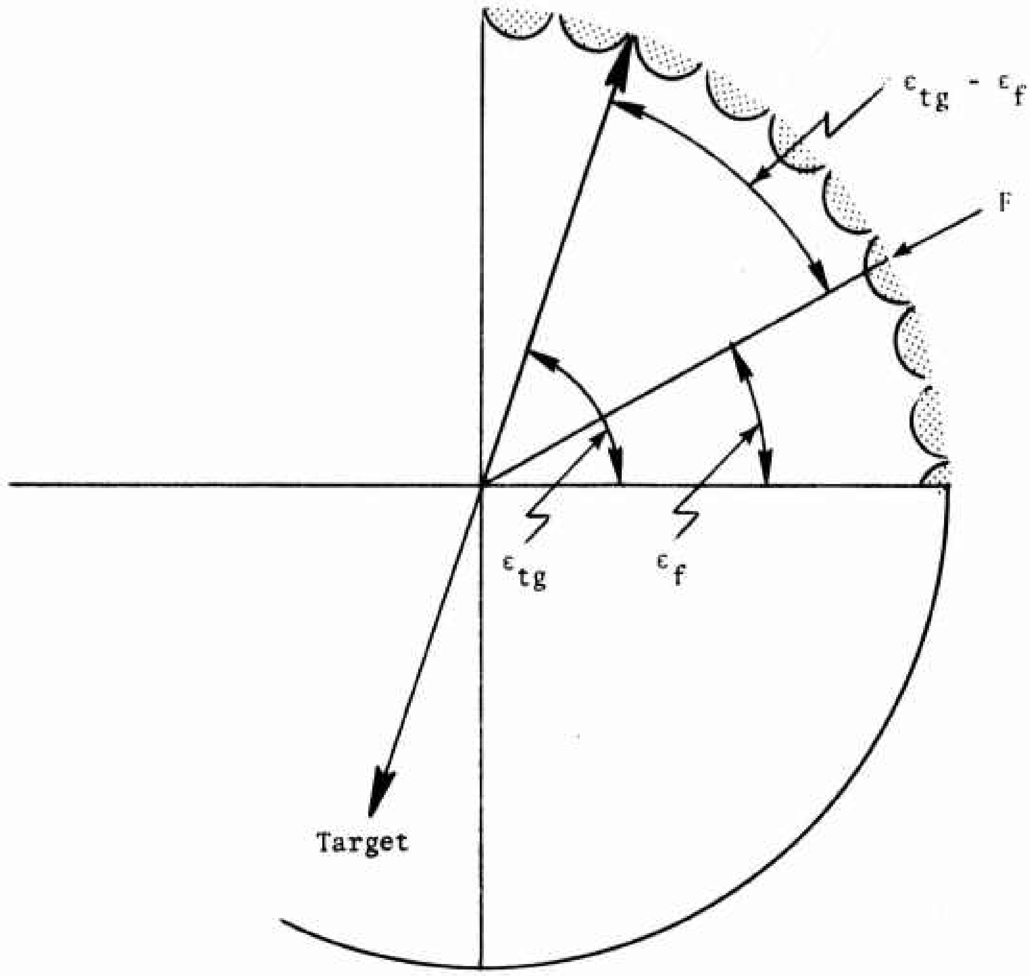

Figure 17. Thruster Correction Error

The expected value of the error angle will depend on the geometry and sequencings of the thrusters and the target image distribution. It is reasonable to assume that the angle position of the target image is a random variable uniformly distributed over the quadrant. In order to simplify the problem, it will be assumed that the thrusters also have a random uniform distribution over a quadrant (that is, no account will be taken of the change in the thruster distribution with thruster depletion).

The problem and solution is as follows:

FIND: $\left\langle \left| \varepsilon_{tg} - \varepsilon_f \right| \right\rangle$ = Expected value of the magnitude of the difference between the thrust and target angle.

Assume a uniform distribution of ε_{tg} and ε_f. Also assume ε_{tg} is independent of ε_f, then the probability density functions for ε_f and ε_{tg} are

$$f(\varepsilon_f) = 1/90 \quad , \quad 0 \leq \varepsilon_f \leq 90 \tag{10}$$

and,

$$f(\varepsilon_{tg}) = 1/90 \quad , \quad 0 \leq \varepsilon_{tg} \leq 90$$

where

f = Probability density function.

Assume
$$\left\langle \left| \varepsilon_{tg} - \varepsilon_f \right| \right\rangle = \sqrt{\left\langle (\varepsilon_{tg} - \varepsilon_f)^2 \right\rangle} \tag{11}$$

Since ε_{tg} is independent of ε_f, it follows that

$$\left\langle (\varepsilon_{tg} - \varepsilon_f)^2 \right\rangle = \left\langle \varepsilon_{tg}^2 \right\rangle - 2 \left\langle \varepsilon_{tg} \right\rangle \left\langle \varepsilon_f \right\rangle + \left\langle \varepsilon_f^2 \right\rangle \tag{12}$$

Using normal procedure in evaluating expected value, it follows that

$$\left\langle \varepsilon_{tg}^2 \right\rangle = \left\langle \varepsilon_f^2 \right\rangle = \int_0^{90} \frac{\varepsilon_{tg}^2}{90} \, d\varepsilon_{tg} = \frac{(90)^2}{3} \tag{13}$$

and

$$\left\langle \epsilon_{tg} \right\rangle = \left\langle \epsilon_{f} \right\rangle = \int_{0}^{90} \frac{\epsilon_{tg}}{90}\, d\epsilon_{tg} = 45 \tag{14}$$

Substituting in Equation (12) gives

$$\left\langle (\epsilon_{tg} - \epsilon_{f})^{2} \right\rangle = 37.74 \text{ degrees} \tag{15}$$

then the expected correction toward the target is

$$\left\langle \delta_{rp} \right\rangle = \delta_{rp} \cos 37.74 = \delta_{rp} \, (.792) \tag{16}$$

3. MAXIMUM EXPECTED CORRECTION FOR NOMINAL CONFIGURATIONS

The utilization of the maximum correction equations will be demonstrated in this section. All the rocket systems which have been considered give the velocity angle correction (δ_s) between 1 and 2 milliradius. Then from Equations (7) and (16) the magnitude of the perpendicular correction will be computed for a one milliradian system (δ_s = 0.001 radians). Table 6 shows the corrections for the nominal trajectories listed in Table 3.

TABLE 6. MAGNITUDE OF CORRECTION - NOMINAL TRAJECTORY

Dive Angle (degrees)	δ_s (radians)	δ_{rp} (feet)	$\left\langle \delta_{rp} \right\rangle$ (feet)
30	0.001	159	126
37.5	0.001	96	76

An example of using the maximum correction equations is given in the following analysis. The planar motion equations and the maximum correction Equation (16) were used to evaluate two guidance configurations for the 37.5-degree dive listed in Table 3. The configurations were the same except for the total impulse of the side thrusters (I_s) and the center of thrust location. The two configurations are listed in Table 7. The table shows that the velocity vector correction (δ_s) is higher on Configuration B giving an expected maximum correction of 108 feet compared to 84 feet on Configuration A.[a]

TABLE 7. MAXIMUM EXPECTED CORRECTION

			Planar Linear Equations			Expected Correction Equation
Configuration	I_s (lb sec)	L (feet)	ω_1 (hertz)	α_m (degrees)	δ_s (radians)	$\langle \delta_{rp} \rangle$ (feet)
A	4	1.174	10.86	0.66	0.00111	84
B	4.4	1.4	10.86	0.951	0.00142	108

The six-degree-of-freedom guidance model was used to evaluate the accuracy of these two configurations. The target array used was that given in Figure 8. This array has five targets within 50 feet and four targets at 100 feet. The two sets were analyzed separately and together. These results are shown in Table 8. Table 8 shows that for configuration A the CEP values get quite large (about 11 feet) for targets at 100 feet. This is readily understood since the maximum expected correction is calculated to be 84 feet. In configuration B the maximum expected correction is brought up to 108 feet by increasing the total impulse and moving the center of thrust forward. This enables the rocket to reach the 100-foot targets and the CEP comes down to a low value (about 1.3 feet). The analysis indicated that the planar equations and the simple maximum correction equations can be used in design of the impulse guided system.

---

[a]The pitch frequencies (ω_1) are the same where the maximum angle of attack (α_m) is higher on configuration B.

TABLE 8. ACCURACY ANALYSIS OF TWO CONFIGURATIONS WITH DIFFERENT EXPECTED CORRECTION

Configuration	$\langle \delta_{rp} \rangle$ (ft)	Target Set	ΔX_{ep} (ft)	ΔY_e (ft)	R (ft)	$\sigma \Delta X_{ep}$ (ft)	$\sigma \Delta Y_e$ (ft)	σcep (ft)
		50-ft targets	-2.4	0.2	2.4	0.5	0.5	0.6
A	84	100-ft targets	-1.7	1.8	2.5	7.6	11.4	11.2
		All targets	-2.2	0.7	2.3	4.4	6.7	6.5
		50-ft targets	-2.7	-0.3	2.7	1.4	0.5	1.1
B	108	100-ft targets	-2.0	0.3	2.0	0.5	1.8	1.3
		All targets	-2.5	-0.1	2.5	1.2	1.1	1.4

SECTION V

TRIM MISALIGNMENT EFFECT

A misalignment of the body components or tail fins will cause aerodynamic forces and moments on the rocket which results in the rocket trimming out at some angle of attack greater than zero. For a spinning rocket this trim misalignment causes the rockets longitudinal axis to perform a lunar type motion about the velocity vector at an angle of attack (trim angle). For the guidance system being considered this will result in error correction and premature expenditure of thrusters giving poor accuracy. This phenomenon was investigated and a method of controlling trim misalignment accuracy error was found.

The magnitude of the dynamic trim arm is primarily a function of the trim moment, the physical and aerodynamic characteristics of the missile, and the missile spin. The magnitude of the dynamic trim arm is given in Equation (B-4). This equation was derived in Appendix B, where only a trim moment is considered[a], and other simplifying assumptions were made.

$$K_t = \delta_m \bigg/ \left| -\left(\frac{p}{\dot{\phi}_{1,2}}\right)^2 \left(1 - \frac{I_x}{I_y}\right) + 1 \right| \qquad \text{(B-4)}$$

δ_m = Static trim misalignment (the trim angle at zero spin rate)

p = Spin rate

$\dot{\phi}_{1,2}$ = Precession or nutation rate for the relatively low spin rate being used

I_x , I_y = Axial and transverse moments of inertia

Figure 18 was generated from Equation (B-4) and is a plot of the trim arm versus the missile spin rate.[b] For the relatively low spin rate being used,

---

[a]No loss in generality in regard to the trim angle of attack is encountered if the trim force term is omitted.

[b]All data generated in this section are for the baseline configuration given in Section II. The spin was varied by changing the spin cant parameter, f_c.

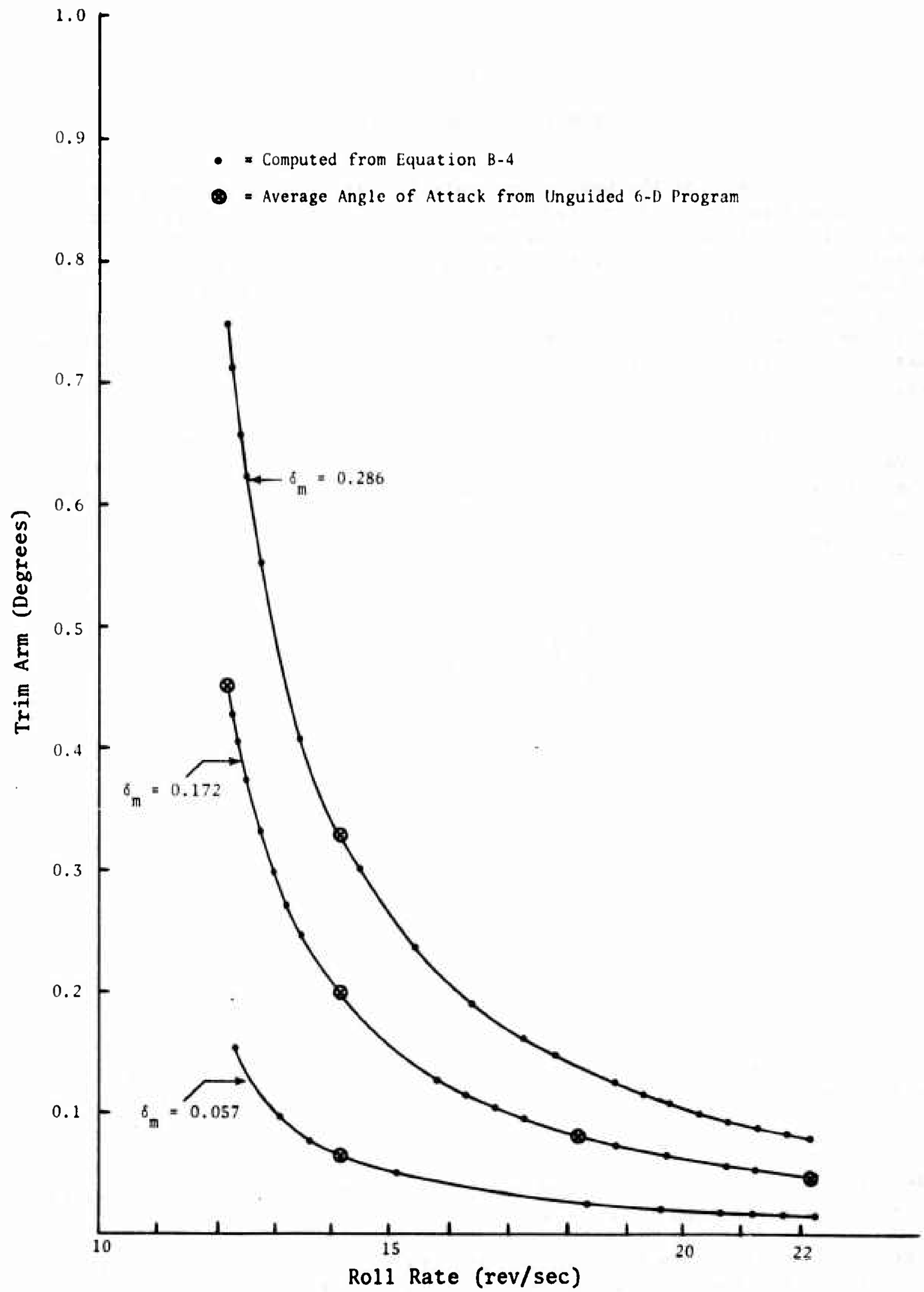

Figure 18. Magnitude of the Trim Arm versus Roll Rate

$\dot{\phi}_{1,2}$ is essentially equal to the one-dimensional pitch frequency (ω_1). The curves in Figure 18 were computed for the 30-degree trajectory given in Table 3. The average conditions during the guidance phase were used in computing the pitch frequency by Equation (A-15). This value for ω_1 (10.29 hertz) was used in Equation (B-4). The same trim moment used in generating Figure 18 was used in the 6-D program on the unguided trajectories. The average angles of attack obtained are also plotted in Figure 18 and are in excellent agreement with Equation (B-4). The curve shows the steep buildup in angle of attack as the spin frequency approaches the pitch frequency (10.29 hertz). Curves are drawn for three static trim misalignments (0.286, 0.127 and .057 degrees). A non-rolling missile trims at the static trim misalignment angle.

Guided trajectories with varying spin and trim misalignment were run using the target array given in Figure 8. Figure 19 is a plot of the average angle of attack at lase time during the guided phase for these trajectories. The curves show that the angle of attack varies in the same manner as that given by Equation (B-4) (See Figure 18).

Also related to the trim induced angle of attack is the depletion of thrusters in the trim angle of attack plane. Figure 20 shows the average number of times a thrust was attempted from a quadrant in which the thrusters had been expended. These curves are drawn from the same guided trajectories mentioned above. The curves follow the same trend as the angle of attack curves going to small values at higher roll rates. It would be expected that the configurations having high average angles of attack, and related over expended quadrant thrusters, would have high miss distances.

Figure 21 shows the total miss distance follows the same trend as the angle of attack and thruster depletion in regard to missile roll rate. Figure 21 consists of plots of the total miss distance (mean point of impact plus the CEP) plotted versus the missile roll rate. The total miss is also plotted for the missile with no trim misalignment.

Figure 22 is the same as Figure 20 with the 2.5-foot gravity sag of the nonperturbed missile[a] (missile with no trim misalignment) taken out. The total miss distance for the low spin (12.25 hertz) and high trim misalignment (0.29 degree) is 22.5 feet but the plot shows that the total miss for any trim misalignment used is less than 2 feet for spins above 19.5 hertz. This analysis indicated that miss distances due to trim misalignment can be reduced to acceptable values by increasing the roll rate to above 1.9 times the pitch frequency.

---

[a]In using this type of guidance system the laser would be aimed high to eliminate part of the normal gravity sag error.

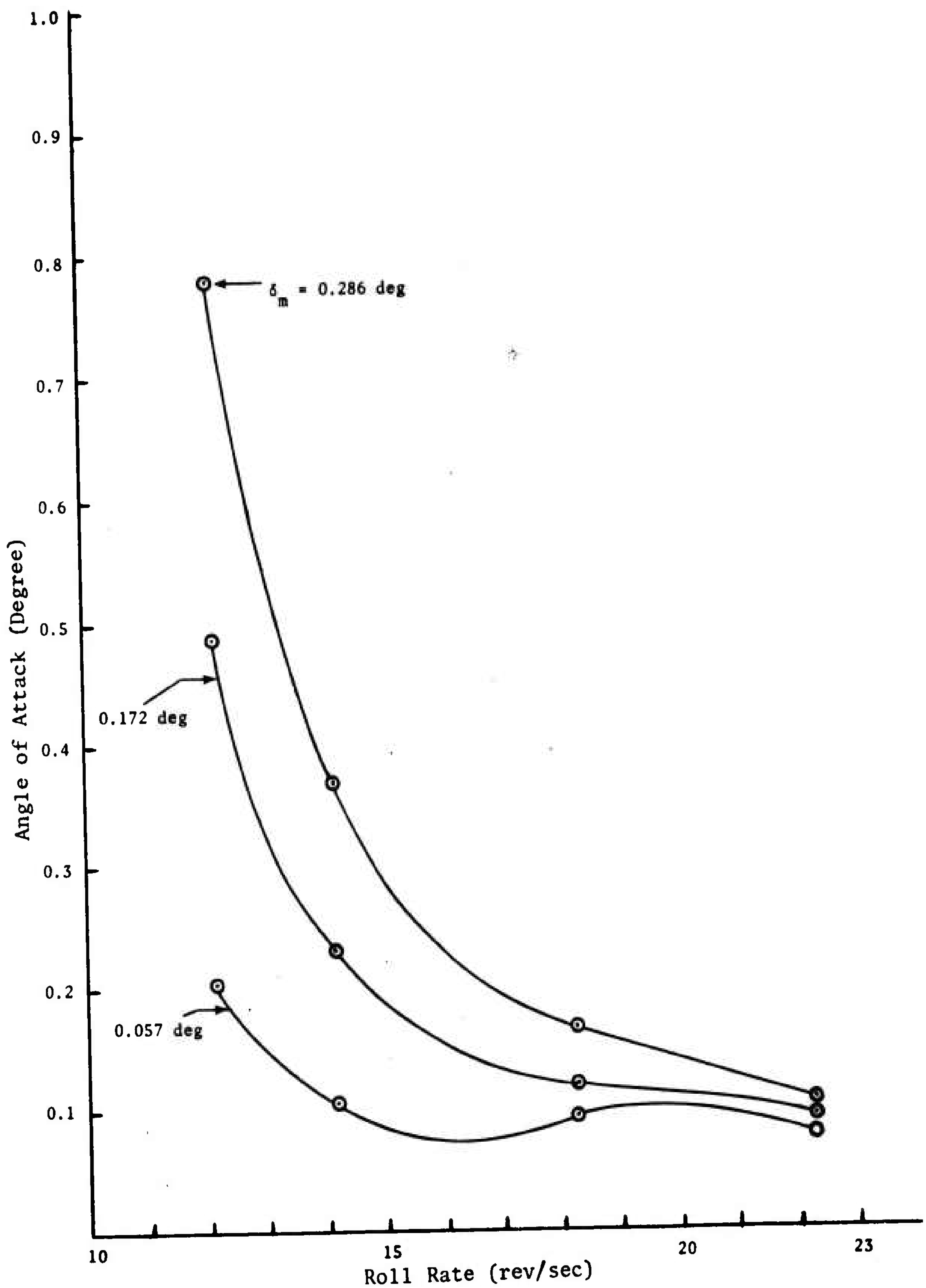

Figure 19. Average Angle of Attack at Lase - Guided Trajectories

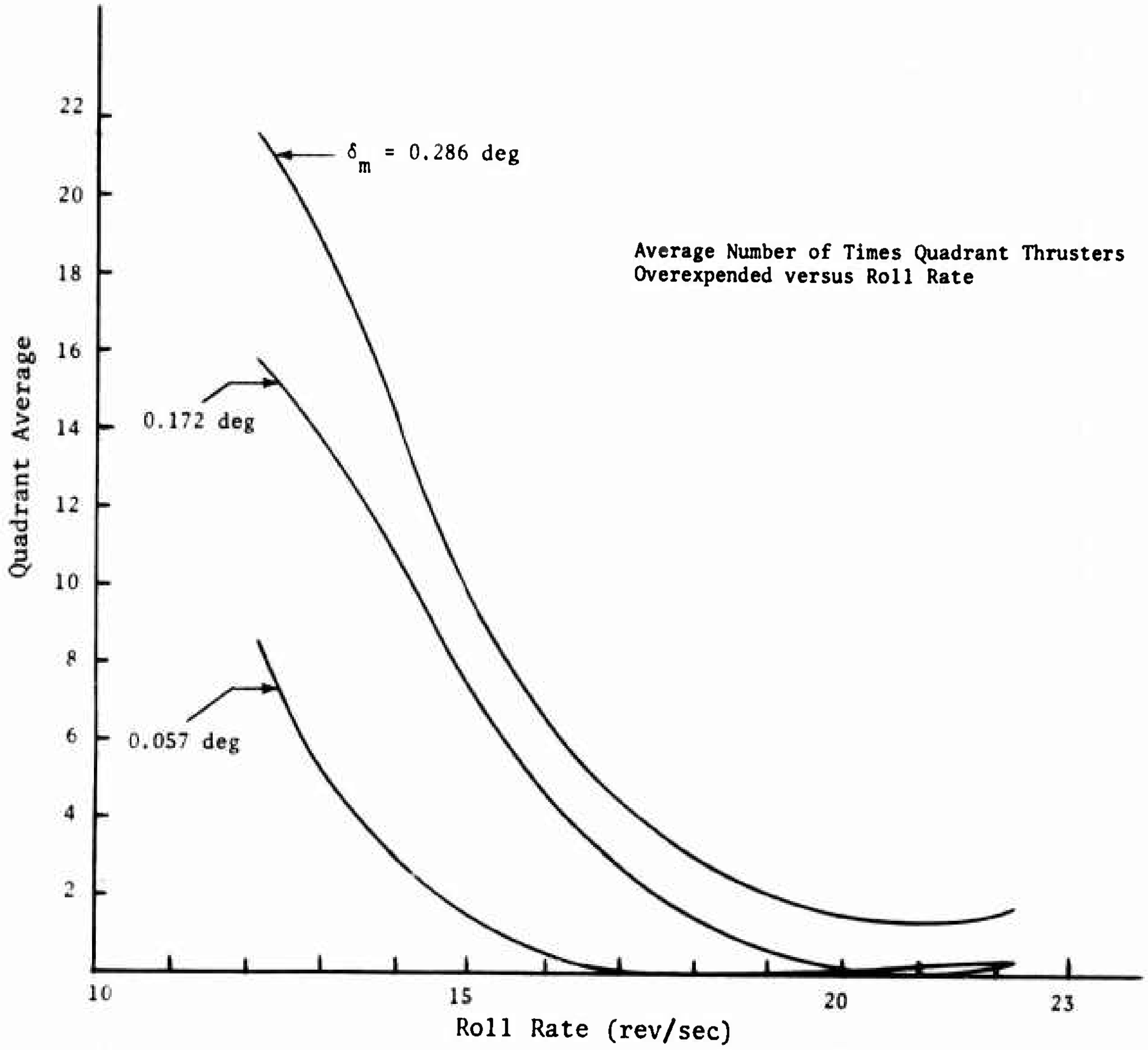

Figure 20. Average Number of Expended Thrusters versus Roll Rate

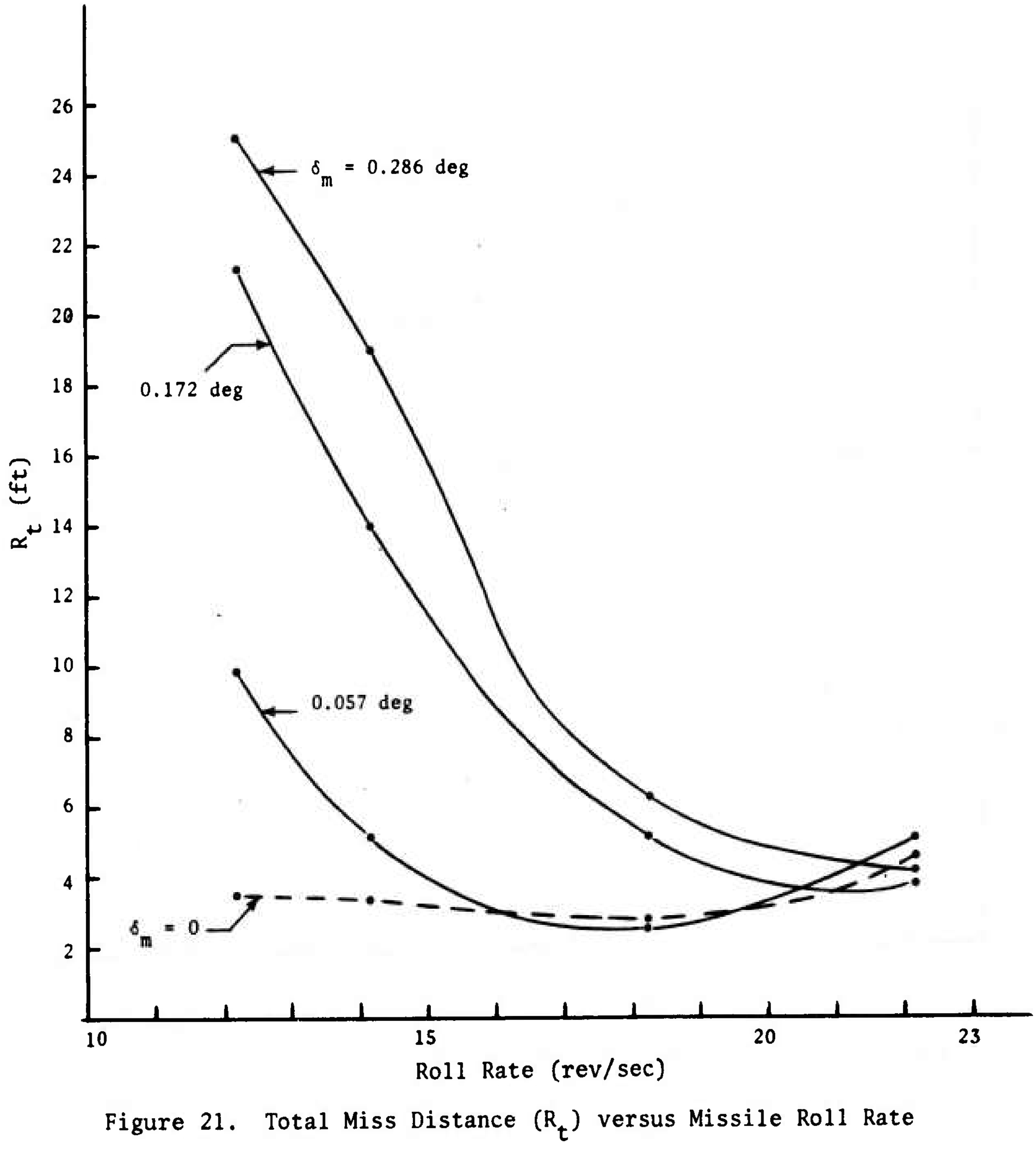

Figure 21. Total Miss Distance (R_t) versus Missile Roll Rate

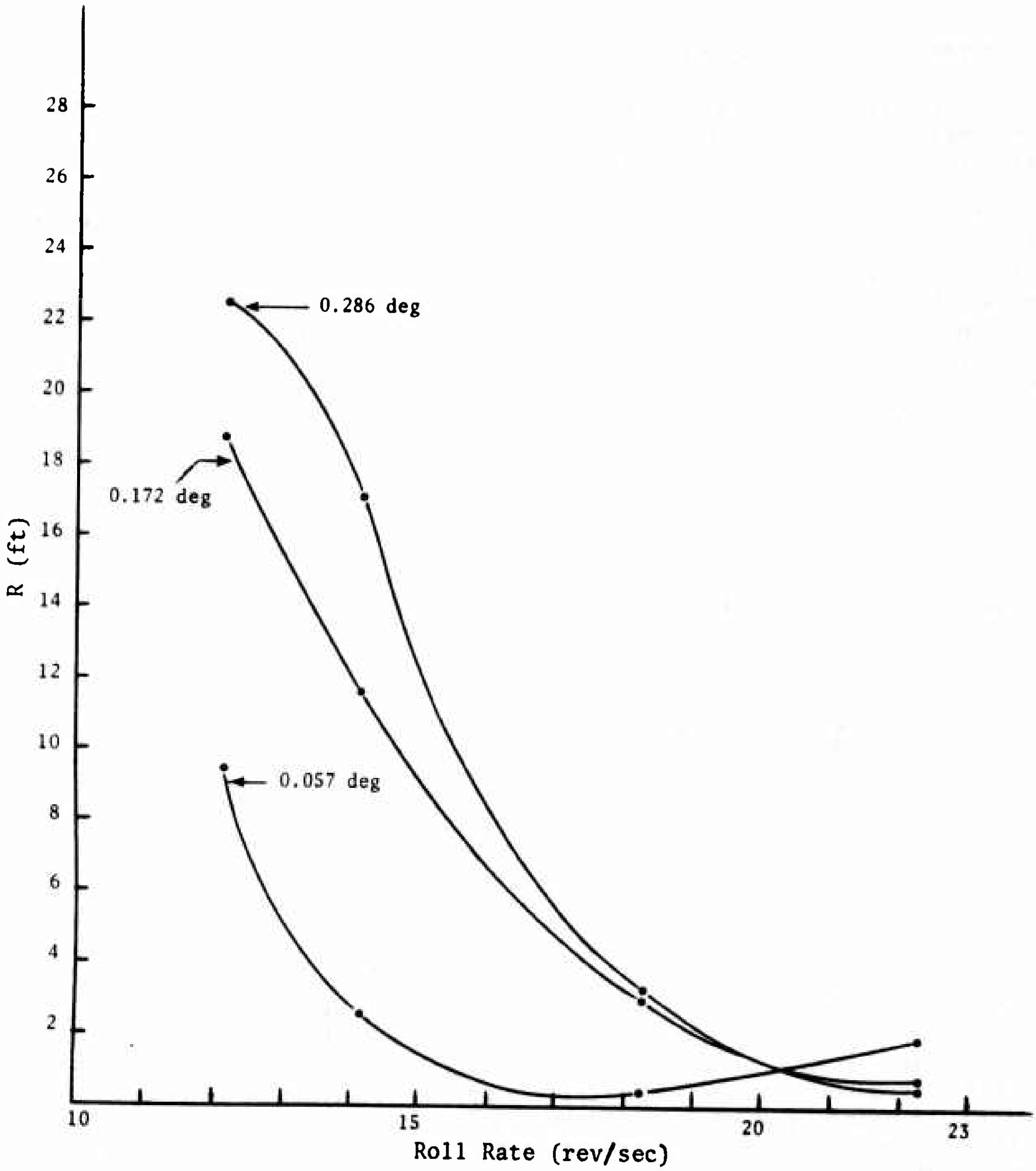

Figure 22. Total Miss Less Gravity Sag (R_{tg}) versus Missile Roll Rate

SECTION VI

OTHER GUIDANCE CONSIDERATION AND ACCURACY ERROR SOURCES

1. PARAMETERS AFFECTING ACCURACY

Several things that affect the accuracy of this type of system will be considered in this section. These are the gravity sag, the aircraft launch velocity, the dead zone size, target motion and wind.

The gravity sag is the target miss due to the natural gravity turn angle of the missile. The velocity vector of the missile at guidance initiation will be pointed downrange of the missile impact point. The logic of the pursuit type guidance system being used will incorrectly call for down corrections for a target at the unguided impact point. This will result in the missile being short of the target in the latter phases of the trajectory and unable to make up the miss. There are a number of parameters that will affect the magnitude of the gravity sag error. Some of these are the velocity of the missile at burnout, the angle and slant range to the target, and the number and magnitude of the thrusters. The gravity sag for the baseline configuration for a 30-degree dive from 6000 feet is 2.5 feet.

The aircraft launch velocity can affect the accuracy of the missile by changing the pitch frequency and by changing the gravity sag. The pitch frequency is given by Equation (A-15). If terms of small magnitude are neglected the pitch frequency reduces to

$$\omega_1 \simeq V \sqrt{\rho C_{m\alpha}(M)} \sqrt{\frac{\pi d^3}{I_y 8}} \quad . \tag{17}$$

The pitch frequency (ω_1) is seen to depend on the velocity linearly and $C_{m\alpha}$. $C_{m\alpha}$ decreases with velocity (in the Mach range of interest) but V is dominant in Equation (17). From Section III it was shown that the pitch frequency must not drop below 1/2 the laser pulse frequency to avoid angle of attack buildup and loss of accuracy. The rocket must be designed so that normal variation in aircraft launch does not change the pitch frequency to less than 1/2 the laser pulse frequency. Figure 23 is a plot of the pitch frequency versus the aircraft launch velocity (this plot was constructed using Equation (17) and unguided trajectory data). The value of the frequency is nearly constant from the initiation of guidance until impact. This occurs since ρ and $C_{m\alpha}$ are increasing during descent as V decreased. The plot shows that the pitch frequency goes above 10 hertz at about 350 knots for the baseline configuration. Table 9 shows the accuracy for a 300-knot aircraft launch (pitch frequency below 10 hertz), and

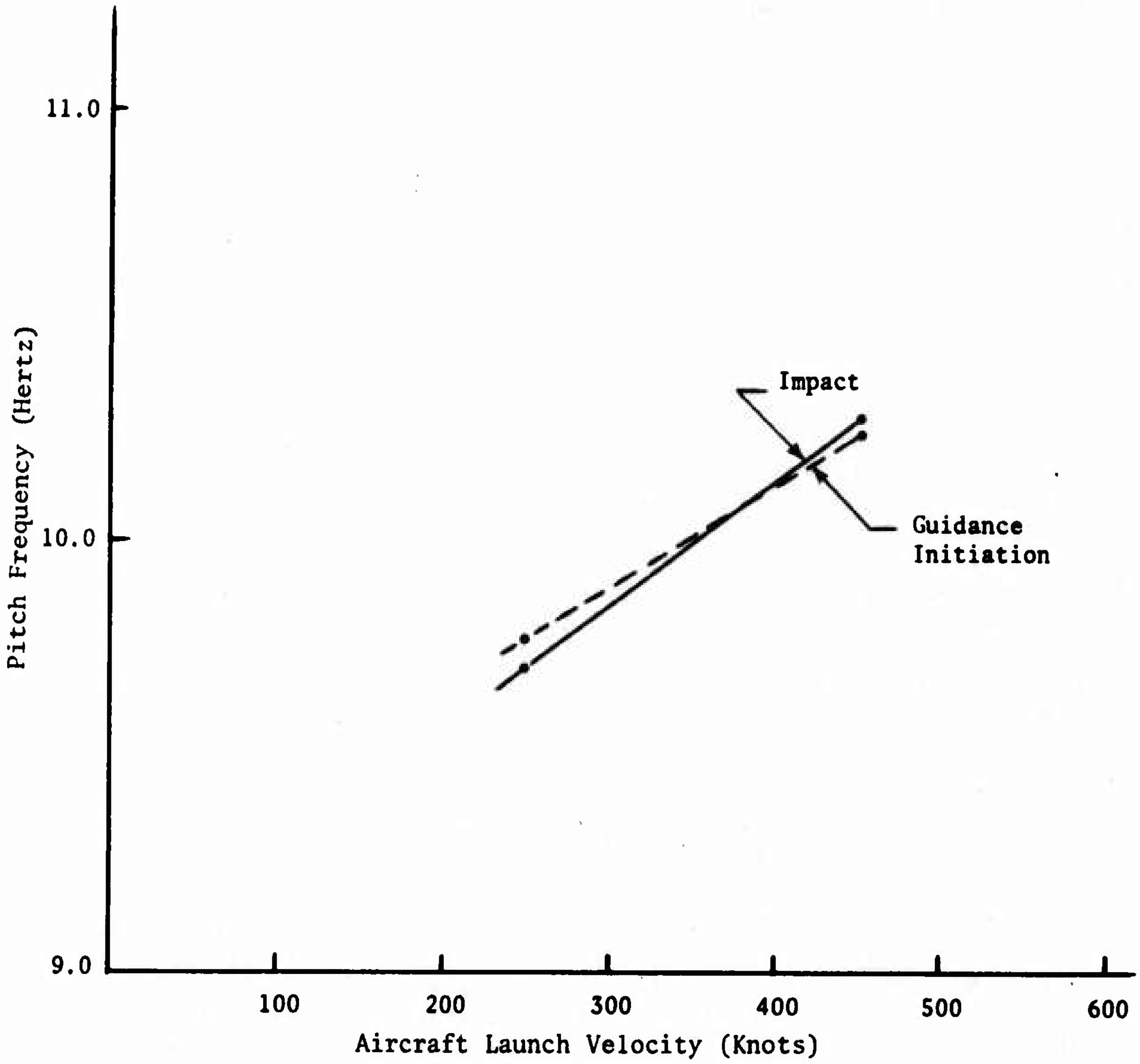

Figure 23. Pitch Frequency versus Average Launch Velocity
Baseline Configuration

the 450-knot aircraft launch (pitch frequency above 10 hertz). The table shows that the lower aircraft launch results in resonant angle of attack buildup and poor accuracy. This particular configuration (baseline configuration) is designed for aircraft launches above 400 knots. If it were desired to design the rocket for lower aircraft launches the pitch frequency would be changed by a cg change, a fin change, or other changes.

TABLE 9. 30-DEGREE DIVE BASELINE CONFIGURATION FOR TWO AIRCRAFT LAUNCH SPEEDS

Aircraft Launch Speed (Knots)	Mean Angle at Lase α_ℓ (Degrees)	R (Feet)	CEP (Feet)
300	0.28	16.5	7.8
450	0.079	2.6	0.96

The dead zone is a region on the image plane where the reflected laser beam does not result in a signal to fire a thruster. The design can be varied so that the dead zone is in the form of a perpendicular cross marking the boundaries of the quadrants or in a central region.[a] An analysis was made to determine the effect of a central dead zone size on the missile accuracy. Figure 24 shows the results of this analysis. Figure 24 shows that for the slant range and dive angle considered (11,300 feet and 30 degrees) the optimum dead zone size is about 0.13 degree. If the dead zone is too large, corrections are not made for targets sufficiently far from the impact point until the missile is too close to the target. For the dead zone too small, an excessive error is picked up because of gravity sag effect and, or depletion of thrusters.

Target motion and wind are similar in causing accuracy errors in pursuit type guidance systems. The error is due to the missile continually correcting directly toward the target. An additional error comes about if, due to target motion or wind, the final position of the target relative to the initial position is beyond the maximum expected correction. Several moving target arrays were simulated on the computer. The standard target array was used (Figure 8), with the target motion beginning at guidance initiation (2.1 seconds). The target motion was perpendicular[b] to the trajectory to the right and varied from 0 to 40 ft/sec. This would correspond to an air

[a]The configuration used in doing most of the error analysis in this report used a cross dead zone of 0.05 degree.

[b]It should be noted that a wind or target motion perpendicular to the trajectory gives about 50 percent greater error than downrange motion.

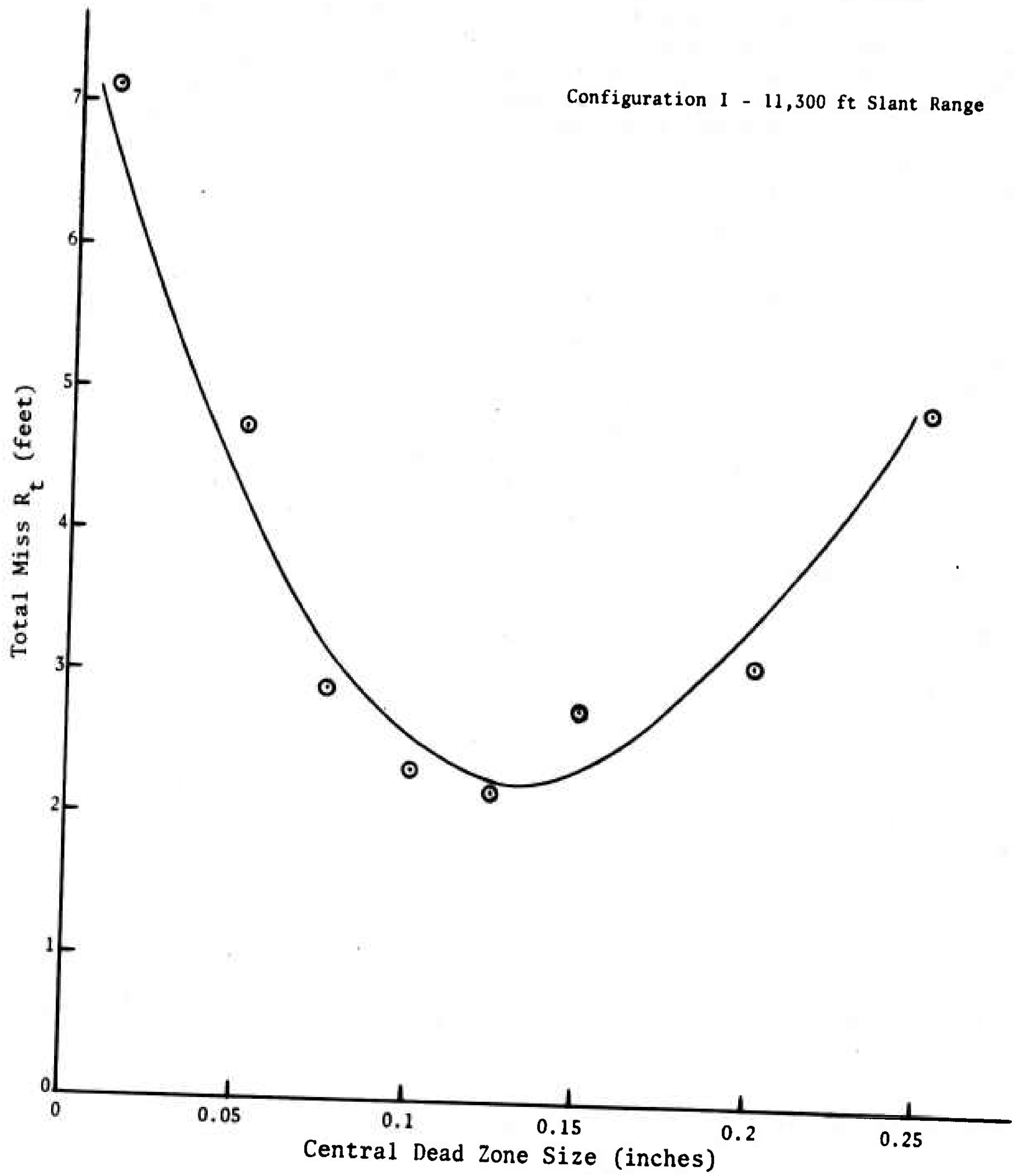

Figure 24. Total Miss Versus Central Dead Zone Size

mass wind with the same speed moving in the opposite direction. The total miss distance less gravity sag (R + CEP - GS) is plotted versus the target speed in Figure 25.[a] The plot shows that this error is large and is up to 17 feet for a 30 ft/sec target speed. The plot shows that the higher impulse reduces the error some. It should be noted that it is common operational practice (laser guided bomb) to eliminate part of this error by leading the target. This correcting procedure would be easier to accomplish for a moving target than for a wind.

2. ESTIMATE OF THE ACCURACY OF THE SYSTEM

Throughout this report the standard target array, (the solid circles in Figure 8), has been used when computing accuracy. A more realistic target array would be that given by the distribution representing the accuracy of the unguided rocket. Let us assume that X and Y (unguided rocket impact points) are normally distributed random variables with standard deviations of 7 mils. This would give the distribution represented by the cross marks in Figure 8 for a 30-degree dive at a slant range of 11,000 feet. For the baseline configuration this gives about 8 percent of the targets beyond the maximum expected correction.[b] The accuracy of the baseline configuration was computed for stationary targets using the normal distribution but not including the 8 percent of the targets beyond the maximum expected correction. A comparison of the accuracy statistics of the standard and the modified normal distributions are given in Table 10.

TABLE 10. BASELINE CONFIGURATION ACCURACY ON STANDARD AND NORMAL DISTRIBUTION ARRAYS

Array	$\overline{\Delta X}$	$\overline{\Delta Y}$	R	CEP
Standard	-2.5	0.86	2.6	0.96
Normal Distribution (Modified)	-2.5	0.14	2.5	1.6

Table 10 shows very little difference between the two arrays except the CEP is slightly higher for the normally distributed array. The standard target array will be used in the following approximate accuracy analysis.

---

[a]The nominal gravity sag of 2.5 feet was subtracted in constructing the curve.

[b]This may be computed approximately by the following formula.

$P_b = \exp\left[-\langle\delta_{rp}\rangle^2 / 2\sigma^2\right]$ where P_b is the percent of target beyond the maximum expected correction, $\sigma = \sigma_x = \sigma_y$ = standard deviation error in x, and y, and $\langle\delta_{rp}\rangle$ = maximum expected correction (see Section IV).

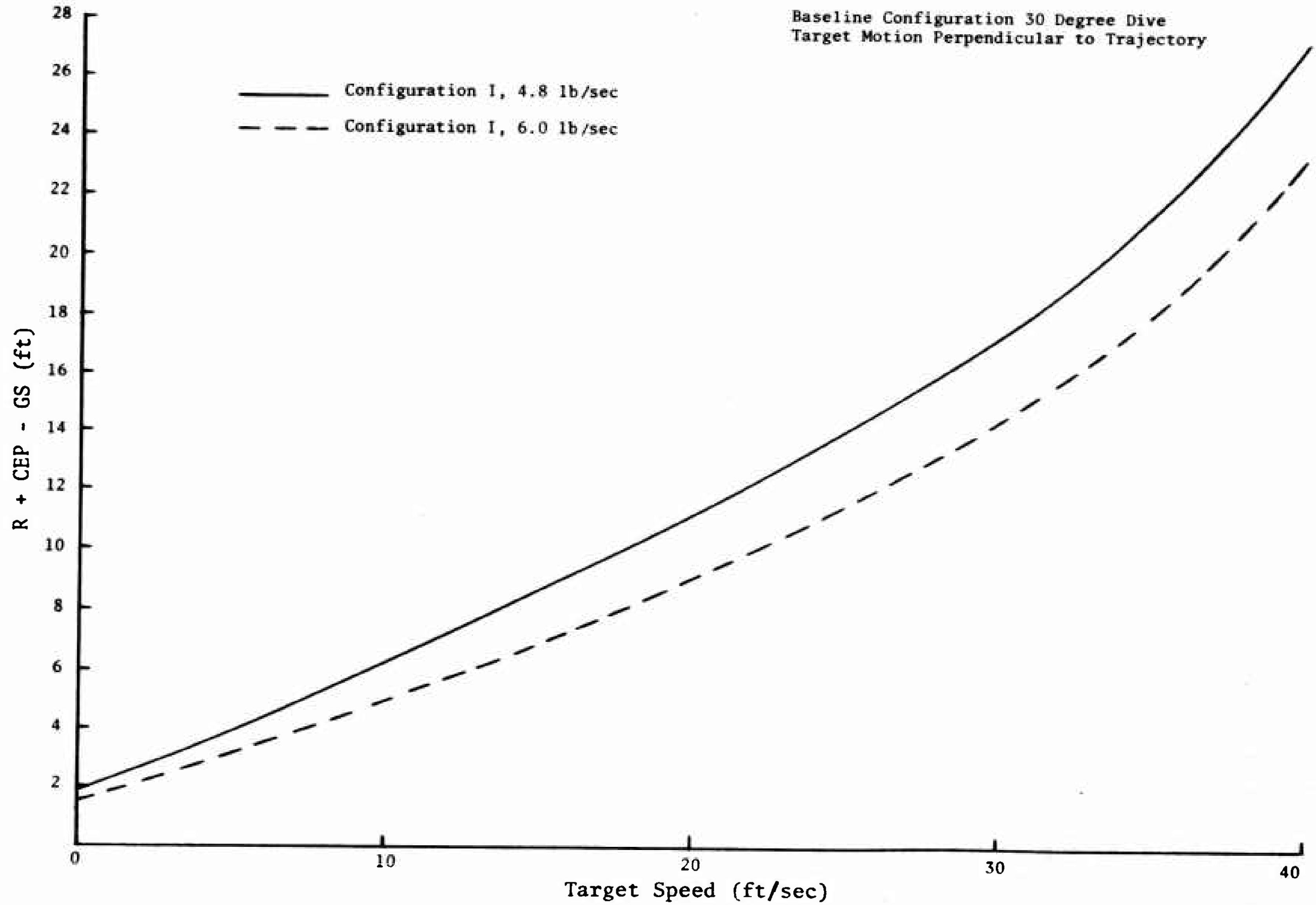

Figure 25. Total Miss Less Gravity Sag versus Target Velocity

The accuracy of the system was very roughly estimated here using somewhat arbitrary assumption on the magnitude of the error sources. The error sources considered are the gravity sag, trim misalignment, target motion, and wind. The errors were assumed to be independent. It was assumed that the laser beam would be aimed in an attempt to reduce the error due to gravity sag, target motion, and wind. The accuracy study was run for the baseline configuration launched from 6000 feet altitude, at an angle of 30 degrees, from an aircraft moving at 450 knots.

A standard deviation for the gravity sag error was taken as 50 percent of the nominal gravity sag or 1.25 feet. A standard deviation error in trim misalignment was taken as a static trim of 0.143 degree for a roll rate of 19 hertz. From Figure 22 this gives an error of 1.2 feet, and this was resolved into a σ_{xt} and σ_{yt} by multiplying by cos 45 degrees.[a] A standard deviation error for target motion was taken as a target moving at 20 ft/sec which was 50 percent corrected. The 20 ft/sec was resolved into a cross range and downrange component of 14.14 ft/sec. From Figure 24 this gives a target motion error of 8.2 feet and if this is corrected by 50 percent then the σ_{ym} error is 4.1 feet for lateral target motion. The error in the downrange direction is about one half this for a 30-degree dive or σ_{xm} is 2.05 feet.

A standard deviation error in wind was taken at 30 percent corrected 10 mph (14.67 ft/sec) in a direction 45 degrees off the downrange direction. The components of wind in the cross range and downrange directions are 10.37 ft/sec. From Figure 24 this gives a wind error of 6.6 feet. Then $\sigma_{yw} = 0.7\ (6.6) = 4.62$ feet and σ_{xw} is one half this or 2.31 feet. These values are listed in Table 11. Table 11 also gives the root mean square value of σ_x and σ_y and a CEP error is computed according to Reference 5.

TABLE 11. ACCURACY FOR BASELINE CONFIGURATION FOR ASSUMED MAGNITUDE OF ERROR SOURCES

	σ_x	σ_y
Gravity sag (50 percent corrected)	1.25	
Trim misalignment static trim 0.143 degree, roll rate 19 hertz	0.85	0.85
Target motion 20 ft/sec 50 percent corrected	2.05	4.1
Wind 10 mph 30 percent corrected	2.31	4.62
$\sqrt{\sum_i \sigma_i^2}$	3.44	6.23
CEP	5.63	

[a] σ_x is taken as downrange and σ_y is cross range standard deviation. The subscript t stands for trim, g gravity sag, m target motion, and w wind.

The error analysis given in Table 11 was done for the target array of Figure 8. This array roughly represents an unguided accuracy of 7 mils in x and y perpendicular to the trajectory with the targets beyond the maximum expected correction (about 8 percent) not considered. The analysis was made for one fixed launch condition and considered only a limited number of error sources. Instrumentation errors were not considered, and it was assumed the target was illuminated without jitter.

SECTION VII

DISTURBED FLOW EFFECT AND TEST

For the guidance system being considered it is important that the explosion from the thruster does not adversely affect the aerodynamic characteristics of the missile. A test was run at AEDC (Reference 2) to determine if the disturbance caused by the explosive strip reacts with the flow to change the aerodynamics of the missile causing changes in the angle of attack or pitch frequency. The time that the blast wave (or disturbed flow) remains over the missile is important in determining its effect.

The solution to the linear equation (Appendix A) was used to estimate the effect of disturbed flow over the missile as a function of the duration of the disturbance (this work was accomplished by the author and reported in a memo in September 1975). If the impulse time of the thruster is very short and the relative magnitude of physical properties and aerodynamics of the missile are considered, then Equations (A-19) and (A-20) reduce to Equation (18)

$$\alpha \sim -\frac{\bar{F}LT^2}{2\,I_y} \quad , \quad \dot{\alpha} \sim \frac{\bar{F}LT}{I_y} \tag{18}$$

and the angle of attack and angular rate of the missile at the end of burning does not depend on the aerodynamics of the missile at all, but only on the thrust, thrust time, moment distance, and missile transverse moment of inertia. The thrust time being considered for the explosive impulse ($\sim 10^{-4}$ seconds) is short enough so that the above conditions prevail. After the explosive impulse the disturbance due to the explosive shock wave and associated perturbed flow will affect the missile aerodynamics in an unknown manner for an unknown period of time. Equations (A-13) through (A-23) were used in an iterative manner to determine the type of motion obtained for a given perturbation as a function of time. It was found that changing the damping coefficient, C_{mq}, had little effect on the maximum angle of attack the missile obtained. The maximum angle of attack was a strong function of the variation in $C_{m\alpha}$ and the time $C_{m\alpha}$ was perturbed.

For the purpose of analysis $C_{m\alpha}$ was reduced by a factor of (0.01) and Equations (A-13) through (A-23) were used to compute the value of $\alpha_{(tp)}$ and $\dot{\alpha}_{(tp)}$ for various perturbing times. Equation (A-13) was used to continue the computation of the angle of attack after the perturbation was terminated. Figure 26 shows the damped oscillation for missile characteristics similar to the baseline configuration. The maximum angle of attack obtained is about 1.18 degrees. The other curve in Figure 26 gives the missile motion if $C_{m\alpha}$ is reduced by a factor of 0.01 for a period of 20 milliseconds after thrust termination. The maximum angle of attack obtained here is 1.91 degrees.

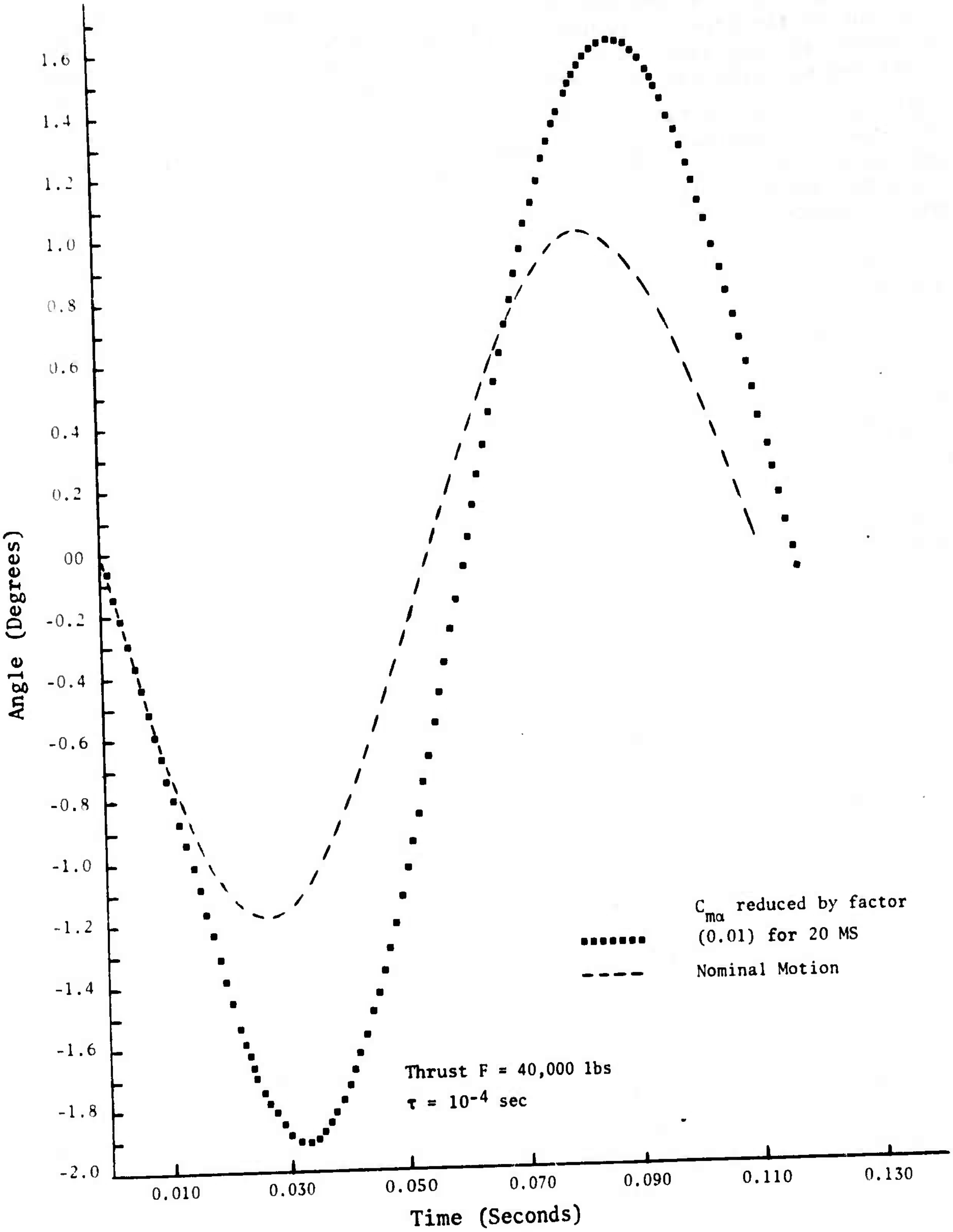

Figure 26. Missile Angle of Attack

The simulations show that the effect on the missile motion is a strong function of the time the perturbing influence acts. Figure 27 shows the missile's maximum angle of attack as a function of the perturbation time where the perturbation is a reduction in $C_{m\alpha}$ by a factor of 0.01. This curve shows that it takes a perturbing time of about 2 milliseconds before any change in maximum angle of attack is noted. After this time the effect multiplies rapidly. Although here the perturbing influence was picked to increase the angle of attack, the perturbation could as well reduce the maximum angle of attack.

The wind tunnel test at AEDC (Reference 2) consisted of measuring the damping ($C_{mq} + C_{m\dot{\alpha}}$) and overturning ($C_{m\alpha}$) moments using a one-degree-of freedom flexure balance. The wind tunnel model had slots which mount the 0.080-inch thick Datasheet-E explosive strip. The strips give various total impulses up to a maximum of 0.294 lb/sec. The angular position of the model, θ, was calculated from strain gage measurements taken at about 3500 data points/sec. These data were plotted automatically after each shot. The predicted angle was plotted on the same plot. The predicted angle is calculated from the measured thrust off aero data ($C_{mq} + C_{m\dot{\alpha}}$, $C_{m\alpha}$), the measured moment of inertia, the balance stiffness, and the statically measured total impulse which varies less than 5 percent from shot to shot.

The Schlieren photographs (frame rate 7500/sec) show that the explosive strip forms a strong shock wave (Figure 28) which appears to move out in a shperical manner. The wave slows as it moves out and then drifts back with the Mach 3 flow. The disturbance appears to be strong enough to have an appreciable effect on the missile aerodynamics while it is acting. The pretest analytical study showed that the time the disturbance persists is an important factor. Using the frame rate (7500/sec), and counting the frames during which the perturbed flow is present, gives a perturbation time of about 1 to 2 milliseconds. From Figure 27 and the analytic study, this is not a sufficient time to cause a noticeable change in the maximum angle of attack.

Figure 29 shows the predicted and measured angles of attack for one shot condition. The plot shows little difference between the predicted and measured motion. Considering all shots, one can conclude that the explosive blast wave and associated disturbed flow has little effect on the missile motion for these test conditions.

Data were taken to determine the effect of the exposed explosive slots on the aerodynamics of the missile. $C_{m\alpha}$ and $C_{mq} + C_{m\dot{\alpha}}$ were measured for no slot exposed, one slot exposed, and all slots exposed. Test results indicate little change in $C_{m\alpha}$ and $C_{mq} + C_{m\dot{\alpha}}$ for the different conditions.

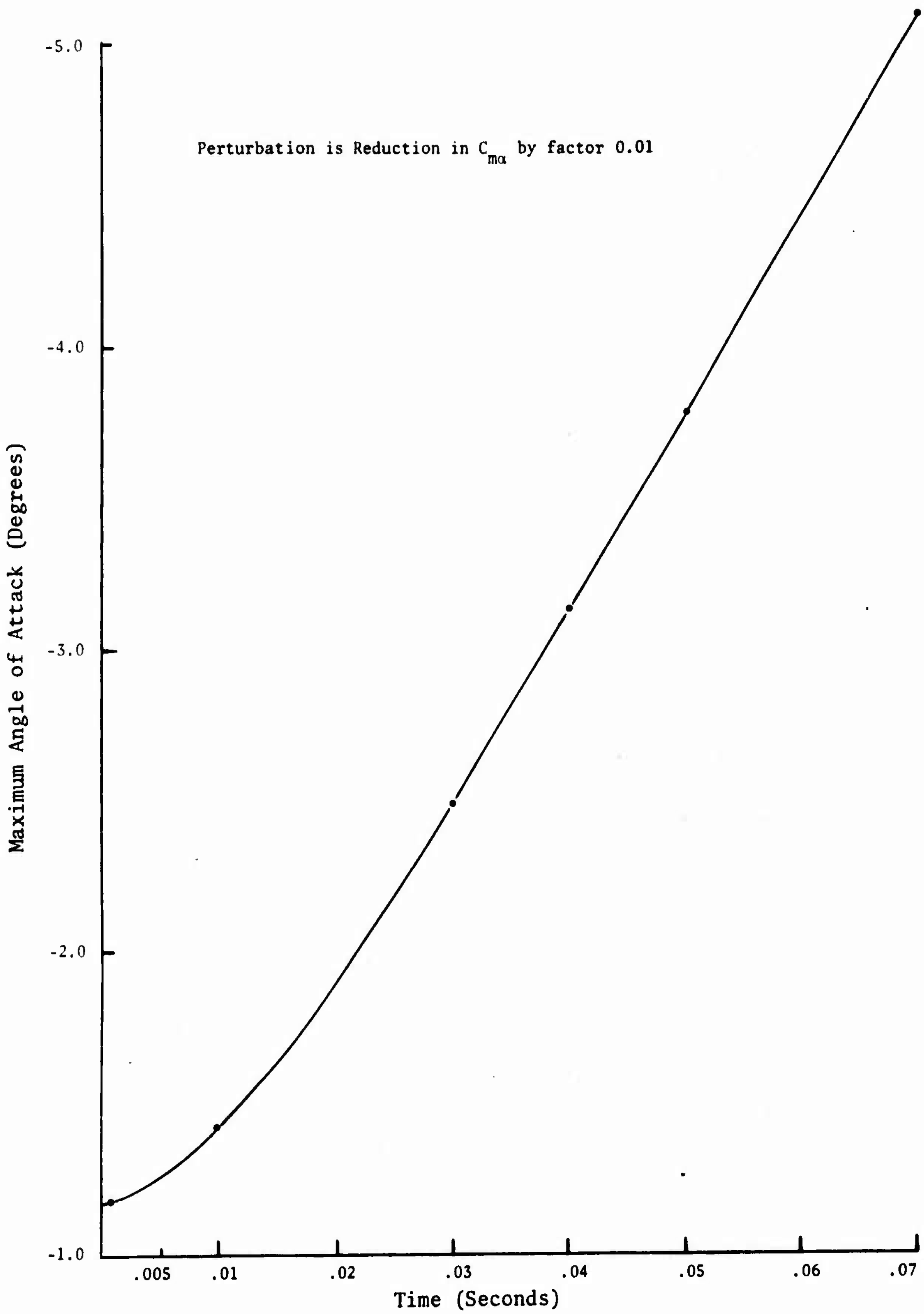

Figure 27. Maximum Angle of Attack versus Perturbation Time

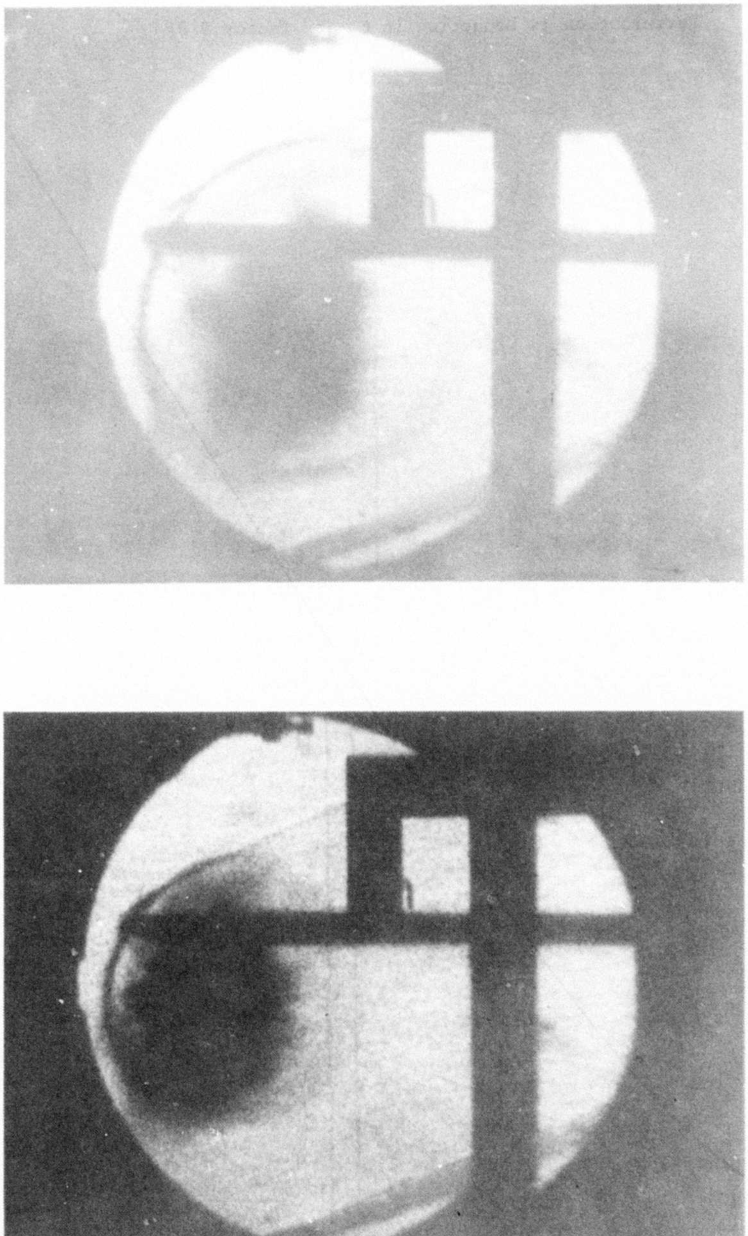

Figure 28. Sequenced Pictures Explosive Blast Wave

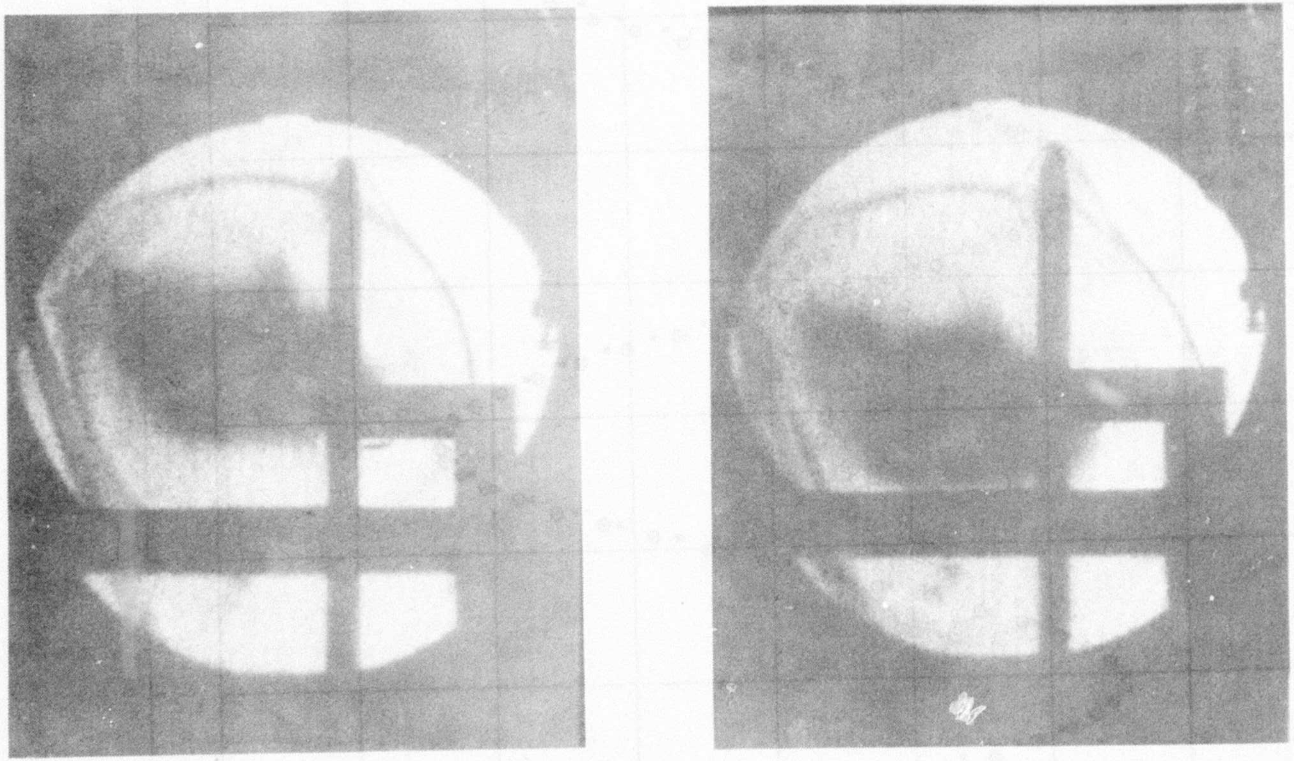

Figure 28. Sequenced Pictures Explosive Blast Wave (concluded)

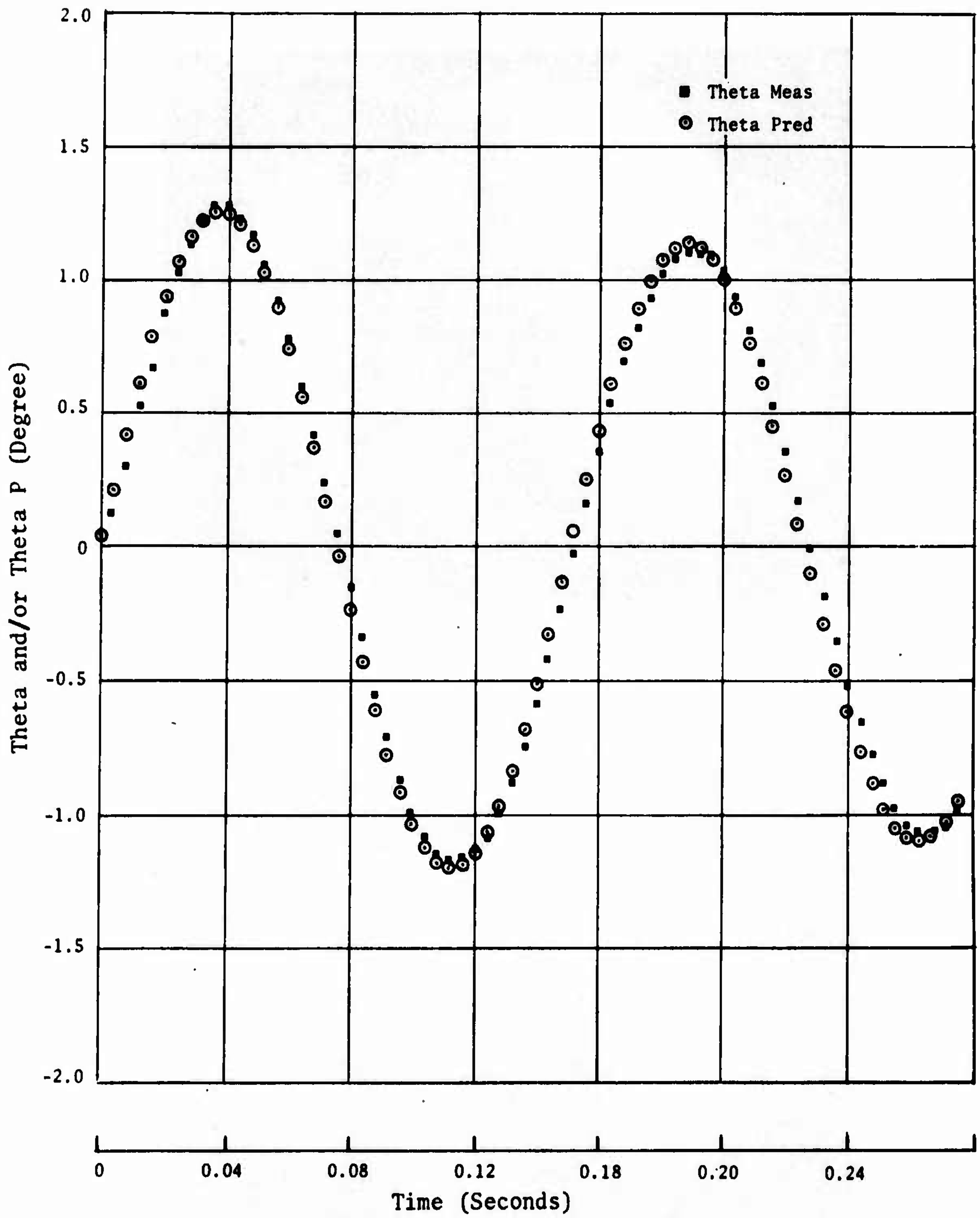

Figure 29. Predicted and Measured Angle of Attack

SECTION VIII

SUMMARY AND CONCLUSIONS

The feasibility of an explosive impulse, laser guided, body fixed (pursuit guidance), fin stabilized rocket was studied. A method of analyzing the system was set up and many important principles affecting the accuracy of the system were determined.

Two computer programs were established to study the system. One of the computer programs simulated simple pitching motion of the rocket and the other program simulated the complete six-degree-of-freedom guidance problem. The pitching motion program gives the pitch frequency, the angle of attack, and the change in the velocity vector when a thruster is fired as a function of the thruster characteristics and the physical and aerodynamic properties of the rocket. The 6-D guidance program simulates the entire guidance problem. The program has variable input for the rocket, atmospheric conditions including wind, initial conditions, target array and target motion. A statistical summary of the accuracy on multiple target arrays is part of the output of the 6-D program.

It was determined that to obtain sufficient accuracy for this system it was necessary to phase the pitch frequency with the laser pulse frequency. The pitch frequency must be slightly greater than 1/2 the laser pulse frequency. A pitch frequency below 1/2 the laser pulse frequency results in resonant buildup of the angle of attack and large miss distances. A gradual increase in miss distance occurs as the pitch frequency is increased above 1/2 the laser pulse frequency. This is due to pitch and laser pulse frequency being out of phase. The rocket can be designed to accommodate pitch frequency changes resulting from nominal changes in aircraft launch velocity without a large loss in accuracy.

Approximate formulas were derived to give the maximum expected correction from a specified rocket configuration. These formulas can be used in preliminary design to determine if the configuration can correct sufficiently far from the unguided trajectory.

The relation between the accuracy of this system and the trim misalignment was determined. A simple equation gives the trim angle as a function of trim misalignment, the pitch frequency, and the roll rate. The 6-D guidance program showed that increasing the roll rate (to reduce the trim angle) from 1.2 to 1.8 times the pitch frequency improved the accuracy by a factor of 10.

Target motion and wind cause large trailing miss distances for this as well as other pursuit type guidance systems. For the baseline configuration considered here, miss distance goes from about 1.8 feet for stationary targets to about 17.2 feet for target motion of 30 ft/sec.

The CEP for the baseline configuration was computed for error sources of gravity sag, trim misalignment, wind, and target motion for a slant range of 11,000 feet. Nominal values were assumed for the error sources and a partial operational correction (by using the laser designator) was assumed for gravity sag, wind, and target motion. The resulting CEP was 5.6 feet.

An AEDC wind tunnel test was run to determine if the explosive impulse caused a blast wave or flow disturbance that adversely affected the aerodynamics of the rocket. Test results indicate that the large explosive blast wave and associated perturbed flow from the terminal guidance explosive strip have little effect on the missile oscillatory motion. This is probably related to the short time the disturbance persists. These test results indicate that the explosive action time may be extended, if desired, without adverse effect on the guidance system.

The initial analytical simulations indicate that the laser guided explosive impulse correction guidance method is a feasible approach for a low cost guidance system. Further development of the explosive correction method, additional analytical studies, and a system demonstration test is required to assure sufficient accuracy of this system.

REFERENCES

1. Uselton, James, Results of an Air Force Advanced Tactical Rocket Development Program, AEDC-TR-71-141, AFATL-TR-71-73, July 1971.

2. Uselton, Bob L., A Wind Tunnel Investigation of Impulse Effects on the Motion of an Impulse Correction Guidance Missile, AEDC-TR-76-6, AFATL-TR-75-164, April 1976.

3. Murphy, C. H., "Free Flight Motion of Symmetric Missiles", BRL Report 1216, July 1963.

4. Laymon, W. A., Proposal to Design, Fabricate, Test and Deliver Terminal Homing Flight Test Vehicles, Digital Simulation Users Manual, North American Rockwell, Columbus Division, 4 June 1970.

5. Groves, A. D., Handbook on the Use of the Bivariate Normal Distribution in Describing Weapon Accuracy, BRL Memorandum Report 1372, September 1961.

APPENDIX A

ANGLE OF ATTACK AND SWERVE FOR PLANAR MOTION, ROLL RATE, AND ROLL AVERAGED THRUST

1. ANGLE OF ATTACK FOR PLANAR MOTION

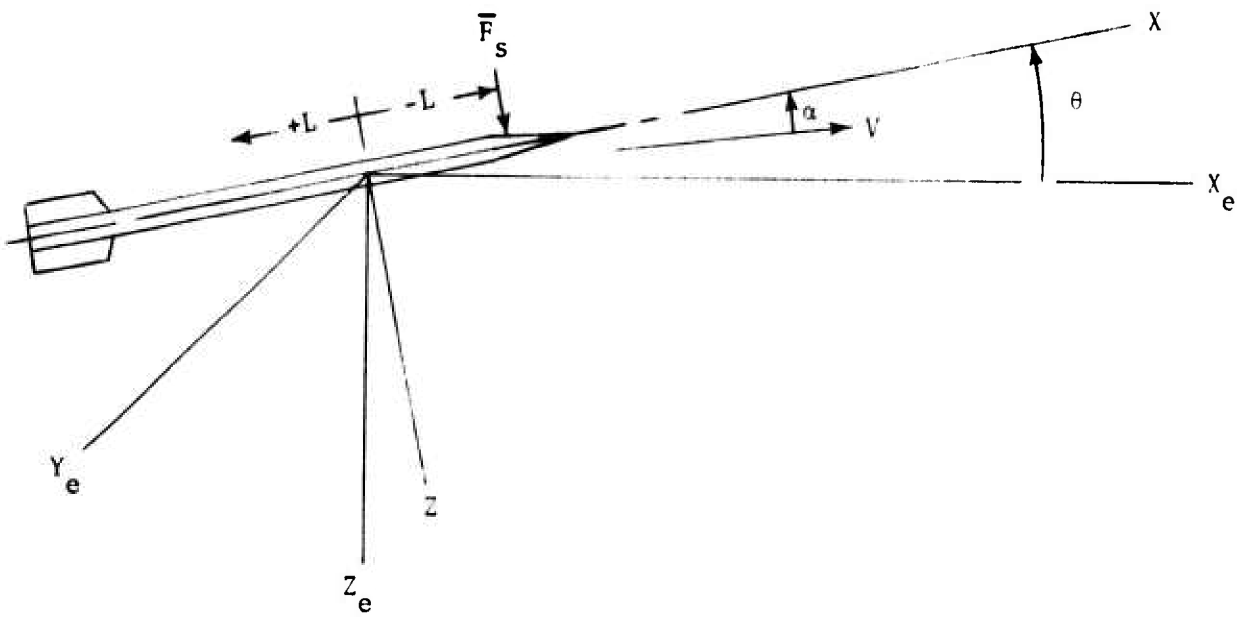

Figure A-1. Missile Pitching Motion

The approximate equations of motion for the missile in the X_e , Z_e plane are

$$M\dot{V} = -D = -\frac{1}{2}\rho V^2 sC_d \sim F_x \tag{A-1}$$

$$M\ddot{Z}_e = F_z \cos\theta - F_x \sin\theta + Mg\cos\theta + \bar{F}_s \cos\theta \tag{A-2}$$

$$I_y\ddot{\theta} = M_y + \bar{F}_s L \tag{A-3}$$

Geometry gives

$$\dot{Z}_e = -V\sin(\theta - \alpha) \simeq -V(\theta - \alpha) \tag{A-4}$$

The swerve force is

$$F_z = QS\ (-C_{N\alpha}) \tag{A-5}$$

The moment

$$M_y = QSd\left[\left(C_{mq}\frac{d\dot{\theta}}{2V} + C_{m\alpha}\frac{d\dot{\alpha}}{2V}\right) + C_{m\alpha}\ \alpha\right] \tag{A-6}$$

If small angle approximations are made and small density factors, such as f, are neglected when summed with 1, g/d neglected compared with $\frac{F_s}{Md}$, and the relative magnitude of the aerodynamic coefficients taken into account, then Equations (A-1) through (A-7) can be combined to give the following differential equation for the angle of attack (α).

$$\ddot{\alpha} - K_{\dot{\alpha}}\ \dot{\alpha} - K_{\alpha}\ \alpha = \frac{L\bar{F}_s}{I_y} - \frac{fC_{mq}\bar{F}_s}{2K_y^2 Md} \tag{A-7}$$

where:

M	=	Missile mass
V	=	Missile velocity
ρ	=	Air density
s	=	Missile reference area
d	=	Missile reference diameter
Q	=	Dynamic pressure = $1/2\rho V^2$
I_x	=	Missile axial moment of inertia
I_y	=	Missile transverse moment of inertia
X_e , Z_e	=	Inertial axes
X , Z	=	Missile axes
θ	=	Missile angle Figure A-1
$\dot{\theta}$	=	Rate of change of θ
α	=	Missile angle of attack
$\dot{\alpha}$	=	Rate of change of α
F_x , F_z	=	Forces along x and z

Mg	=	Gravitational force
$C_{N\alpha}$	=	Normal force coefficient slope
C_{mq}	=	Damping moment coefficient slope with respect to $q = \dot{\theta}$ here
$\bar{F}_s$	=	Average side force
L	=	Position of application of $\bar{F}_s$ (Figure 1)
$C_{m\dot{\alpha}}$	=	Damping moment coefficient with respect to $\dot{\alpha}$
$C_{m\alpha}$	=	Moment coefficient slope $\partial C_m / \partial \alpha$

$$f = \rho s d/2M \tag{A-8}$$

$$K_y^2 = I_y / Md^2 \tag{A-9}$$

$$K_\alpha = \frac{F_1}{2}\left(\frac{V}{d}\right)^2 C_{m\alpha} = \rho V^2 \pi d^3 C_{m\alpha} / I_y 8 \tag{A-10}$$

$$F_1 = \rho s d d^2 / I_y \tag{A-11}$$

$$K_{\dot{\alpha}} = \frac{F_1}{4}\,\frac{V}{d}\left(C_{mq} + C_{m\dot{\alpha}}\right) = \frac{\rho \pi d^4 V}{16\, I_y}\left(C_{mq} + C_{m\dot{\alpha}}\right) \tag{A-12}$$

The solution to Equation (A-7) is

$$\alpha = e^{\lambda t}\left[A \cos \omega_1 t + B \sin \omega_1 t\right] + \alpha_p \tag{A-13}$$

$$\dot{\alpha} = e^{\lambda t}\left[A\left[\frac{K_{\dot{\alpha}}}{2} \cos \omega_1 t - \omega_1 \sin \omega_1 t\right] + B\left[\frac{K_{\dot{\alpha}}}{2} \sin \omega_1 t + \omega_1 \cos \omega_1 t\right]\right] \tag{A-14}$$

$$\lambda = K_{\dot{\alpha}}/2$$

A, B = arbitrary constants

$$\omega_1 = \sqrt{-K_\alpha - K_{\dot\alpha}^2/4} \quad \text{, pitch frequency} \tag{A-15}$$

$$\alpha_p = \frac{\bar{F}_s}{K_\alpha}\left[\frac{L}{I_y} - \frac{fC_{mq}}{2K_y^2 Md}\right] = -\frac{\bar{F}_s L}{K_\alpha I_y} + \frac{\bar{F}_s C_{mq} d}{2MV^2 C_{m\alpha}} \tag{A-16}$$

At $t = 0$, $\alpha = \alpha_0$ $\dot\alpha = \dot\alpha_0$ then

$$A = \alpha_0 - \alpha_p \tag{A-17}$$

$$B = \left[\dot\alpha_0 - \frac{K_{\dot\alpha}}{2}\left(\alpha_0 - \alpha_p\right)\right] \Big/ \omega_1 \tag{A-18}$$

For case $\alpha_0 = \dot\alpha_0 = 0$, the values of α and $\dot\alpha$ at thruster burnout time (τ) are

$$\alpha_\tau = \alpha_p \left[e^{\lambda\tau}\left(-\cos\omega_1\tau + \frac{K_{\dot\alpha}}{2\omega}\sin\omega_1\tau\right) + 1\right] \tag{A-19}$$

$$\dot\alpha_\tau = \alpha_p\omega_1 e^{\lambda\tau}\sin\omega_1\tau\left[1 + \left(\frac{K_{\dot\alpha}}{2\omega_1}\right)^2\right] \tag{A-20}$$

If $\omega_1 >> K_{\dot\alpha}/2$

$$\alpha_\tau \simeq \alpha_p\left\{1 - \left(\cos\omega\tau\right)e^{\lambda\tau}\right\} \tag{A-21}$$

$$\dot\alpha_\tau \simeq \alpha_p\omega_1 e^{\lambda\tau}\sin\omega_1\tau \tag{A-22}$$

Now use Equation (A-13) to give the value of α after termination of the side thrust. For these conditions, $A = \alpha_0 = \alpha_\tau$, $B = \left(\dot{\alpha}_\tau - \frac{K_{\dot{\alpha}}\alpha_0}{2}\right)\Big/\omega_1$

$$\alpha_{(t_2)} = e^{\lambda t_2}\left\{\alpha_\tau \cos \omega_1 t_2 + \left(\frac{\dot{\alpha}_\tau}{\omega_1} - \frac{K_{\dot{\alpha}}\alpha_\tau}{2\omega_1}\right)\sin \omega_1 t_2\right\} \tag{A-23}$$

$t_2 = 0$ at thrust termination

α_τ and $\dot{\alpha}_\tau$ may be taken from Equations (A-19) and (A-20) or (A-22) and (A-20).

2. SWERVE FOR PLANAR MOTION

The differential equation for the swerve (side deflection) may be obtained from Equations (A-1), (A-2), (A-4) and (A-5). Assume small angles, $\cos\theta = 1$, $\sin\theta = \theta$; neglect Mg ; substitute (A-4) in (A-2). The result is

$$M\ddot{Z}_e \simeq F_z - F_x\left(-\frac{\dot{Z}_e}{V} + \alpha\right) + \overline{F}_s$$

Divide by V

$$\frac{\ddot{Z}_e}{V} \sim \frac{\rho s V}{2M}\left(-C_{N\alpha} + C_d\right)\alpha - \frac{\rho s C_d \dot{Z}_e}{2M} + \frac{\overline{F}_s}{MV}$$

Assume $\dot{Z}_e/V$ is order of α and $C_d << |C_{N\alpha}|$

Then

$$\frac{\ddot{Z}_e}{V} \sim -\frac{\rho s V}{2M} C_{N\alpha}\alpha + \frac{\overline{F}_s}{MV} \tag{A-24}$$

Define: $\delta \equiv \dot{z}_e / V$

Integrating Equation (A-24) with α given by Equation (A-13), from time 0 to time τ gives

$$\delta_\tau = \frac{fV}{d}\left(-C_{N\alpha}\right)\left\{ e^{\frac{K_{\dot{\alpha}}\tau}{2}} A \frac{\left(\frac{K_{\dot{\alpha}}}{2}\cos\omega_1\tau + \omega_1 \sin\omega_1\tau\right)}{-K_\alpha} \right.$$

$$+ e^{\frac{K_{\dot{\alpha}}\tau}{2}} B \frac{\left(\frac{K_{\dot{\alpha}}}{2}\sin\omega_1\tau - \omega_1\cos\omega_1\tau\right)}{-K_\alpha}$$

$$\left. + \alpha_p \tau \right\} + \frac{\bar{F}_s \tau}{MV} + \delta_{\tau 0}$$

$$- \frac{fV}{d}\left(C_{N\alpha}\right)\left\{ \frac{AK_{\dot{\alpha}}}{2K_\alpha} - \frac{B\omega_1}{K_\alpha} \right\} \qquad \text{(A-25)}$$

From Equation (A-17) and Equation (A-18)

if at $t = 0$ $\alpha_0 = \dot{\alpha}_0 = \delta_{\tau 0} = 0$

$A = \alpha_p$, $B = \frac{K_{\dot{\alpha}}}{2\omega_1}\alpha_p$

and Equation simplifies to

$$\delta_\tau \simeq \frac{fV}{d} C_{N\alpha} \frac{K_{\dot{\alpha}}}{2K_\alpha}\alpha_p \left\{ e^{\lambda\tau} \left(-2\cos\omega_1\tau - \frac{2\omega_1}{K_{\dot{\alpha}}}\sin\omega_1\tau\right)\right.$$

$$\left. + 2 - \frac{2K_\alpha}{K_{\dot{\alpha}}}\tau \right\} + \frac{\bar{F}_s\tau}{MV} \qquad \text{(A-26)}$$

δ may be found after burnout by integrating Equation (A-24) with $\bar{F}_s = 0$ and using α with $\bar{F}_s = 0$.

$$\alpha_{(t_2)} = e^{\lambda t_2} \left\{ A \cos \omega_1 t_2 + B \sin \omega_1 t_2 \right\}$$

$$A = \alpha_\tau \quad , \quad B = \frac{\dot{\alpha}_\tau}{\omega_1} - \frac{K_{\dot{\alpha}}}{2\omega_1} \alpha_\tau$$

$$\delta_{t_2} \simeq \frac{fV}{d} C_{N\alpha} \frac{K_{\dot{\alpha}}}{2K_\alpha} \left\{ e^{\lambda t_2} \left[\alpha_\tau \left(\cos \omega_1 t_2 + \frac{2\omega_1}{K_{\dot{\alpha}}} \sin \omega_1 t_2 \right) \right. \right.$$

$$\left. \left(\frac{\dot{\alpha}_\tau}{\omega_1} - \frac{K_{\dot{\alpha}}}{2\omega_1} \alpha_\tau \right) \left(\sin \omega_1 t_2 - \frac{2\omega_1}{K_{\dot{\alpha}}} \cos \omega_1 t_2 \right) \right]$$

$$\left. - \left(2\alpha_\tau - \frac{2}{K_{\dot{\alpha}}} \dot{\alpha}_\tau \right) \right\} + \delta_\tau \qquad \text{(A-27)}$$

Considering only the part of Equation (A-27) which does not damp out with time the result is

$$\delta_{t_2} \; (t_2 \rightarrow \text{large}) = \frac{-fV}{d} \frac{C_{N\alpha} K_{\dot{\alpha}}}{2K_\alpha} \left(2\alpha_\tau - \frac{2\dot{\alpha}_\tau}{K_{\dot{\alpha}}} \right) + \delta_\tau \qquad \text{(A-28)}$$

substituting from Equations (A-19), (A-20), and (A-26) and canceling terms

$$\delta_s \equiv \delta_{t_2}\ (t_2 \rightarrow \text{large}) = -\frac{fV}{d} C_{N\alpha}\alpha_p \left\{ e^{\lambda\tau} \frac{K_{\dot{\alpha}}^2}{4K_\alpha \omega_1} \sin \omega_1 \tau + 2\tau \right\} + \frac{\bar{F}_s \tau}{MV} \tag{A-29}$$

3. ROLL RATE

The spin differential equation is

$$\dot{p} - \frac{C_{\ell p}\, Qsd^2}{2V\ I_x} p - \frac{C_{\ell\delta} Qsd}{I_x} = 0 \tag{A-30}$$

p = Spin

I_x = Axial moment of inertia

$C_{\ell p}$ = Spin damping moment coefficient derivative (constant)

$C_{\ell\delta}$ = Spin driving moment coefficient (constant)

Q = Dynamic pressure

Define:

$$C_1 \equiv \frac{C_{\ell p} Qsd^2}{2V\ I_x} \quad , \quad C_2 \equiv \frac{C_{\ell\delta} Qsd}{I_x} \tag{A-31}$$

The solution of Equation (A-30) is

$$p = -\frac{C_2}{C_1}\left(1 - e^{C_1 t}\right) + p_0 e^{C_1 t}$$

$$p = p_\delta \left(1 - e^{C_1 t}\right) + p_0 e^{C_1 t} \tag{A-32}$$

$$-\frac{C_2}{C_1} \equiv p_\delta = -\frac{C_{\ell\delta}}{C_{\ell p}} \frac{2V}{d} \tag{A-33}$$

4. ROLL AVERAGED THRUST

The rocket will be rolling while the thrust is being applied. If the thrust is applied for a time period (roll angle $\phi_\tau = \dot{\phi}\tau$), what is the average value of the thrust in the mid angle direction. (See Figure A-2). In Figure A-2 it is desired to compute the average value of the thrust along the mid angle direction.

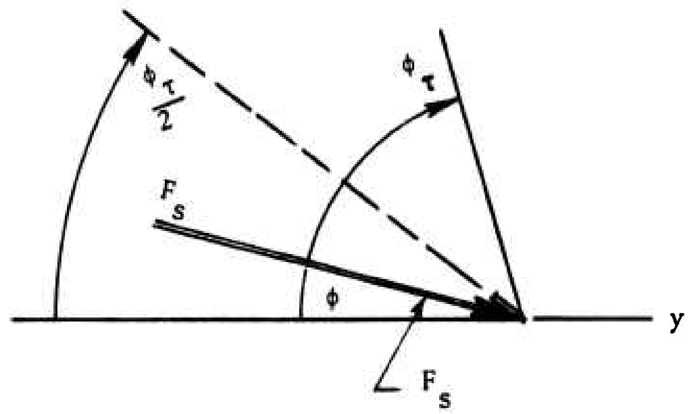

Figure A-2. Thrust Averaged about Mid Roll Angle

$$\dot{\phi} \simeq \text{constant} \quad , \quad \phi = \dot{\phi}t \quad , \quad \phi_\tau = \dot{\phi}\tau \quad , \quad \phi_\tau/2 = \dot{\phi}\tau/2$$

$$\bar{F}_s = \text{Average thrust} = \frac{1}{\tau}\int_0^\tau F_s \cos\left(\frac{\dot{\phi}\tau}{2} - \dot{\phi}t\right) dt$$

$$\bar{F}_s = -\frac{F_s}{\tau}\frac{1}{\dot{\phi}}\left[\sin\dot{\phi}\left(\frac{\tau}{2} - t\right)\right]_0^\tau$$

$$\bar{F}_s = \frac{2F_s}{\tau\dot{\phi}} \sin\frac{\dot{\phi}\tau}{2}$$

Note if $\dot{\phi}\tau = \pi$, (i.e., 1/2 revolution) then

$$\bar{F}_s = \frac{2F_s}{\pi}$$

APPENDIX B

LINEARIZED SOLUTION FOR THE MOTION OF A FIN-STABILIZED MISSILE WITH TRIM MISALIGNMENT

Linearized solution for the motion of a fin-stabilized missile with trim misalignment:

$$\S = K_{10}\, e^{\lambda_1 t}\, e^{i\dot{\phi}_1 t} + K_{20}\, e^{\lambda_2 t}\, e^{i\dot{\phi}_2 t} + K_t\, e^{i\phi_t} \qquad \text{(B-1)}$$

Where

$\S$ = Angle of attack of the missile in the complex plane (see Figure B-1)

K_{10}, K_{20} = Nutation and precession arms

λ_1, λ_2 = Nutation and precession damping rates

$\dot{\phi}_1$, $\dot{\phi}_2$ = Nutation and precession frequencies

i = $\sqrt{-1}$

t = Time

ϕ_t = $\int_0^t p\, dt$

p = Spin rate

K_t = Trim arm.

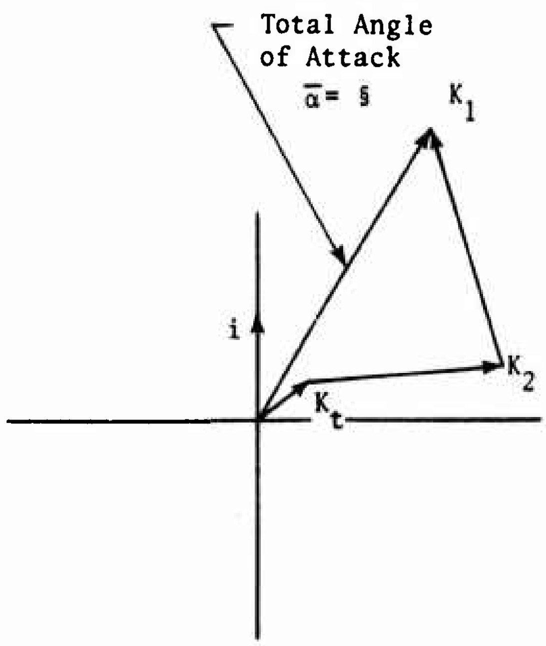

Figure B-1. Geometric Notation for Pitching and Yawing Motion

If the magnitude of the aerodynamic coefficients, the mass and moments of inertia, and the relatively low roll rate of the missile are taken into account the damping rates and frequencies of the missile reduce to a simple form.[a]

$$\dot{\phi}_{1,2} \simeq \frac{I_x}{I_y} \frac{p}{2} \pm \sqrt{-K_\alpha - \frac{K_{\dot{\alpha}}^2}{4}} \tag{B-2}$$

$$\lambda_{1,2} = K_{\dot{\alpha}}/2 \tag{B-3}$$

For a simple type of trim misalignment where the zero yaw trim moment is $QsdC_{m\alpha}\delta_m$, the non-rolling missile will trim at an angle δ_m, and the rolling missile has a trim arm given by

$$K_t \simeq \frac{\delta_m}{\left| -\left(\frac{p^2}{\dot{\phi}^2_{1,2}}\right)\left(1 - \frac{I_x}{I_y}\right) + 1 \right|} \tag{B-4}$$

For the case being considered

$$\dot{\phi}_{1,2} \simeq \pm \sqrt{-K_\alpha} \quad , \text{ and } \quad \left(\dot{\phi}_{1,2}\right)^2 \simeq \omega_1^{\,2}$$

This can be done since K_α is the dominating term in Equation (B-2).

---

[a]An assumption has been made that for the small angle of attack anticipated the nonlinear magnus moment coefficient will be small. Although there is no magnus wind tunnel data on the ATR, magnus data on similar missiles indicate this is so.

APPENDIX C

FORCES AND MOMENTS

1. THRUSTER FORCES AND MOMENTS

For the computer program the position of the target is established in body axis system by the equations below.

$$\varepsilon_q = \tan^{-1} R_z / R_x \tag{C-1}$$

$$\varepsilon_r = \tan^{-1} R_y / R_x$$

The computer flow chart logic Figure C-1 establishes the body fixed quadrant as seen in Figure C-2. The sequencing of the thruster may be done in any number of ways. The methods shown here are for inside out or outside in. The angle ζ is used in conjunction with the number of the thrust ($n = 1, 2, 3, - - N$) to determine the angle χ (chi) which is used in trigonometric function determining components of thruster force and associated moments. For equation logic see Figure C-3. Symbol definitions are at the end of this appendix.

2. AERODYNAMIC FORCES AND MOMENTS

The equations for the aerodynamic forces and moments in the body axis system are given in Figure C-4. These are commonly used equations for the more important forces and moments for a fin stabilized missile. The magnus moment and trim misalignment terms are included in the moment equations. Figure C-4 defines all the terms used in this Appendix.

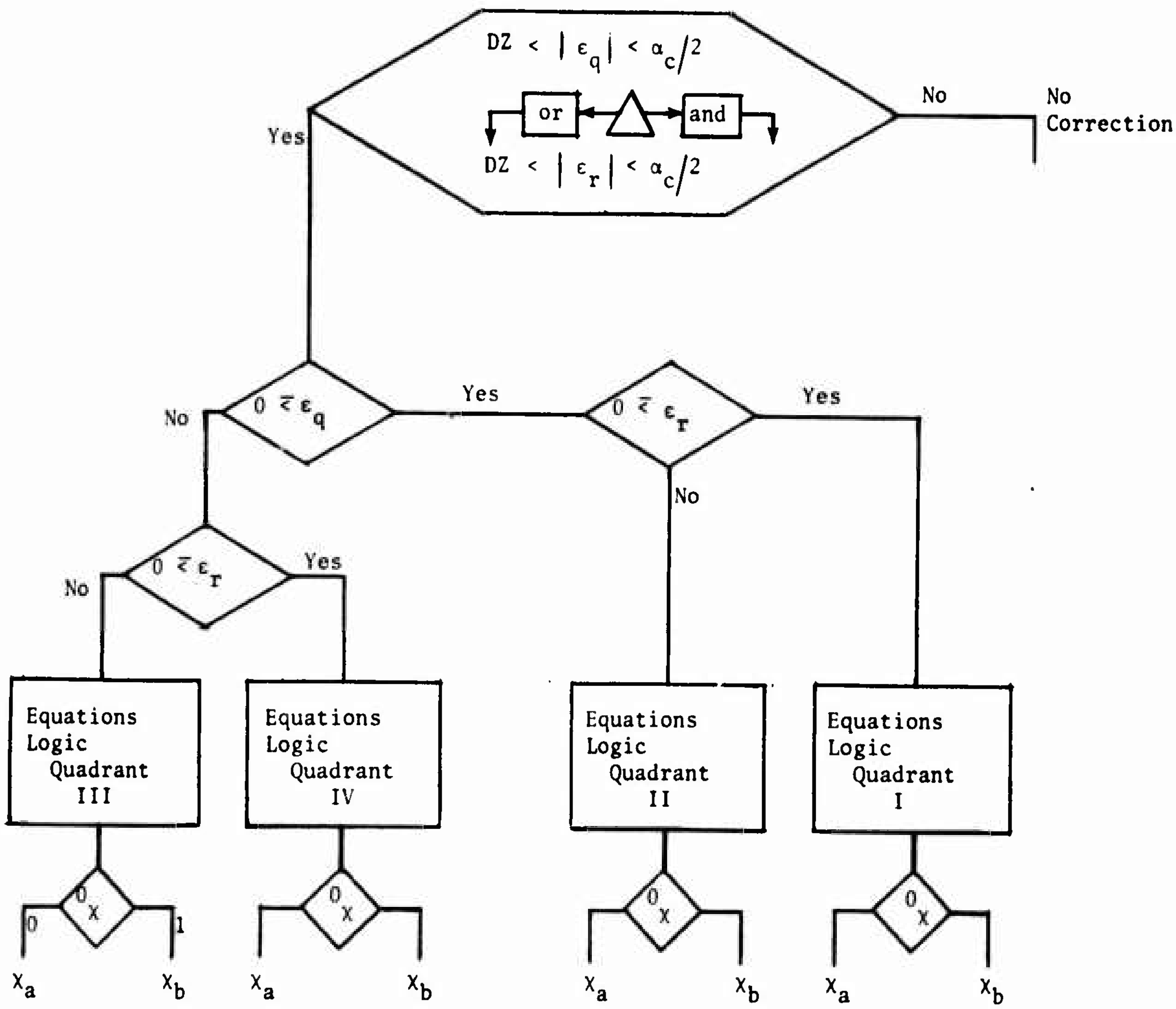

Figure C-1. Thruster Logic Flow Chart

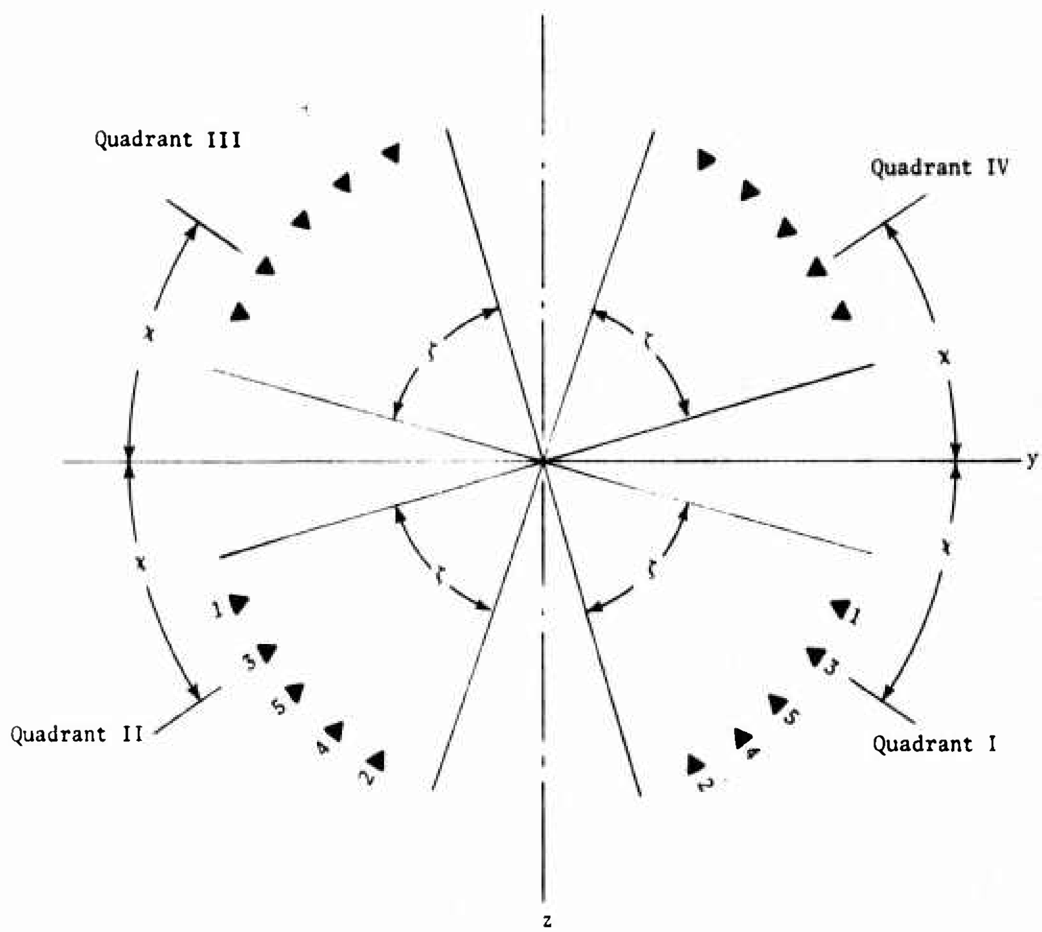

Example N = 5

Thruster positions looking forward along x.
x , y , z are body axes.

Figure C-2. Thruster Geometry

$$n = 1, 2, 3 \text{ --- } N$$

	n Odd		n Even	
N Even or Odd	$\chi_{a0} = \frac{90 - \zeta}{2} + \frac{(n + 1)\zeta}{2(N + 1)}$	,	$\chi_{\alpha e} = \frac{90 - \zeta}{2} + \frac{n\zeta}{2(N + 1)}$	Option a Outside In
N Even	$\chi_{b0} = \frac{90 - \zeta}{2} + \frac{(N - n + 1)\zeta}{2(N + 1)}$	,	$\chi_{be} = \frac{90 - \zeta}{2} + \frac{(N - n + 2)\zeta}{2(N + 1)}$	Option b Inside Out
N Odd	$\chi_{b0} = \frac{90 - \zeta}{2} + \frac{(N - n + 2)\zeta}{2(N + 1)}$	,	$\chi_{be} = \frac{90 - \zeta}{2} + \frac{N - n + 1}{2} \quad \frac{\zeta}{(N + 1)}$	

(n Odd) Body Forces and Moments

$$F_{yt} = \begin{bmatrix} + \\ = \\ + \end{bmatrix} T_{(n)} \cos \chi$$

$$F_{zt} = \begin{bmatrix} + \\ + \\ = \end{bmatrix} T_{(n)} \sin \chi$$

$$M_{yt} = \begin{bmatrix} = \\ + \\ + \end{bmatrix} T_{(n)} L_{(n)} \cos \chi$$

$$M_{\alpha t} = \begin{bmatrix} + \\ = \\ + \end{bmatrix} T_{(n)} L_{(n)} \cos \chi$$

(n Even) Body Forces and Moments

$$F_{yt} = \begin{bmatrix} + \\ = \\ + \end{bmatrix} T_{(n)} \sin \chi$$

$$F_{zt} = \begin{bmatrix} + \\ + \\ = \end{bmatrix} T_{(n)} \cos \chi$$

$$M_{yt} = \begin{bmatrix} = \\ + \\ + \end{bmatrix} T_{(n)} L_{(n)} \cos \chi$$

$$M_{zt} = \begin{bmatrix} + \\ = \\ + \end{bmatrix} T_{(n)} L_{(n)} \sin \chi$$

The signs preceding the forces and moments correspond to Quadrant I, II, III, IV in order.

Figure C-3. Thruster Logic Equations

$$F_x = Q_s \left[C_x \right]$$

$$F_y = Qs \left[C_{y\beta}\beta \right]$$

$$F_z = Qs \left[C_{z\alpha}\alpha \right]$$

$$L = Qsd \left[C_{\ell\delta}\, f_c + C_{\ell p}\left(\frac{pd}{2V}\right) \right]$$

$$M = Qsd \left[C_{mp\beta}\left(\frac{pd}{2V}\right)\beta + C_{m\alpha}\alpha + C_{m\dot{\alpha}}\left(\frac{\dot{\alpha}d}{2V}\right) + C_{mq}\left(\frac{qd}{2V}\right) - \delta_m C_{m\alpha} \cos\left(\phi + \phi_m\right) \right]$$

$$N = Qsd \left[C_{np\alpha}\left(\frac{pd}{2V}\right)\alpha + C_{n\beta}\beta + C_{n\dot{\beta}}\left(\frac{\dot{\beta}d}{2V}\right) + C_{nr}\left(\frac{rd}{2V}\right) + \delta_m C_{m\alpha} \sin\left(\phi + \phi_m\right) \right]$$

$$\alpha = \tan^{-1} w/u, \quad \beta = \tan^{-1} v/u, \quad \bar{\alpha} = \tan^{-1} \sqrt{v^2 + w^2} \Big/ \sqrt{u^2 + v^2 + w^2}$$

Figure C-4. Aerodynamic Forces and Moments in Body Axis System

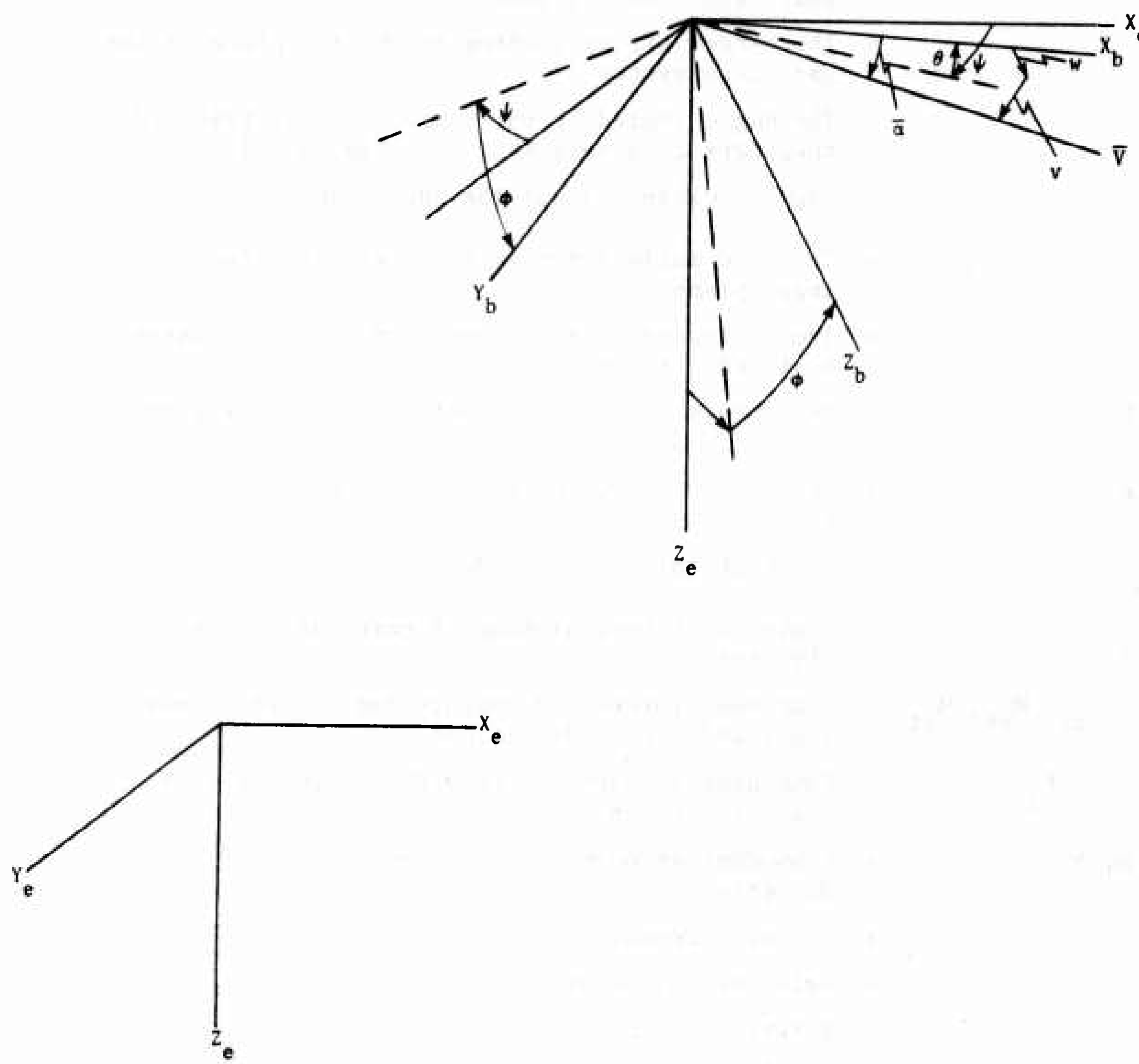

Figure C-5. Rocket Orientation and Angle of Attack Geometry

DEFINITION OF SYMBOLS IN APPENDIX C

ϵ_q	=	The target off axis error in the X-Z plane of the body axis system (Equation 1)
ϵ_r	=	The target off axis error in the X-Y plane of the body axis system
ζ	=	The angle including the symmetrical distributed thrusters of a quadrant. See Figure C-1
DZ	=	Angular dimensions of the dead zone
α_c	=	The cone angle defining the field of view from the image plane
χ	=	The angle defining the position of the thruster to be fired. Figure C-1
a, b	=	Subscripts referring to option a or b. Figures C-1 and C-3
o, e	=	Subscripts referring to n odd or even. Figures C-2 and C-3
$T_{(n)}$	=	Constant thrust magnitude for thruster n
$L_{(n)}$	=	Center of thrust distance forward of the cg for thruster n
F_{yt}, F_{zt}, M_{yt}, M_{zt}	=	Component forces and moments due to side thrust in the Y and Z body directions
F_x, F_y, F_z	=	Component aerodynamic body forces in the X, Y, Z body directions
L, M, N	=	Component aerodynamic body moments in XYZ body directions
Q	=	Dynamic pressure
d	=	Reference diameter
s	=	Reference area
C_x	=	Axial force coefficient. Computer tabulated and a function of Mach (M) and $\overline{\alpha}$
$C_{y\beta}$	=	Y force coefficient slope $\partial C_y/\partial\beta$. computer tabulated (M, β)
$C_{z\alpha}$	=	Z force coefficient slope $\partial C_z/\partial\alpha$. Computer tabulated (M, α)
$C_{\ell\delta}$	=	Spin driving moment computer tabulated (M, $\overline{\alpha}$)

f_c	=	Fin cant constant input
C_{lp}	=	Spin damping coefficient. Computer tabulated (M, $\bar{\alpha}$)
p, q, r	=	X Y Z body axis roll rates
V	=	Magnitude of missile velocity
ν	=	pd/2V = non-dimensional spin
$C_{mp\beta}$	=	Magnus moment coefficient $\partial^2 C_m / \partial\nu\partial\beta$. Computer tabulated (M, β)
$C_{m\alpha}$	=	Pitching moment coefficient slope $\partial C_m / \partial\alpha$. Computer tabulated (M, α)
$C_{m\dot{\alpha}}$	=	Damping moment derivative coefficient $\partial C_m / \partial \frac{\dot{\alpha} d}{2V}$. Computer tabulated (M, α)
$C_{np\alpha}$	=	Magnus moment coefficient $\partial^2 C_n / \partial\nu\partial\alpha$. Computer tabulated (M, α)
C_{mq}	=	Damping moment derivative coefficient $\partial C_m / \partial \frac{qd}{2V}$. Computer tabulated (M, α)
$C_{n\beta}$	=	Yawing moment coefficient slope $\partial C_n / \partial\beta$. Computer tabulated (M, β)
$C_{n\dot{\beta}}$	=	Damping moment derivative coefficient $\partial C_n / \partial \frac{\dot{\beta} d}{2V}$. Computer tabulated (M, β)
C_{nr}	=	Damping moment derivative coefficient $\partial C_n / \partial \frac{rd}{2V}$.
δ_m	=	Trim misalignment angle

(The reverse of this page is blank)

APPENDIX D

EQUIVALENT CEP CHART

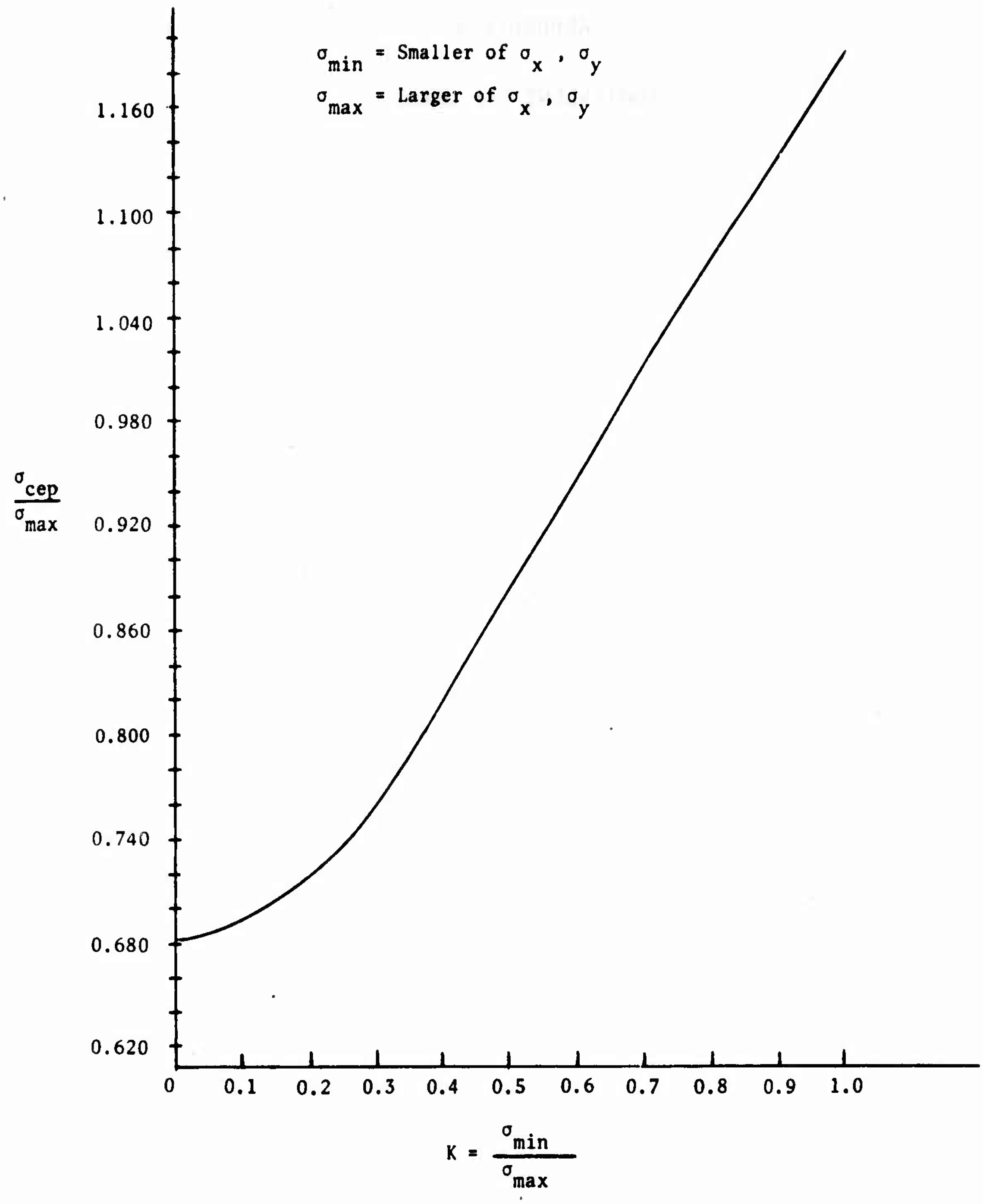

Figure D-1. Equivalent CEP Chart

INITIAL DISTRIBUTION

HQ USAF/RDQRM	2
HQ USAF/SAMI	1
HQ USAF/XOXFCM	1
HQ USAF/XOOWA	2
AFSC/IGFG	1
AFSC/SDWM	1
HQ AFSC/DLCAW	1
AFML/DO/AMIC	1
AFIT/LD	1
ASD/YEM	10
ASD/ENFEA	1
ASD/ENAZ	1
AFFDC/PTS	1
TAC/DRA	1
SAC/LGWC	1
HQ SAC (NRI/STINFO LIB)	1
WRAMA/MMEBL	1
CIA/CRE/ADD/PUBS	2
AFWL/LR	1
AUL/AUL-LSE-70-239	1
Redstone Sci Info Ctr/Doc Sec	2
USA Weapons Comd/SAPRI-LW-A	1
AMXSY-DD	1
AMXSY-A	1
AMXBR-TB	1
Frankford Arsenal/K2400	1
SARPA-TS	1
USN Weapons Lab	1
USN Nav Ord Lab/Tech Lib	2
Nav Ord Stn/Tech Lib	1
Nav Weapons Stn/20323	1
Nav Sys Cntr/Tech Lib	1
USN Wea Cntr/Code 533	2
China Lake/Code 40	1
Air Force Weapons Lab/Tech Lib	1
Nav Air Sys Comd/Code-Air 5323	1
Off Nav Res/Code 473	1
NASA STINFO Fac/Acquisitions Br	1
Inst for Defense Analysis/Class Lib	1
The RAND Corp/Lib-D	1
DDC/TC	2
USAFTFWC/TA	1
Nav Weapons Lab	1
SARWV-RDT-L	1
Honeywell, Inc/Aero & Defense Gp	1
Alpha Research Inc	1
Ogden ALC/MMWM	2
AF SPEC COMM CNTR/SUR	2
DAMA/WSA	1
SARPA-FR-S-A	1
US ATOMIC ENERGY COMM/Hqs Lib	1
AEDC/ARO, Inc/Lib/DLCS	1
AMXSY-DS	1
AMCR-WM	1
Nav Weapons Eval Fac/WE	1
Off of Chief of Nav Opns(OP-982E)	1
Nav Research Lab/Code 2627	1
Cal Inst of Tech/Propulsion Div	5
HQ PACAF/LGWLE	4
USAFTAWC/AY	1
TAWC/TRADOCLO	1
AFATL/DL	1
AFATL/DLB	1
AFATL/DLY	1
AFATL/DLOU	1
ADTC/XR	2
AFATL/DLOSL	2
AFATL/DLYV	1
AFATL/DLYD	3
AFATL/DLDL	15
AFATL/DLDE	1
AFATL/DLDT	1
ADTC/WE	1
AFATL/DLDG	6
AFATL/DLMA	2
AFATL/DLMT	2
ADTC/AD	1
Texas Instruments Inc	2
Thiokol Corp	1
AFRPL/MKMB	2
AAI Corp	1
Aerojet Solid Propulsion Co	2
NAVWPNCEN/Code 0632	1
Arnold Engr Development Cntr	1
Hughes Aircraft Co/Mail Sta N-77	1
GE Armament Sys Dept	2
Rockwell Intl/D-183	1
AFIS/INTA	1
BRL/EBL	1
AGARD/NATO	1

(The reverse of this page is blank)